NASA Contractor Report 195333

15725
p. 204

Processing and Mechanical Properties of NiAl-Based In-Situ Composites

David R. Johnson
The University of Tennessee at Knoxville
Knoxville, Tennessee

(NASA-CR-195333) PROCESSING AND MECHANICAL PROPERTIES OF NiAl-BASED IN-SITU COMPOSITES Ph.D. Thesis Final Report (Tennessee Univ.) 204 p

N94-36954

Unclas

G3/26 0015725

May 1994

Prepared for
Lewis Research Center
Under Grant NAG3–876

National Aeronautics and
Space Administration

PROCESSING AND MECHANICAL PROPERTIES OF NiAl-BASED IN-SITU COMPOSITES

A Dissertation
Presented for the
Doctor of Philosophy
Degree
The University of Tennessee, Knoxville

David R. Johnson
May 1994

ACKNOWLEDGMENT

The author is indebted to a number of individuals who have participated in the research presented in this dissertation. Mrs. X. F. Chen has performed all the TEM analysis presented here and her work and many helpful discussions are gratefully acknowledged. Mrs. Chen is a visiting scholar from the Materials Science Department at Shanghai Jiao Tong University, China. Dr. J. D. Whittenberger of NASA Lewis Research Center has performed all the elevated temperature compression tests and has supplied many helpful reviews. The author is also indebted to Dr. R. D. Noebe of NASA Lewis Research Center his many helpful discussions, suggestions, reviews, and guidance.

Appreciation is also expressed for the helpful guidance of my committee members. I would like to thank Dr. W. T. Becker for his many helpful discussions on interpreting the fracture behavior of the materials is this study. Dr. C. R. Brooks and Dr. A. J. Pedraza were always available to answer my questions and their help is gratefully acknowledged. I would like to thank Dr. C. T. Liu of the Oak Ridge National Laboratory for his time, interest, and assistance. My major professor, Dr. B. F. Oliver, was instrumental in all aspects of this research and I would like to thank him for his guidance, patience, and support.

I would like to thank Mr. B. L. McGill for his help and training on the SEM. Mr. McGill also performed the EDS analysis.

Appreciation is also extend to Mr. Ron Johnson of the electronics shop for his help with programing the DEC RT-11. Mr. Johnson specified, installed, and tested all the computer hardware in Dr. Oliver's solidification laboratory. In addition, the parallel processing setup was Ron's idea.

The author would like to thank his fellow students, specifically Preston Smith, Rob Reviere, Steve Joslin, and Tim Newport for their friendship and many helpful discussions.

ABSTRACT

Many ordered intermetallic alloys possess an unique combination of properties making them extremely attractive for high temperature applications. These advantageous properties include: high melting point, high thermal conductivity, low density, excellent oxidation resistance, and low material costs. However, the use of ordered intermetallic alloys for structural applications have been limited due to their brittleness at room temperature. Also, the elevated temperature strength of many intermetallic alloys such as NiAl is poor.

The objective of this research was to improve both the room temperature fracture toughness and elevated strength of NiAl-based materials by producing in-situ composites from directional solidification of eutectic alloys. Directional solidification was performed by containerless processing techniques in a levitation zone refiner to minimize alloy contamination. Three classes of NiAl-based in-situ composites were examined. These were the NiAl-Cr eutectic system, the NiAl plus Laves phase eutectics, and ternary eutectic systems containing NiAl, a refractory metal phase, and a Laves phase. Room temperature fracture toughness of these materials was determined by four-point bend test. Preliminary creep behavior was determined by compression tests at elevated temperatures, 1200-1400 K.

In-situ composites based on the NiAl-Cr eutectic system were successfully produced by containerless processing and evaluated. Molybdenum additions of 0.6 to 6 at.% were used to change the eutectic microstructure. The NiAl-Cr alloys had a fibrous microstructure while the NiAl-(Cr,Mo) alloys containing 1 at.% or more molybdenum exhibited a lamellar structure. The effect of eutectic morphology on both the room temperature fracture toughness and the 1300 K creep strength was investigated. The NiAl-28Cr-6Mo alloys exhibited the best creep resistance and additional creep testing was performed at 1200 and 1400 K. This NiAl-(Cr,Mo) eutectic displays a promising high temperature strength while still maintaining a reasonable room temperature fracture toughness when compared to other NiAl-based materials.

The Laves phase NiAlTa was used to strengthen NiAl and very promising creep strengths were found for the directionally solidified NiAl-NiAlTa eutectic. The eutectic composition was found to be near NiAl-15.5Ta (at.%) and well aligned microstructures were produced at this composition. An off-eutectic composition of NiAl-14.5Ta was also processed. The off-eutectic composition resulted in microstructures consisting of NiAl dendrites surrounded by aligned eutectic regions. The room temperature toughness of these two phase alloys was similar to that of polycrystalline NiAl even with the presence of the brittle Laves phase NiAlTa. Evidence of a ternary peritectic reaction: NiAl+NiAlTa+liquid=Ni_2AlTa was also found from cast microstructures of Ni-Al-Ta alloys.

Polyphase in-situ composites were generated by directional solidification of ternary eutectics. This work was performed to discover if a balance of properties could be produced by combining the NiAl-Laves phase and the NiAl-refractory metal phase eutectics. The systems investigated were the Ni-Al-Ta-X (X=Cr, Mo, or V) alloys. Ternary eutectics were found in each of these systems and both the eutectic composition and temperature were determined. Of these ternary eutectics, the one in the NiAl-Ta-Cr system was found to be the most promising. The fracture toughness of the NiAl-(Cr,Al)NiTa-Cr eutectic was intermediate between those of the NiAl-NiAlTa eutectic and the NiAl-Cr eutectic. The creep strength of this ternary eutectic was similar to or greater than that of the NiAl-Cr eutectic.

TABLE OF CONTENTS

CHAPTER PAGE

PART 1: GENERAL INTRODUCTION AND OVERVIEW

PART 2: PROCESSING AND EXPERIMENTAL PROCEDURES

PART 3: DIRECTIONAL SOLIDIFICATION AND MECHANICAL PROPERTIES OF NiAl-Cr and NiAl-(Cr,Mo) EUTECTIC ALLOYS

PART 4: DIRECTIONAL SOLIDIFICATION AND MECHANICAL PROPERTIES OF NiAl-NiAlTa ALLOYS

PART 5: POLYPHASE IN-SITU COMPOSITES

PART 6: SUMMARY

LIST OF TABLES

TABLE PAGE

LIST OF FIGURES

PART 1: GENERAL INTRODUCTION AND OVERVIEW

CHAPTER 1

OVERVIEW AND OBJECTIVES

To meet the requirements of advancing technologies in the aerospace and other industries, materials are needed with application temperatures higher than those of the nickel-based superalloys currently in use. Intermetallics systems are being considered as candidate materials for advanced high temperature aerospace applications. In particular, the B2 compound NiAl is being extensively studied due to its superior oxidation resistance, high melting point, low density, and high thermal conductivity [1]. However, NiAl is brittle at room temperature and has poor elevated temperature strength, both of which render this material inadequate for structural applications. Reinforcing NiAl with second phases to form composite materials may eliminate these problems.

One method for producing NiAl-based composites is by controlling the eutectic solidification process of NiAl based alloys. During eutectic growth, two or more solid phases form simultaneously from the liquid. Directional solidification of these eutectic alloys may produce in-situ composites, where one or more phases are aligned parallel to the growth direction.

One advantage of producing in-situ composites by directional solidification is that the phases are thermodynamically stable even up to the melting point. A disadvantage is that alloy compositions are limited by the appropriate phase equilibria needed for eutectic growth. Unfortunately, the eutectic compositions for many systems of interest are unknown.

The objective of this research was to develop high temperature, NiAl based, in-situ composites. The research objectives may be stated as:

1. locate NiAl based eutectic systems for directional solidification,
2. develop computer controlled containerless processing conditions for these NiAl based systems,
3. grow in-situ composites by directional solidification from the systems of interest, and to
4. examine the room temperature and the elevated temperature mechanical properties of the materials so processed.

CHAPTER 2

LITERATURE REVIEW

The intermetallic compound NiAl

Nickel aluminide (NiAl) is a potential material for use at elevated temperatures, due to many excellent properties as listed in Figure 1.1. The Ni-Al phase diagram is shown in Figure 1.2. It is characterized by the presence of five intermetallic compounds. Of these, NiAl has the highest melting temperature at 1911 K. This is 240 K greater than melting temperature of Ni_3Al, the strengthening phase in many nickel-based superalloys [2]. In addition, NiAl has a wide phase field of more than 5 at.% nickel making it suitable for alloying studies without entering a two phase field [1].

Nickel aluminide (NiAl) has a simple CsCl crystal structure as shown in Figure 1.3. The predominate slip system in NiAl at room temperature is the <100>{110} system [3-7]. This gives only three independent slip systems for plastic deformation which is less than the five independent deformation modes needed for polycrystalline deformation. However, single crystals of NiAl are brittle regardless of the loading orientation [8]. Single crystals of NiAl tested along a non-<100> orientation (the "soft" orientation) exhibit poor tensile ductility at room temperature with typical values near 2% total elongation. Thus, the limited number of slip systems operative at room temperature in NiAl is not sufficient to accommodate the complex stress states that may develop at surface flaws [9].

The brittle behavior of NiAl single crystals is further characterized by cleavage on the {110} type planes [10-13]. Crystal orientations that maximize the resolved shear stresses on the {110} slip planes also produce large normal stresses on the cleavage

ADVANTAGES OF NICKEL ALUMINIDE (NiAl)

- DENSITY IS TWO-THIRDS THAT OF THE NICKEL-BASED SUPERALLOYS.
- THERMAL CONDUCTIVITY IS FOUR TO EIGHT TIMES THAT OF THE NICKEL-BASED SUPERALLOYS.
- EXCELLENT OXIDATION RESISTANCE – COMMONLY USED AS A PROTECTIVE COATING FOR THE NICKEL-BASED SUPERALLOYS.
- LOW DUCTILE TO BRITTLE TRANSITION TEMPERATURE OF 300–400 C. LOWER THAN MANY INTERMETALLICS
- SIMPLE CRYSTAL STRUCTURE. NiAL HAS AN ORDERED BODY-CENTERED CUBIC CRYSTAL STRUCTURE (CsCl).

Figure 1.1: Attractive properties of the intermetallic compound NiAl [1].

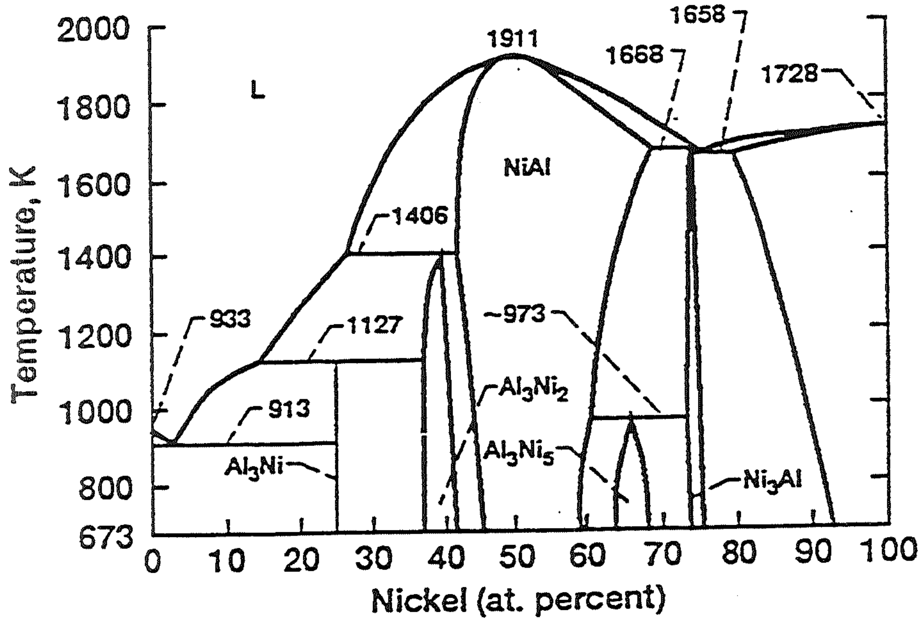

Figure 1.2: Ni-Al phase diagram [8].

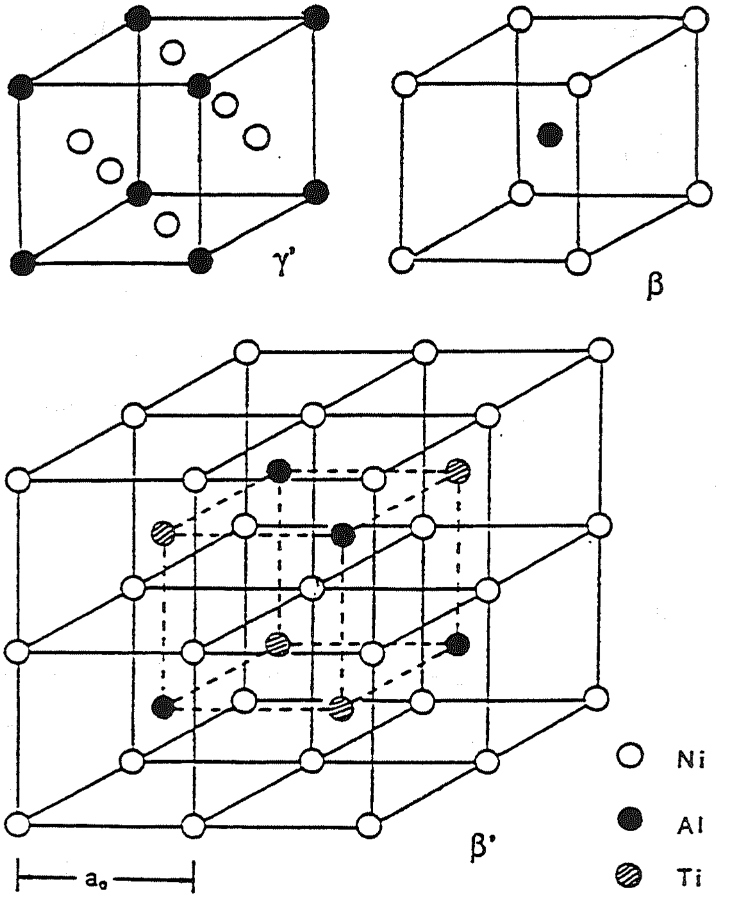

Figure 1.3: Crystal structures of Ni_3Al (γ'), NiAl (β), and Ni_2AlTi (β') [3].

planes as shown in Figures 1.4 and 1.5. Thus, the crystal orientations needed to maximize both the tensile ductility and the plane strain fracture toughness are not initially obvious.

As expected, the fracture toughness of single crystal NiAl is strongly dependent upon the test orientation. Typical fracture toughness values between 4-5 MPa√m are observed when the notch is perpendicular to the <110> direction, while values between 8-10 MPa√m are observed when the notch is perpendicular to the <100> direction [13]. Fracture toughness as a function of test orientation has been found to scale with the magnitude of the resolved normal stresses on the <110> type cleavage planes [13] as shown in Figure 1.6.

While the toughness is poor at room temperature, one attractive property of NiAl is its low ductile to brittle transition temperature (DBTT). Within the temperature range of 573-673 K, there is a large increase in both the tensile elongation and the fracture toughness of single crystal NiAl [12,14] as shown in Figure 1.7. From Figure 1.7, the maximum tensile elongation is observed at intermediate temperatures with decreasing values at higher temperatures.

Room temperature ductility

While the intermetallic phase NiAl possesses many excellent properties, it use for load bearing applications is limited due to its inadequate low temperature mechanical properties. Considerable research has been exerted to understand the deformation processes of NiAl at room temperature and to develop strategies to improve its poor room temperature mechanical properties. Such investigations include macroalloying, microalloying, and ductile phase toughening of NiAl.

Many recent investigations have examined the possibility of activating additional slip systems such as <111> slip through macroalloying additions (say greater than 1 at.%). Alloying elements considered have been Cr, V, and Mn [8]. The elements

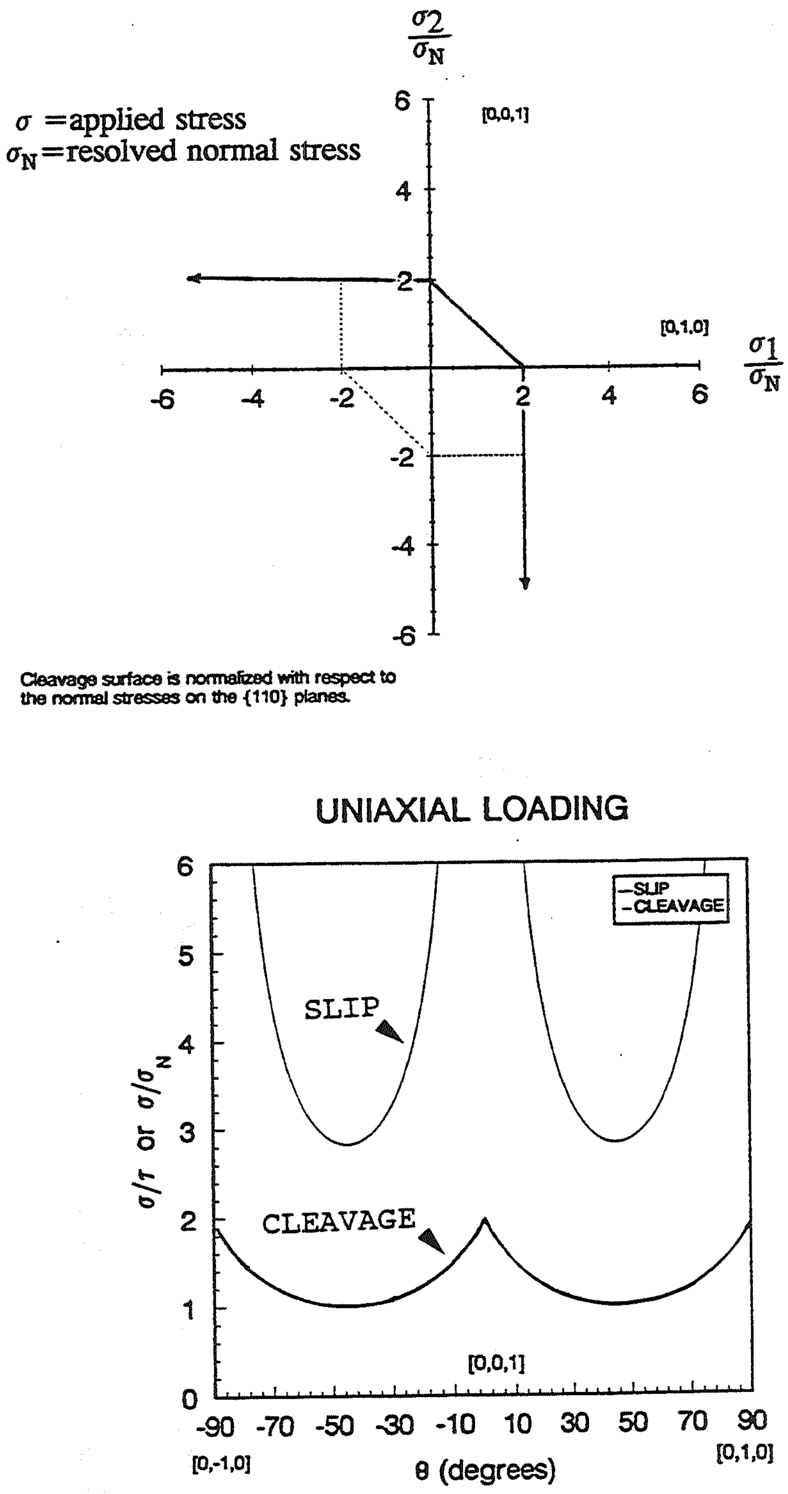

Figure 1.4: Cleavage and yield surfaces for NiAl in the (a) "hard" <100> orientation and (b) non-<100> orientation.

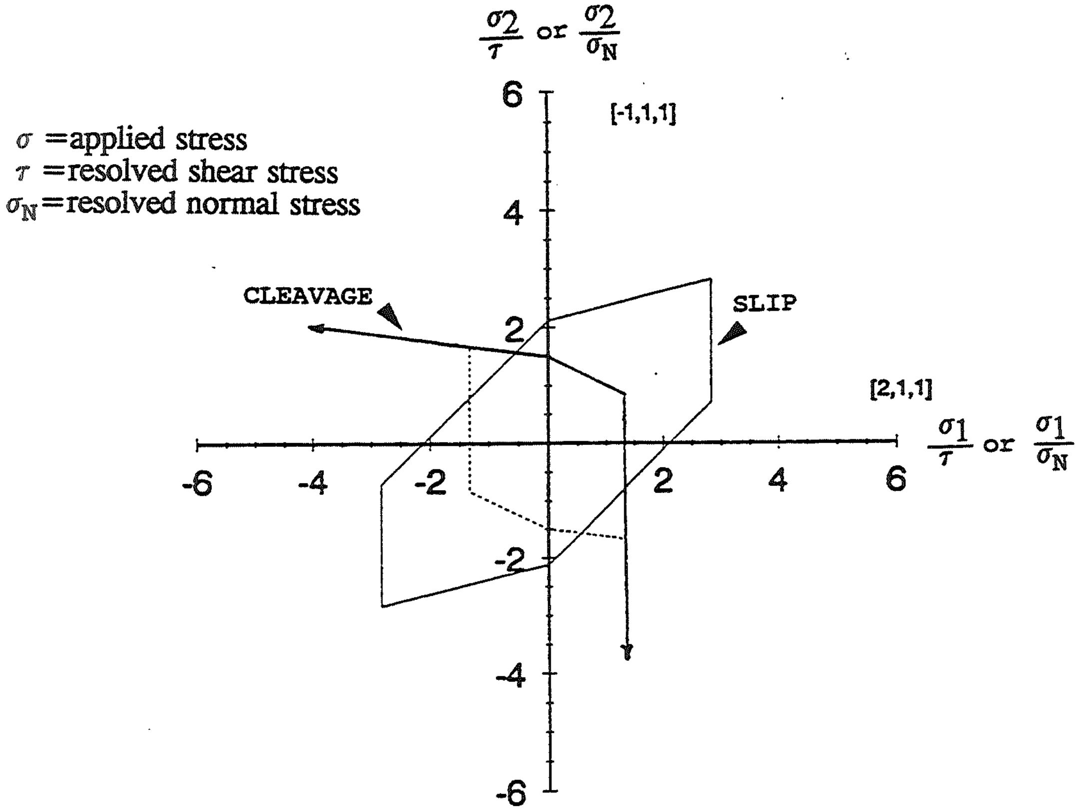

Yield surface for {110}<001> slip systems. Cleavage surface is normalized with respect to the normal stresses acting on the {110} planes.

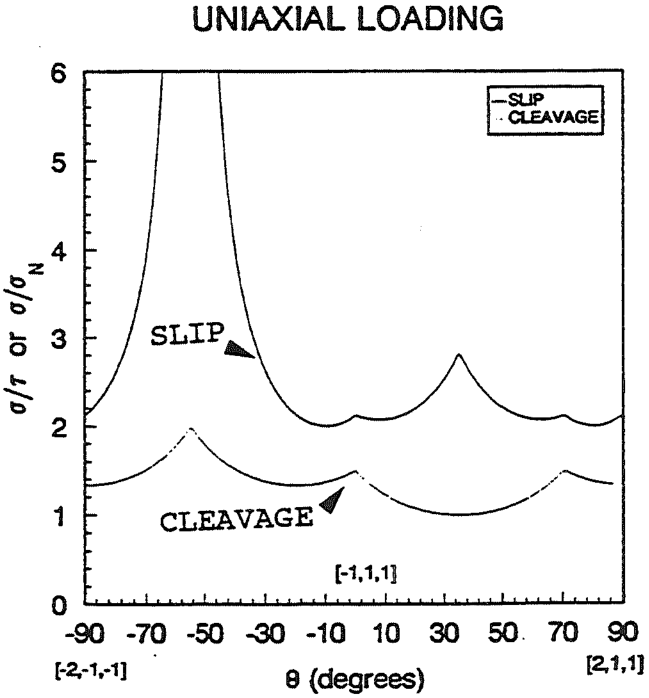

Figure 1.5: Cleavage and yield surfaces for NiAl (a) in the "soft" <111> orientation and (b) rotated away from <111> axis.

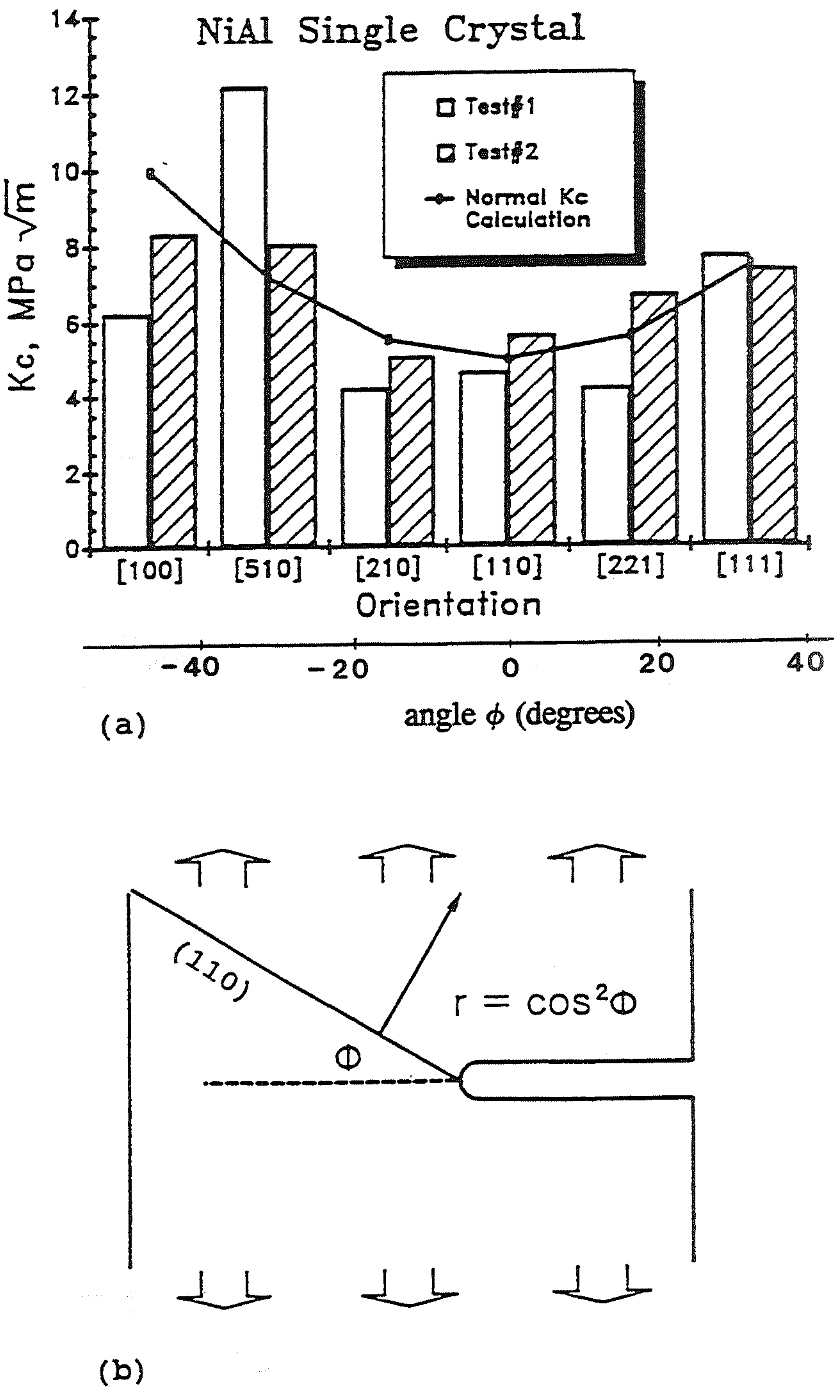

Figure 1.6: Fracture toughness for single crystal NiAl (a) as a function of orientation given by (b) the relationship between the cleavage plane and the notch plane [13].

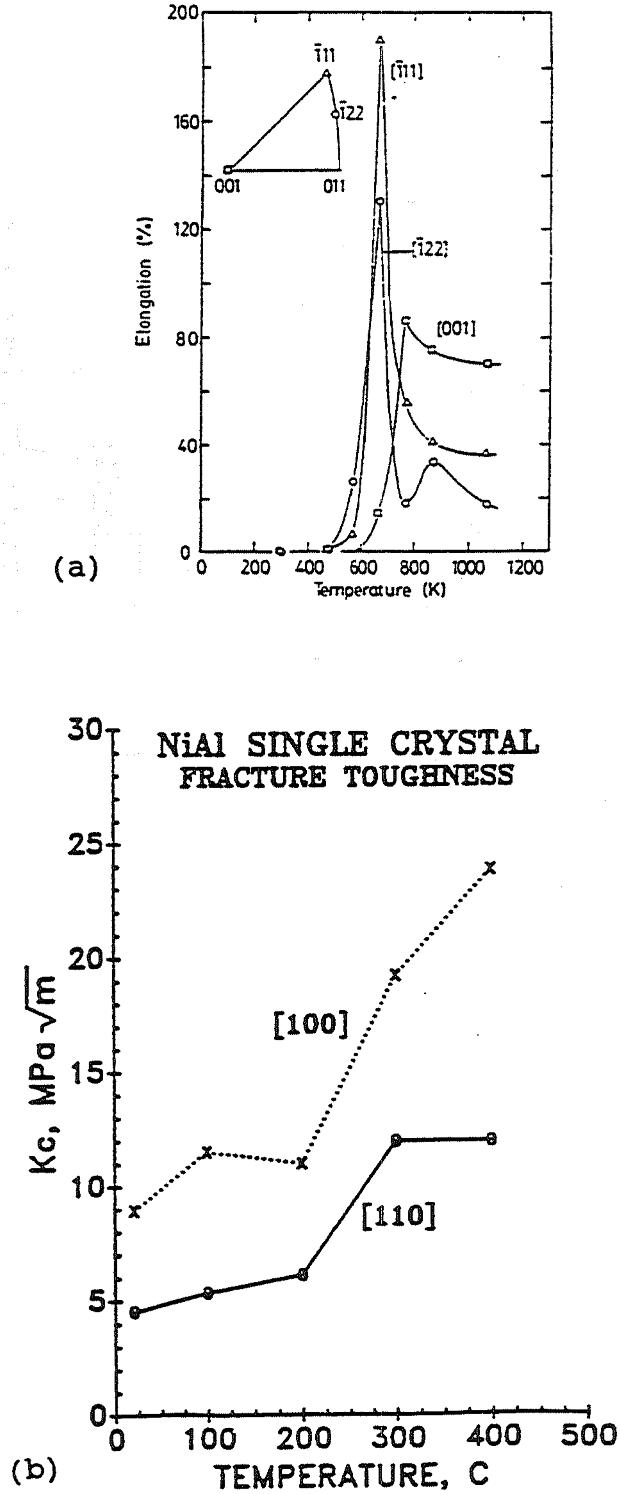

Figure 1.7: The ductile brittle transition temperature in single crystal NiAl demonstrated by (a) tensile elongation versus temperature [12] and (b) fracture toughness versus temperature [13].

Cr, V, and Mn all have limited solubility in NiAl. A few studies have indicated that <111> slip occurs in NiAl due to Cr or Mn additions when tested in the hard orientation [15,16]. However, these alloys showed no signs of improved room temperature tensile ductility [15]. In addition, there has been no evidence of <111> slip in polycrystalline NiAl alloyed with Cr or Mn when tested in compression [8,17].

Increases in tensile ductility have been observed for single crystal NiAl microalloyed with Mo, Ga, and Fe within the 0.1 to 0.25 at.% range [18]. Measured plastic strains in tension as high as 6% were seen when these alloys were tested in the <110> orientation. At higher alloying additions the effect of increased ductility disappears. The mechanisms for the improved ductility from microalloying have not yet been identified but are speculated to involve impurity trapping or dislocation core interactions with point defects [18]. However, tests performed on polycrystalline NiAl specimens microalloyed with Ga or Mn showed no improvement in tensile ductility [19].

Ductile phase toughening is another method for improving the toughness and ductility of brittle materials. The improved toughness is provided by the interaction between the propagating crack and the ductile phase during fracture. The challenge is to increase the toughness without sacrificing the attractive high temperature properties of the intermetallic compound. For example, introducing Ni_3Al as a ductile phase in NiAl improves the ductility and toughness of the composite material over that of binary NiAl [9]. Unfortunately, the melting temperature is depressed and the creep strength of the two phase alloy can be significantly lower than that of binary NiAl [9].

On the other hand, a number of eutectic microstructures consisting of NiAl and a refractory metal phase show both improved toughness and creep strength. Two example systems are the NiAl-Cr, and the NiAl-Mo eutectic alloys [20-24]. The reinforcing refractory metal phase provides increases in both the toughness and creep strength of the composite material. The NiAl-Cr eutectic was one of the initial NiAl based systems studied for possible high temperature use [20]. This system has displayed promising room temperature fracture toughness [24] and promising elevated temperature strength [25]. These properties make the NiAl-Cr eutectic a good choice for comparison when evaluating other NiAl-based in-situ composites. Furthermore, different processing procedures and alloying additions may enhance the mechanical properties of this eutectic. The Cr-NiAl quasi-binary phase diagram is shown in Figure 1.8.

The different possible toughening mechanisms provided by a ductile second phase within a brittle matrix are shown in Figure 1.9. These different mechanisms are classified as crack bridging, crack blunting, or crack deflection [9]. Crack bridging occurs when a moderately strong bond exist between the ductile phase and the matrix phase [9]. The plastic deformation experienced by the second phase in the crack wake inhibits further crack propagation. Crack blunting occurs when the stresses at the crack tip are relaxed sufficiently by the ductile phase preventing further crack propagation. Crack deflection occurs when a weak bond exist between the second phase and the matrix phase. Debonding between the two phases may causes the crack to branch decreasing its energy. Of these different toughening mechanism, crack bridging is commonly observed in eutectic microstructures due to the strong interfacial bond between the different phases.

Elevated temperature properties

Most intermetallics with high melting temperatures have complex crystal structures with strong directional atomic bonding. This strong bonding in general leads to a retention of mechanical properties at high temperatures. To a first approximation, mechanical properties such as strength and creep resistance scale directly with melting temperature. However, NiAl with its simpler crystal structure exhibits poorer creep resistance than either Ni_3Al or TiAl even though NiAl has the greater melting temperature [25,26].

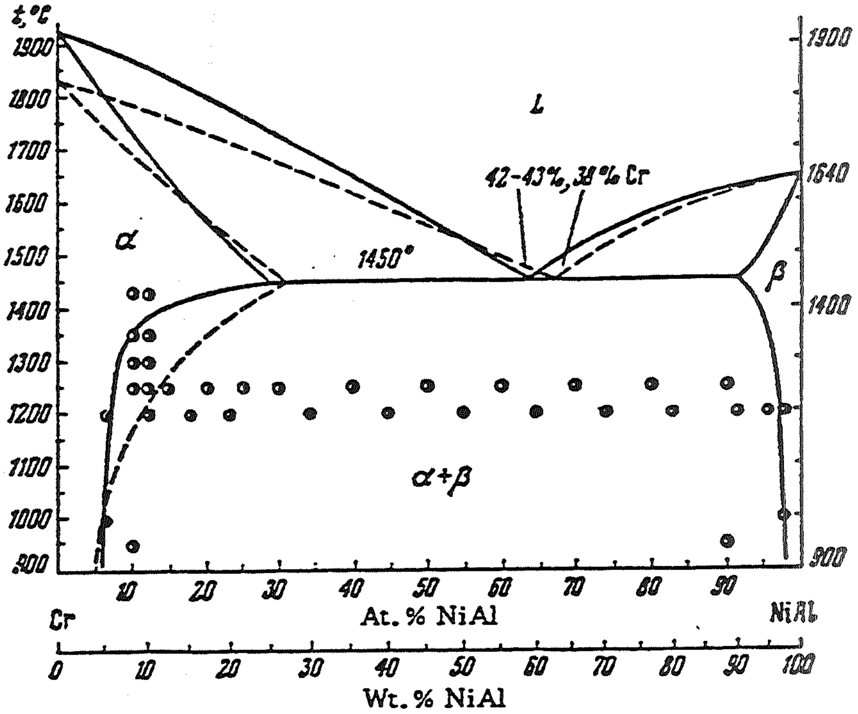

Figure 1.8: The Cr-NiAl quasi-binary phase diagram [34].

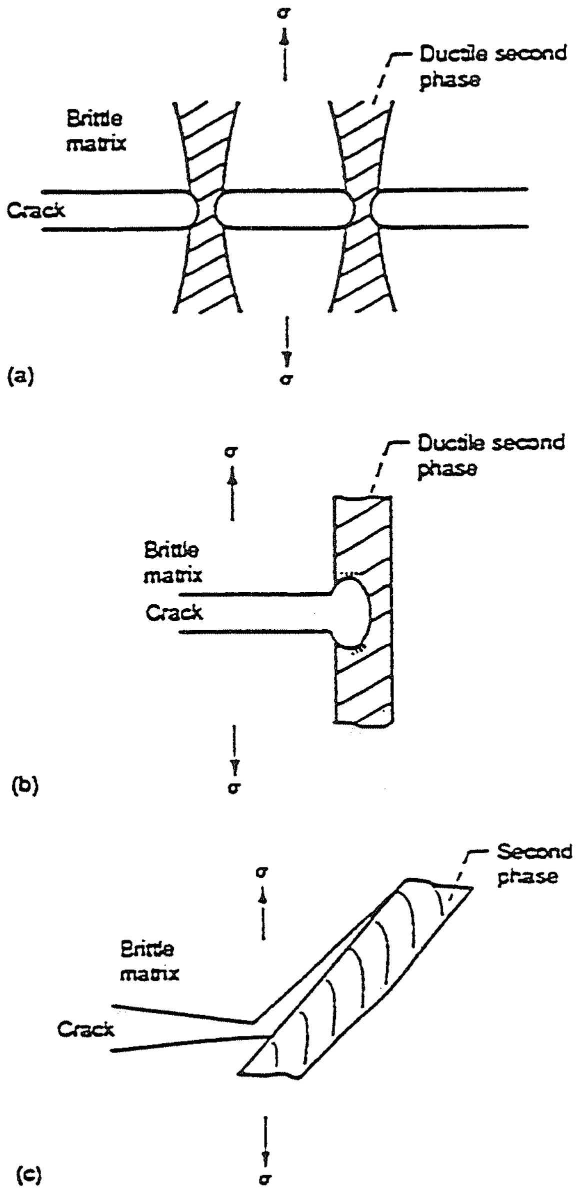

Figure 1.9: Examples of ductile phase toughening by (a) crack bridging, (b) crack blunting, and (c) crack deflection mechanisms [9].

The high temperature strength of NiAl is poor when compared to those of a nickel-based superalloy, Figure 1.10. Methods to improve the high temperature strength of NiAl by solid solution strengthening or precipitation hardening are generally successful for fast deformation rates but the improvement is diminished at slow deformation rates [27]. Alloys containing precipitates of Heusler phases such as Ni_2AlHf have shown promising creep properties [1]. However, some of the most promising elevated temperature strengths have been displayed by NiAl-Laves phase systems. An example of such a system is the NiAl-NiAlNb eutectic [25,28]. By directional solidification of this eutectic, an order of magnitude increase in creep resistance was measured when compared to material processed using a casting and extrusion procedure [28]. These results are shown in Figure 1.11.

Polyphase in-situ composites

Also of interest are composites structures containing more than two phases. Systems of interest would include a metallic phase for better low temperature toughness combined with several intermetallic phases for good elevated temperature strength. Such systems considered are the NiAl-refractory metal eutectics and the NiAl-Laves phase eutectics. Based on the room temperature toughness imparted by the metallic phase, the elevated temperature strength of the Laves phase, and the oxidation resistance of the NiAl phase, optimum properties may be achieved in a directionally solidified three phase eutectic.

The intermetallic compound NiAl forms eutectic microstructures with the refractory metals Cr, Mo, V, W, and Re [8]. The NiAl-Laves phase NiAlNb eutectic has shown promising high temperature properties [28]. In addition, the Laves phase NiAlTa forms stable equilibria with NiAl and such alloys have also displayed promising high temperature properties [25,26].

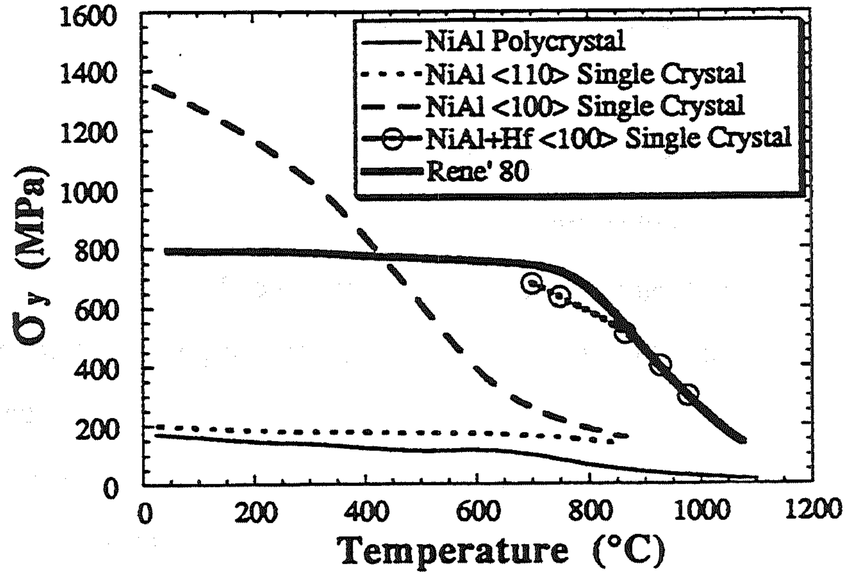

Figure 1.10: Yield strength of NiAl compared to a nickel-base superalloy at elevated temperatures [38].

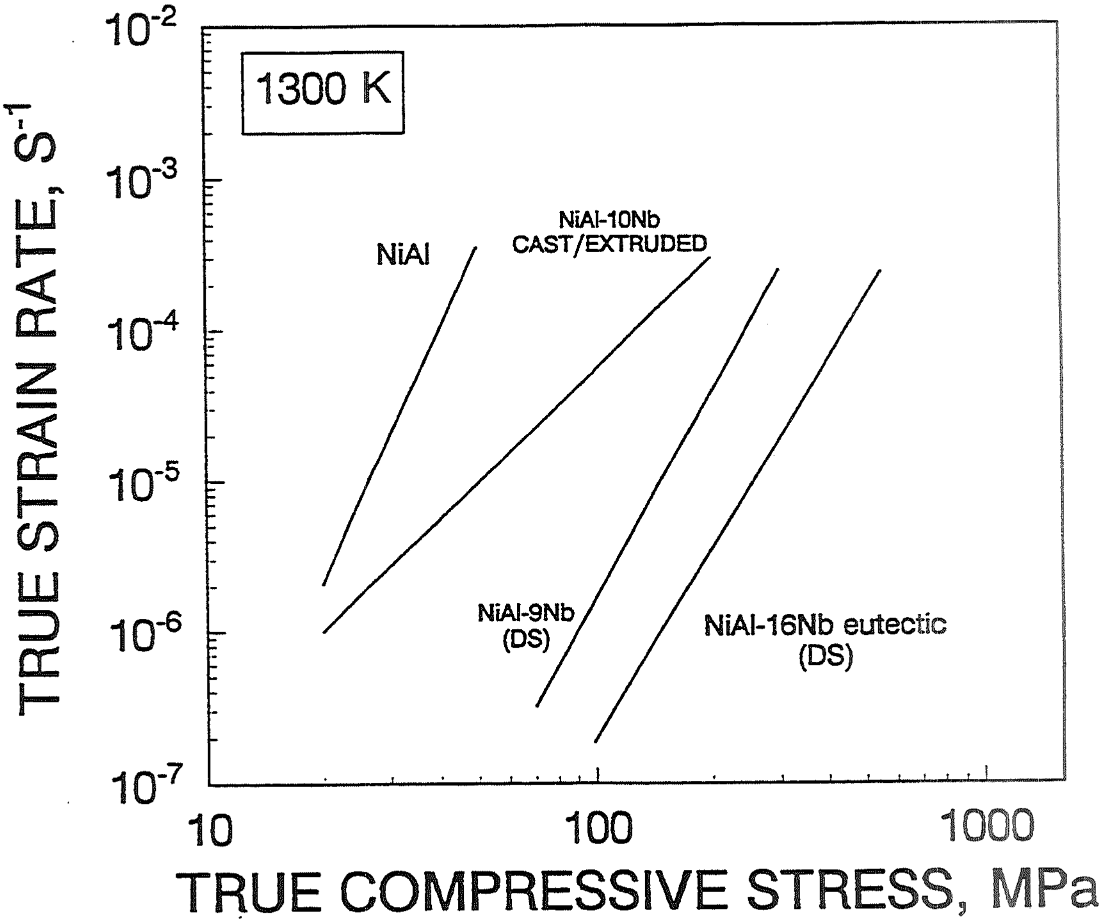

DS = DIRECTIONALLY SOLIDIFIED

Figure 1.11: 1300 K compressive stress-strain behavior of NiAl alloys strengthened with the Laves phase NiAlNb [28].

Thus, the systems to study are the Ni-Al-Nb refractory metal systems and the Ni-Al-Ta-refractory metal systems. Unfortunately, much of the alloying work to date on these systems considers only the nickel rich alloys [30-33].

CHAPTER 3

SCOPE OF RESEARCH

Ordered intermetallics such as NiAl are considered candidate for high temperature structural applications provided that the proper combination of room temperature toughness and elevated temperature strength can be developed. Improvements in these areas are generally found for multi-phase alloys. However, processing of intermetallics is usually difficult due to their refractory nature. Before mechanical properties can be measured and optimized, processing routes must produce sound bulk material which can be reliably tested. Part of the present research was to develop containerless processing techniques for producing composite materials. In-situ composites were generated by directional solidification in a levitation zone refiner. The facility design of the directional solidification laboratory allows automated process control of the levitation zone refiner. Much of the present research consisted of software development to allow automated processing of a wider range materials than previously possible.

After the upgrade of the levitation zone refiner, two classes of NiAl-based in-situ composited were examined. These were the NiAl plus refractory metal eutectic systems and the NiAl plus Laves phase eutectics. The ductile phase toughening of brittle materials was examined in the NiAl-refractory metal eutectics. Conversely, the very hard and brittle Laves phases in the NiAl-Laves phases eutectics were expected to provide improvements in the creep resistance compared to other NiAl based materials.

Lastly, polyphase in-situ composites were generated by directional solidification of ternary eutectics. This work was performed to discover if a balance of properties could be produced by combining the NiAl-Laves phase and the NiAl-refractory metal phase eutectics.

REFERENCES

1. R. Darolia, JOM 43[3], (1991), 44-49.
2. C.T. Sims and W.C. Hagel, The Superalloys, John Wiley & Sons, New York, 1972.
3. R.W. Cahn, MRS BULLETIN, May (1991), 18-21.
4. R.D. Field, D.F. Lahrman, and R. Darolia, Acta Metall.Mater., 39 (1991), 2951-2959.
5. M. Dollar, S. Dymek, S. J. Hwang, and P. Nash, Scripta Metall. Mater., 26 (1992), 29-43.
6. R.T. Pascoe, and C.W.A. Newey, Met. Sci., 5 (1971), 50-55.
7. M.J. Mills, and D.B. Miracle, Acta Metall. Mater., 41 (1993), 85-95.
8. R.D. Noebe, R.R. Bowman, and M.V. Nathal, Int. Mat. Rev., 38 (1993), 192-232
9. R.D. Noebe, F.J. Ritzert, A. Misra, and R. Gibala, Prospects for Ductility and Toughness Enhancement of NiAl by Ductile Phase Reinforcement, NASA TM-103796, 1991.
10. Keh-minn Chang, R. Darolia, and H.A. Lipsitt, MRS Proceedings, 213 (1991), 597-602.
11. M.H. Yoo, and C.L. Fu, Scipta Metall. Mater., 25 (1991), 2345-2350.
12. T. Takasugi, S. Watanabe, and S. Hanada, Mat. Sci. Engr., A149 (1992), 183-193.
13. K.M. Chang, R. Darolia, and H.A. Lipsitt, Acta Metall. Mater, 40 (1992), 2727-2737.
14. S.V. Raj, R.D. Noebe, and R. Bowman, Scripta Met., 23 (1989), 2049-2054.
15. R.D. Field, D.F. Lahram, and R. Darolia, Acta Metall. Mater., 39 (1991) 2961-2969.
16. D.B. Miracle, S. Russell, and C.C. Law, MRS Proceedings, 133 (1988), 225-230.
17. J.D. Cotton, M.J. Kaufman, R.D. Noebe, and M.K. Behbehani, HITEMP Review-1991, NASA CP-10082 (1991), 23-1.
18. R. Darolia, D. Lahrman, and R. Field, Scripta Metall. Mater., 26 (1992), 1007-1012.
19. R.D. Noebe and M.K. Behbehani, Scripta Metall. Mater., 27 (1992), 1795-1880.
20. J.L. Walter and H.E. Cline, Met. Trans., 1 (1970), 1221-1229.
21. H.E. Cline and J.L. Walter, Met. Trans., 1 (1970), 2907-2917.
22. J.L. Water and H.E. Cline, Met. Trans., 4 (1973), 33-38.
23. H.E. Cline, J.L. Water, E. Lifshin, and R.R. Russel, Met. Trans., 2 (1971), 189-194.
24. R. Darolia, D.F. Lahrman, R.D. Field, J.R. Dobbs, K.M. Chan, E.H. Goldman, and D.G. Konitzer, in Ordered Intermetallics-Physical Metallurgy and Mechanical Behavior, C. T. Liu, et. al., eds., Kluwer Academic Publishers, The Netherlands (1991), 679-698.
25. G. Sauthoff, Z. Metallkde., 81 (1990), 855-861.
26. G. Sauthoff, in Intermetallic Compounds - Structure and Mechanical Properties, O. Izumi, ed., Japan Institute of Metals, Sendai, Japan (1991), 371-378.
27. J.D. Whittenberger and M.J. Luton, J. Mater. Res., 5 (1990), 2819-2827.
28. J.D. Whittenberger, R. Reviere, R.D. Noebe and B.F. Oliver, Scripta Metall. Mater., 26 (1992), 987-992.
29. R.D. Reviere, B.F. Oliver, and D.D. Bruns, Mat. and Manuf. Proc., 4 (1989), 103-131.
30. M. Durand-Charre, D. David and J. Wang, High Temp. Mat. and Proc, 10 (1991), 1-12.
31. S. Chakravorty and D. R. F. West, Mat. Sci. and Tech., 1 (1985), 978-985.
32. S. Chakravorty and D. R. F. West, Metal Sci., 18 (1984), 207-215.
33. S. Chakravorty, S. Sadiq, and D. R. F. West, J. Mat. Sci., 24 (1989), 577-583.
34. Yu. A. Bagaryatskiy, J. Inorganic Chem., USSR, 3 (1958), 247-252.

36. V.M. Pathare, Ph.D. Thesis, Case Western Reserve University, 1987. (Also available as NASA CR-182113, 1988).

35. D.R. Johnson, S.M. Joslin, B.F. Oliver, R.D. Noebe, and J.D. Whittenberger, MRS Proceedings, 273 (1992).
37. S. Reuss, H. Vehoff, Scripta Metall. Mater., 24 (1990), 1021-1026.
38. R. Darolia, in Structural Intermetallics, R. Darolia, et al., eds., TMS, Warrendale PA (1993), 495-502.

PART 2: PROCESSING AND EXPERIMENTAL PROCEDURES

CHAPTER 1

CONTAINERLESS PROCESSING

In-situ composites generated by directional solidification can possess more attractive high temperature properties than those produced by other techniques such as casting and extrusion. Containerless processing offers the additional advantage of enhanced purity by eliminating alloy contamination from the crucible. The crucible is eliminated by using induction power to heat, levitate, and constrain the liquid zone. Directional solidification is then accomplished by moving the liquid zone through the length of the ingot. A schematic of the levitated molten zone is shown in Figure 2.1. Without crucible containment, precise dimensional control of the freezing ingot requires that the shape and position of the molten zone within the induction coils be controlled. Thus, the control variables are the position of the solid-liquid interface and the liquid zone diameter. The design of the solidification laboratory allows ingots to be processed under full computer control independent of any temperature measurements [1].

The following procedure is used to control the solidification process. A digitized image of the molten zone is captured by an image processing camera that is computer addressable. The interface location is held to a target position by controlling the induced power. The shape of the zone is controlled by maintaining a constant melt diameter by a stretch-squeeze action on the liquid. Both the interface position and the melt diameter are held to their target values by proportional, integral control loops. An infrared pyrometer is also used to record the temperature near the solid-liquid interface.

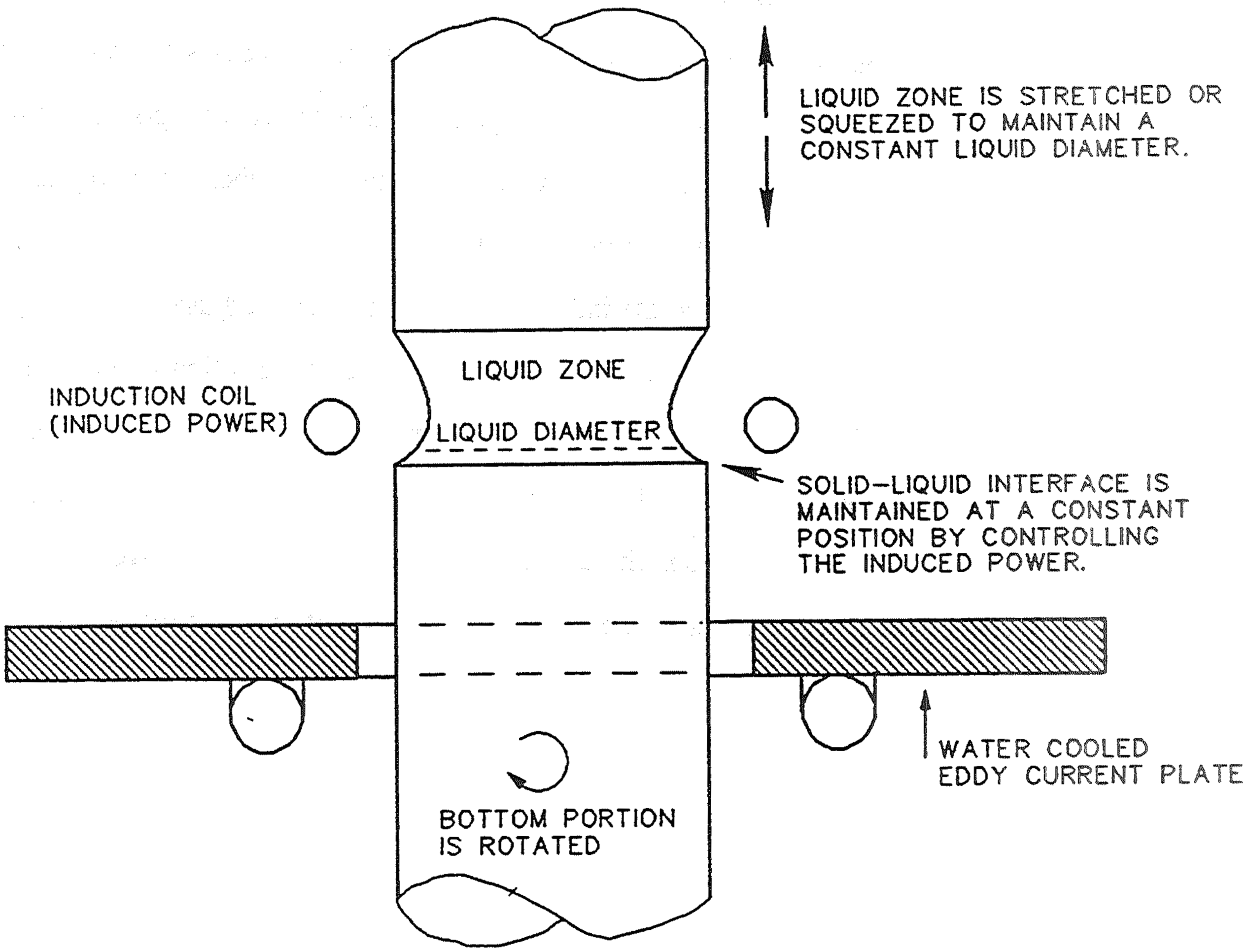

Figure 2.1: Schematic of molten zone during directional solidification.

The method for producing the electromagnetically constrained liquid zone is shown in Figure 2.2. To allow for volume expansion upon melting, a gap is left between the upper and lower portions of the ingot during initial heating. As the material is melted, liquid is levitated until it comes in contact with the upper portion of the ingot. After thermal equilibrium is reached, the induced power is controlled to establish a stable liquid zone. The shape of the molten zone and dimensional control of the freezing solid-liquid interface can be maintained by moving the top portion of the ingot relative to the bottom (stretch/squeeze). The lower solid portion of the ingot is rotated to maintain a smooth solid-liquid interface. The whole assembly is moved through the heating and shaping induction field.

During a typical run, the induced power is manually adjusted at the beginning of the process to place the solid-liquid interface at a stable position in the constraining field. The power is then placed under computer control using software to locate the solid-liquid interface. As the liquidus temperature and composition of the interface change during directional solidification, the controller adjusts the power to maintain the interface position at the desired position independent of direct temperature measurements.

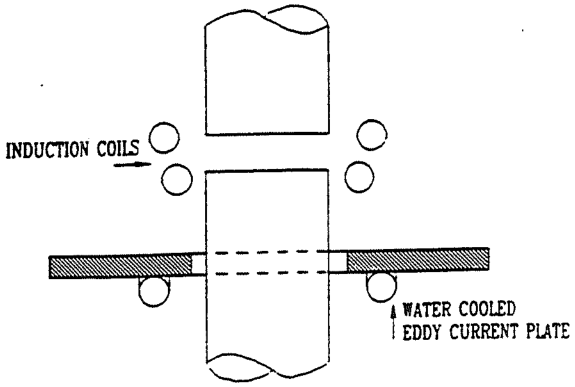

(a) POSITION AT START

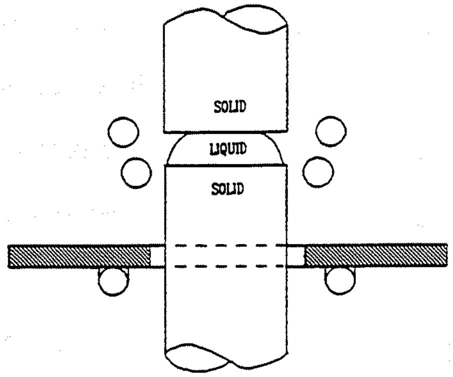

(b) ZONE PARTIALLY ESTABLISHED
LIQUID PARTIALLY LEVITATED

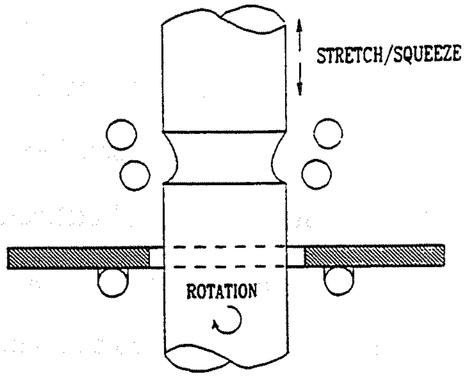

(c) ZONE ESTABLISHED

Figure 2.2: Formation of an electromagnetically constrained liquid zone during containerless processing.

CHAPTER 2

FACILITY DESIGN

The thermal response of high temperature intermetallics such as NiAl is very fast. To maintain steady state heat and mass transfer processes in these high energy input/output systems, the control system must maintain the solid-liquid interface at a fixed position within the thermal field. Experience has shown that control actions are needed 4 to 5 times per second to maintain the shape of the molten zone for many high temperature systems. Times longer than this are insufficient to control the shape of the zone. Unfortunately, the computer acquisition and interrogation of the digitized image are very time consuming. This allows only a small portion of the digitized image to be transferred to the computer within the given time constraints. Furthermore, simultaneous control of both the liquid diameter and the position of the solid-liquid interface is needed for precise dimensional control of the processed ingot. The liquid diameter is measured along a fixed pixel line during the control process, Figure 2.1. Thus, to maintain an accurate reading of the liquid zone diameter, a constant solid-liquid interface position must be maintained. However, a variety of different zone shapes and geometries have been observed for materials processed to date making effective computer control difficult.

To overcome the time limitations imposed by the image processing hardware, a parallel processing scheme using two computers was employed. With parallel processing, the position of the solid-liquid interface is found on one computer without interfering with the control actions of the second computer. A schematic of the previous and upgraded facility design is shown in Figure 2.3. Computer control of the levitation zone refiner is divided into three parts. First, a central processing

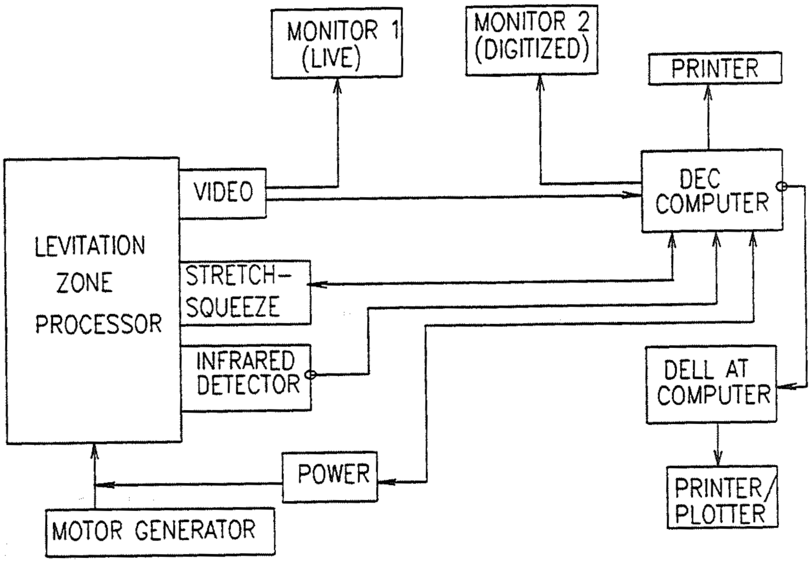

(a) previous facility design.

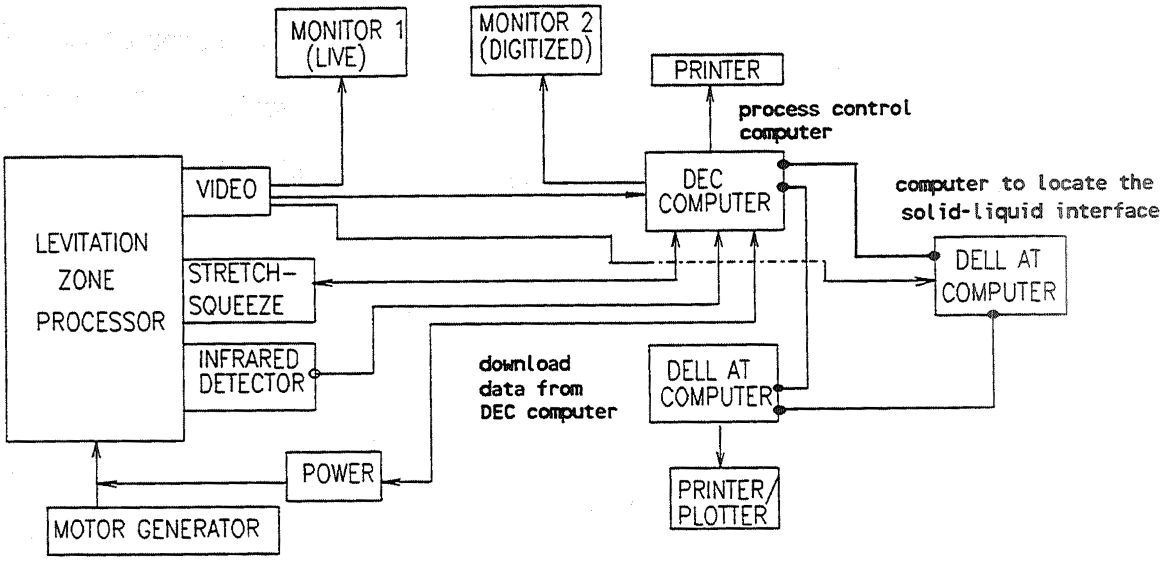

(b) Parallel processing setup.

Figure 2.3: System upgrade to include parallel processing capabilities.

computer is used to vary the power and stretch/squeeze action of the levitation zone refiner. Also, the length of the liquid zone diameter is found by this central processing computer. Next, the position of the solid liquid interface is found on a second computer. This measurement is transferred to the main processing computer where the appropriate control action is performed. Lastly, a third computer is used for data acquisition of the run time variables. Details of the hardware setup and a listing of the software code are given in appendix A.

Dividing the tasks needed to control the zone melter among different computers allows for development of more extensive software. The difficulties experienced in developing algorithms to locate the solid-liquid interface were caused by the time constraints imposed by the image processing hardware. The distance over which the solid-liquid interface can move during a typical run is small and less than 20 pixels lines. With such a coarse resolution, the interface position must be found within one or two pixel lines to successfully control the induction power. Increasing the camera magnification and the working resolution would not allow the full width of the zone to be captured. The rotation of the solid-liquid interface may also create a slight wobble in the ingot complicating matters further.

Hence, the most successful algorithms were ones where the solid-liquid interface was determined from the average of a large number of readings over a short time period. With the parallel processing arrangement, the frequency of the control actions was increased by a factor of two. In addition, for each control action, the average interface position was determined from twice the number of reading than that previously allowed.

Typical as-processed NiAl ingots are shown in Figure 2.4. These single crystal ingots were produced by containerless processing under full computer control. The melt record for one of these ingots is shown in Figure 2.5. Computer control was initiated at about 3000 seconds. From Figure 2.5, a constant interface position

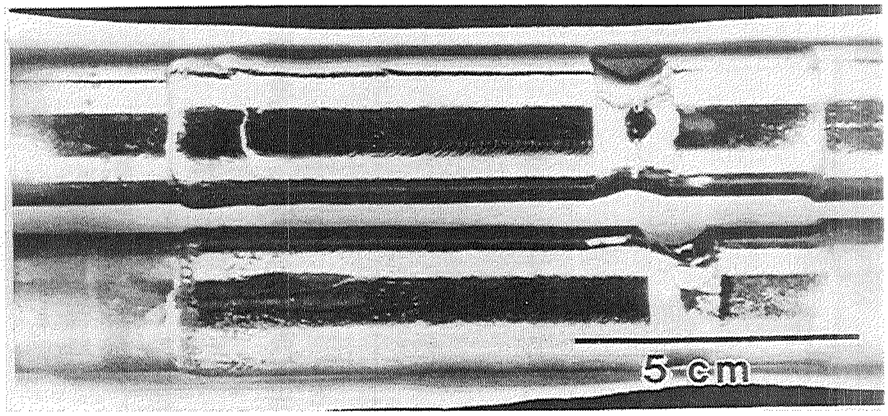

Figure 2.4: Typical as-processed single crystal NiAl ingots.

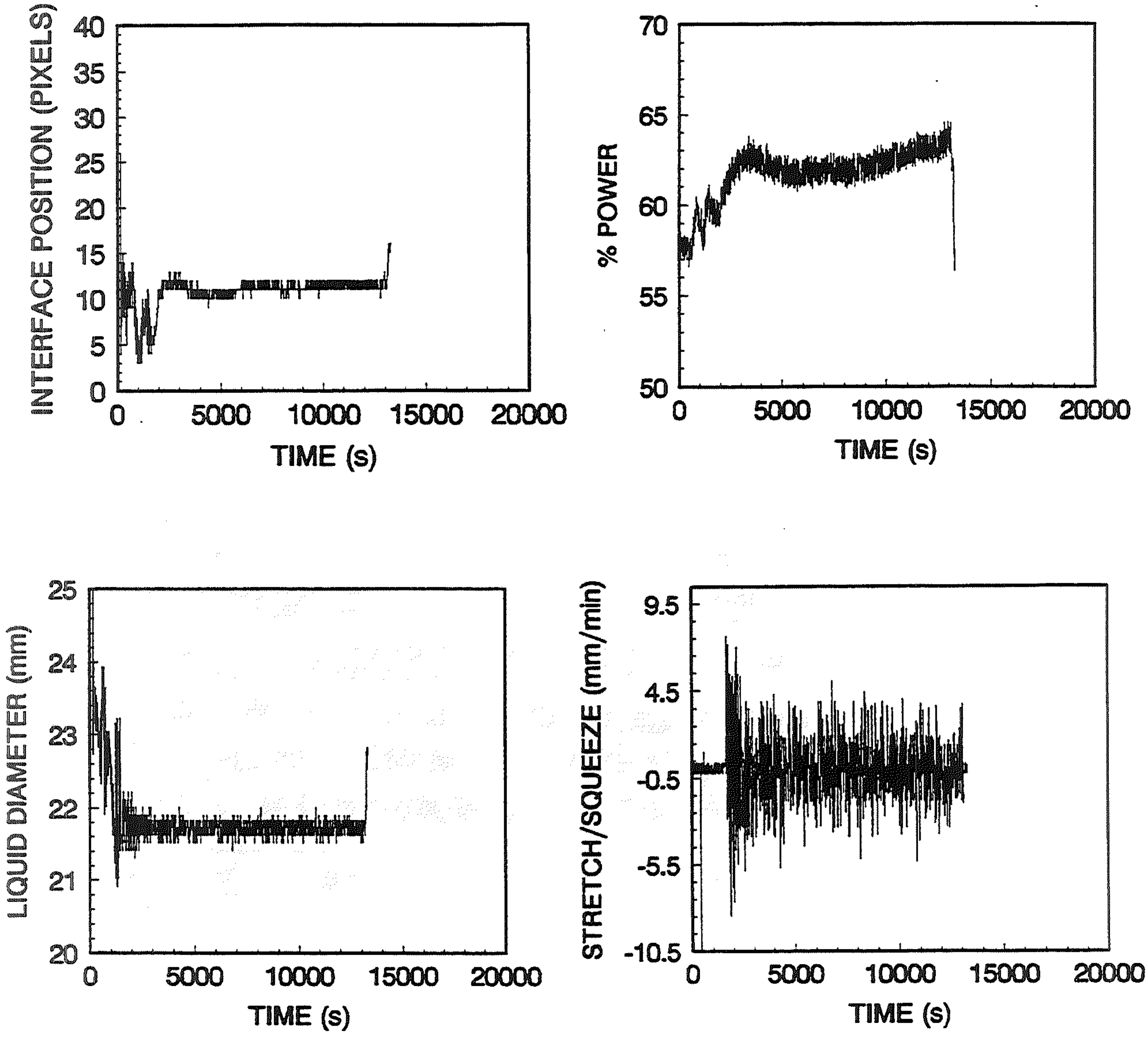

Figure 2.5: Processing record for a NiAl ingot.

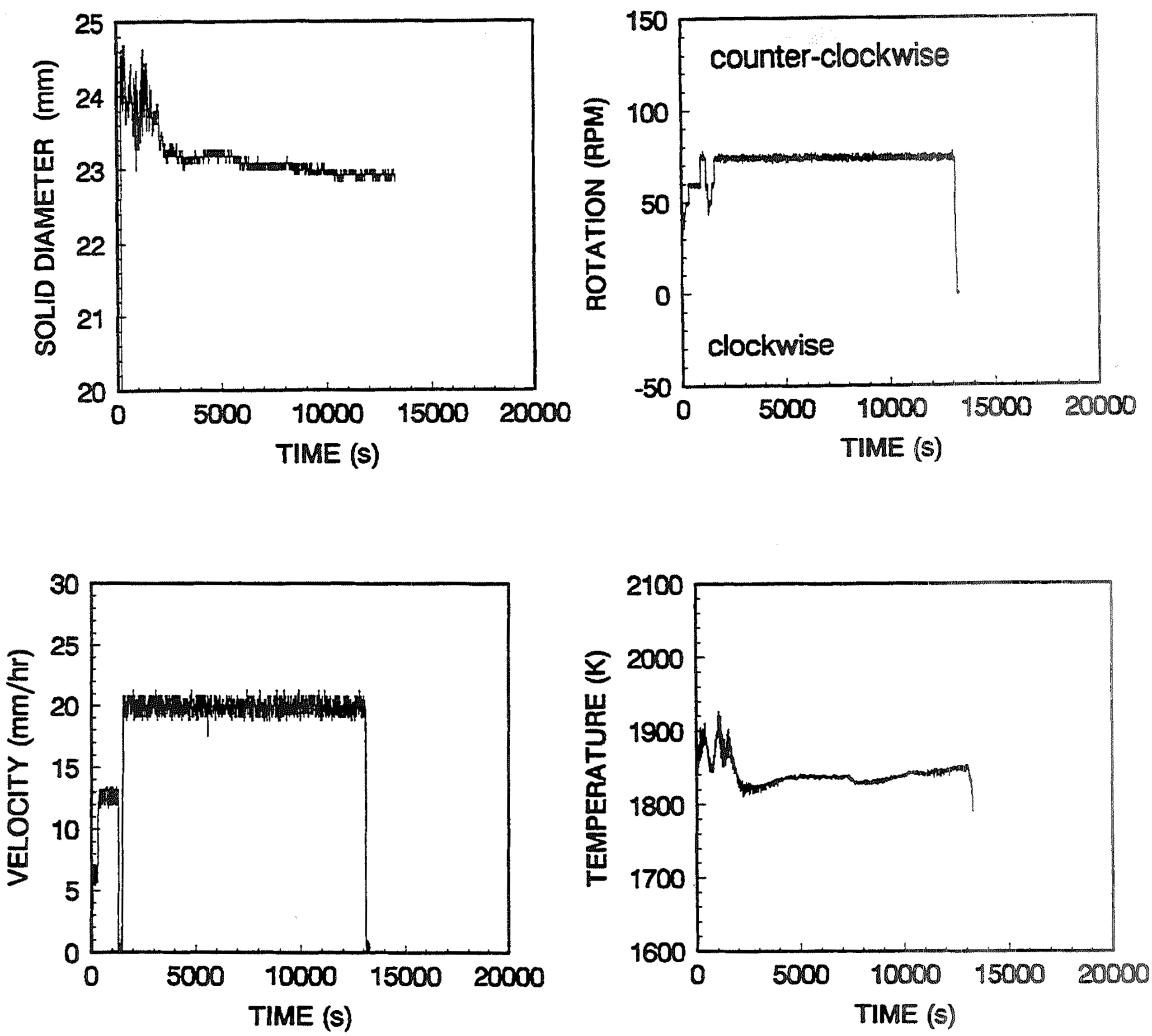

Figure 2.5 (continued).

was maintained by varying the induced power. Similarly, constant liquid diameter was maintained by a stretch-squeeze action. Control of these two variables resulted in excellent dimensional control as represented by the plot of the solid diameter. Completing the melt record are the velocity of the scan frame, the rotation of the interface, and the temperature near the solid-liquid interface.

CHAPTER 3

EXPERIMENTAL PROCEDURES

Compression testing

Compression testing at elevated temperature was performed by Dr. J. D. Whittenberger at NASA Lewis Research Center. Cylindrical compression specimens, 5 mm diameter by 10 mm length, with the compression axis parallel to the growth direction, were electrical discharge machined from selected ingots. The elevated temperature mechanical behavior of these specimens was then determined. If promising strengths were measured at 1300 K, further testing at 1200 and 1400 K was performed. Compressive properties were generated under both constant velocity conditions in a screw driven universal machine and under constant load conditions in lever-arm creep machines. In general, constant velocity experiments were used to determine behavior at the higher strain rates ($>10^{-7}\ s^{-1}$) while constant load testing was employed for lower rates. Overlapping stress-strain rate data from the two techniques indicated excellent correlation between constant load and constant rate tests. All testing was performed in air as a secondary check for environmental resistance under load.

Flexure testing

Room temperature fracture toughness was determined by performing four--point bend tests on notched samples. The specimen size and test geometry are shown in Figure 2.6. Bend specimens were electrical discharge machined from the directionally solidified ingots and notched perpendicular to the growth direction using a slow speed diamond impregnated saw. A fatigue crack was not initiated at the

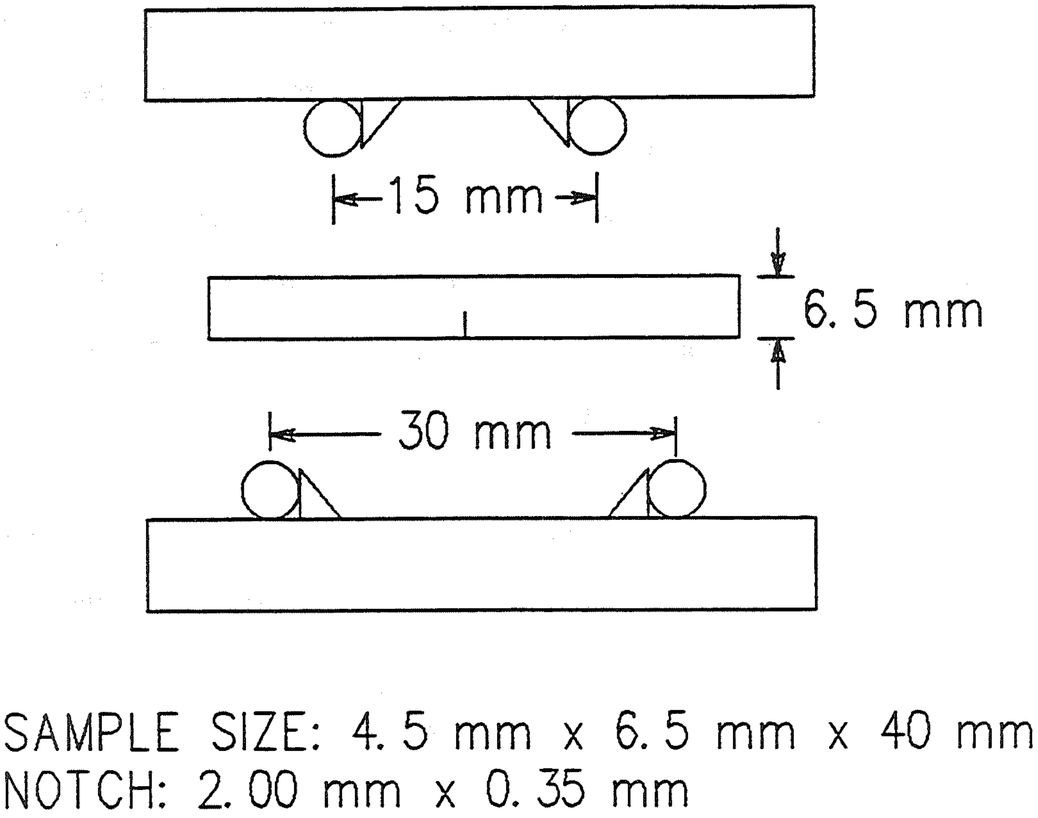

Figure 2.6: Geometry of the four-point flexure testing fixture and bend sample.

notch tip prior to testing. Bend tests were performed on a screw driven test frame using a displacement rate of 1.4×10^{-4} mm/s. Fracture toughness values were calculated using the K calibration for pure bending [2].

Metallography

Optical microscopy was used to characterize the general morphology and the degree of alignment for the eutectic microstructures after directional solidification. Longitudinal and transverse sections taken from each directionally solidified ingot were metallographically prepared and etched with a solution of $5\%HF$-$5\%HNO_3$-$90\%H_2O$ by volume.

Scanning electron microscopy (SEM) was also used to characterize the microstructure. Backscattered electron imaging was used to help identify the phases present in the arc-melted and directionally solidified ingots. Quantitative X-ray analysis on as-polished un-etched specimens was performed on a scanning electron microscope equipped with an energy dispersive spectrometer (EDS) detector. The "ZAF" method which attempts to correct the data for Z-atomic number, A-absorption, and F-fluorescence, effects was used to determine the phase compositions.

Secondary electron imaging was used to examine the topology of the fracture surfaces from broken bend specimens. However, backscattered electron imaging was often used in conjunction with secondary electron imaging to enhance phase contrast. The sides of the bend specimens were also studied under backscattered electron conditions near the notch to characterize the microcracking adjacent to the fracture surface. In all cases, the sides of the bend specimens were polished prior to testing.

Transmission electron microscopy (TEM) was used to further characterize the microstructure and to study the dislocation structure. Sample preparation and TEM analysis were performed by Mrs. X. F. Chen. Mrs. Chen is a visiting scholar from the Materials Science Department at Shanghai Jiao Tong University, China.

Thin slices were taken from broken bend specimens both parallel and perpendicular to the growth direction using a low speed diamond saw. The TEM specimens were taken as close to the fracture surface as possible. The thin slices of material were cut to 3 mm disks with a small pair of wire cutters. The corners of the slices were sniped off with the wire cutters until the desired shape was obtained. Thinning was performed by grinding and dimple grinding followed by twin-jet electropolishing in a solution of 5 vol.% perchloric acid, 95 vol.% acetic acid at 40 volts and 300 K.

REFERENCES

1. R.D. Reviere, B.F. Oliver, and D.D. Bruns, Mat. and Manuf. Proc., 4(10) (1989), 103-131.

2. W. F. Brown and J. E. Srwaley, in Plane Strain Crack Toughness Testing of High Strength Metallic Materials, ASTM Special Publication No. 410, ASTM, Philadelphia, PA (1966), 13-14.

PART 3: DIRECTIONAL SOLIDIFICATION AND MECHANICAL PROPERTIES OF NiAl-Cr AND NiAl-(Cr,Mo) EUTECTIC ALLOYS

CHAPTER 1

INTRODUCTION

Ductile phase toughening is one method for improving the fracture resistance and ductility of brittle materials. Increased toughness is provided by the interaction between the propagating crack and the ductile phase during the fracture process. The challenge is to increase the toughness and at the same time improve the high temperature strength of the intermetallic compound. For example, introducing Ni_3Al as a ductile phase in NiAl improves the ductility and toughness of the composite material over that of binary NiAl. Unfortunately, the effective melting point is depressed and the creep strength of the two phase alloys, depending on the specific composition, is about the same or less than that of binary NiAl [1].

On the other hand, a number of eutectic alloys consisting of NiAl and a refractory metal phase, such as NiAl-Cr, show both improved toughness and creep strength compared to single phase nickel aluminide alloys [2-5]. Directional solidification of these eutectic alloys results in in-situ composites where one or more phases are aligned parallel to the growth direction. In this case, the reinforcing refractory metal phase provides increases in both the toughness and creep strength of the composite material.

One advantage of producing composites by directional solidification of eutectic alloys is that the phases are thermodynamically stable even up to the melting point. A disadvantage is that alloy compositions are limited by the appropriate phase equilibria needed for eutectic growth. In many systems these compositions are often unknown. Fortunately, the NiAl-Cr system is well characterized in terms of processing-microstructure relationships, second phase morphology, and constitutional associations

[2,5-9]. The morphology of the NiAl-34Cr (atomic percent) eutectic consists of chromium rods within a NiAl matrix, both having a <100> growth orientation. The early work by Walter and Cline [6] has shown that small additions of impurity elements such as Mo, V, and W will change the growth direction to <111> for both phases while changing the microstructure to a lamellar morphology. For example, additions of molybdenum greater than 0.6 atomic percent will result in a lamellar chromium morphology with a {112} facet plane. Thus, the effects of second phase morphology and the orientation of the reinforcing phase may be studied without large changes in the volume fraction of reinforcement.

While the microstructures of these NiAl-Cr,X alloys have been characterized, mechanical property data are sparse. Furthermore, processing procedures and resulting microstructures generally vary with each investigator, making comparisons between research groups difficult. Therefore, the purpose of this study was to characterize the effects of containerless processing on the microstructure and subsequently the fracture toughness and elevated temperature strength of in-situ composites based on the NiAl-Cr and NiAl-(Cr,Mo) eutectic systems.

CHAPTER 2

EXPERIMENTAL PROCEDURES

Processing and materials

Directional solidification of near-eutectic alloys was used to produce in-situ composites with aligned microstructures for mechanical testing. Precursor ingots consisting of the NiAl-Cr eutectic and those alloyed with molybdenum were supplied by NASA Lewis research center. These ingots were produced by induction melting of elemental Ni, Al, Mo and a Ni-Cr master alloy. The 1-kg charge was then chill cast into a copper mold. After removal of the hot-top, precursor ingots were nominally 25 mm in diameter and 300 mm in length. These ingots were then directionally solidified in the containerless mode by the electromagnetically-levitated zone process in an ultra-pure helium atmosphere.

Typically, two processing passes are necessary to produce clean bulk metallurgical samples from the NiAl-Cr precursor ingots. During the first pass, oxide inclusions and other impurities migrate to the surface of the liquid zone and are deposited on the surface of the ingot as shown in Figure 3.1a. The surface of the ingot and associated impurities are then removed by machining and the ingot is processed a second time, Figure 3.1b. Automated control of the solidification process is performed by image analysis (real-time) of the molten zone. During the first pass, oxide particles (with a higher spectral emissivity) make the image analysis difficult and prevent tight dimensional control of the freezing solid-liquid interface. After a cleaning pass is made, automated control is possible and good dimensional control can be maintained as demonstrated by the NiAl-33.4Cr-0.6Mo ingot shown in Figure 3.2.

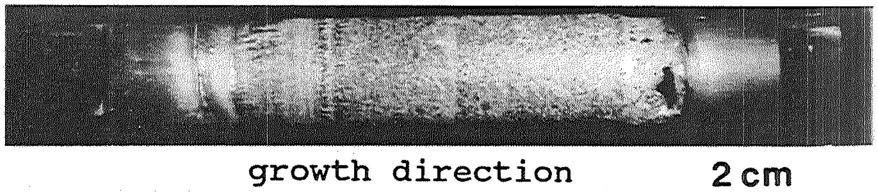

(a) NiAl-34Cr (first pass)

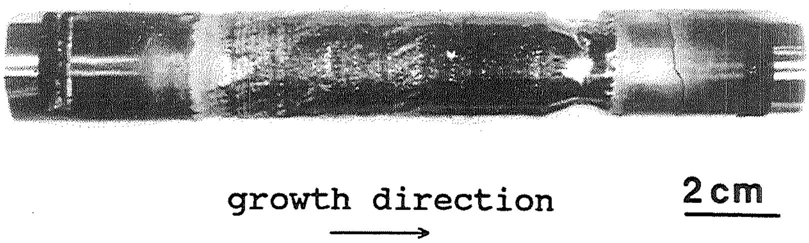

(b) NiAl-34Cr (second pass)

Figure 3.1: directionally solidified NiAl-34Cr eutectic showing difference between (a) the first processing pass and (b) the second processing pass.

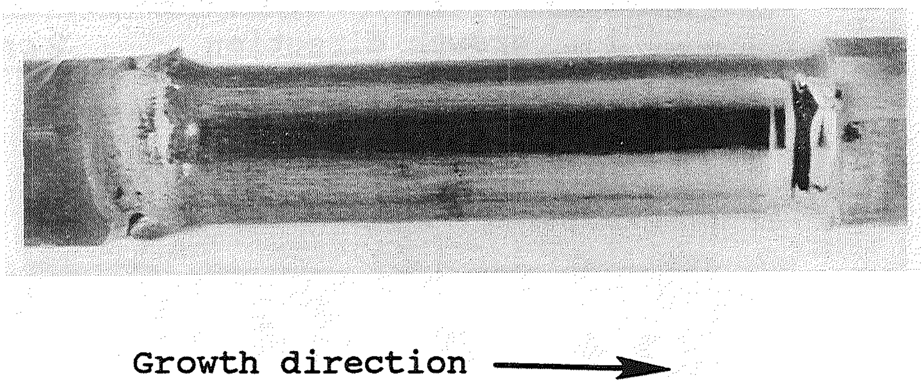

Figure 3.2: as-processed NiAl-33.4Cr-0.6Mo ingot (2 passes).

To compare the behavior of a directionally solidified eutectic to conventionally cast material, a NiAl-34Cr alloy was induction melted and cast into bars using an alumina shell mold. Fracture toughness samples were then machined from the conventionally cast ingot. In addition, the thermal gradient through the liquid/solid interface was increased during one directional solidification run in an attempt to produce a better aligned microstructure. To produce the steeper thermal gradient, a cooling jacket was mounted below the eddy current plate in the levitation zone refiner. The cooling jacket consisted of four water cooled rings (40 mm diameter) that supported a series of thin copper strips that made mechanical contact with the ingot. A NiAl-31Cr-3Mo ingot was directionally solidified using this cooling jacket. The compositions and processing conditions for all the materials used in this study are listed in Table 3.1.

Flexure testing

Most of the bend specimens were tested in the as-processed condition. However, heat treatments were performed on a number of specimens to investigate the effect of long term thermal exposure on properties. Selected bend specimens were encapsulated in silica tubing and back filled with argon to produce one atmosphere pressure at 1300 K. The samples were then heat treated at 1300 K for 1.8×10^6 s (500 hours) and air cooled. After heat treatment, the samples were notched and the room temperature fracture toughness was determined by performing four-point bend tests.

Table 3.1: Composition and processing conditions for NiAl-Cr alloys.

Nominal Composition (at.%)	Growth velocity (mm/hr)	Rotational velocity (rpm)	Number of passes
NiAl-34Cr	25	140	2
NiAl-34Cr-0.1Zr	13	100	3
NiAl-33.4Cr-0.6Mo	19	100	2
NiAl-33Cr-1.0Mo	13	40	2
NiAl-31Cr-3Mo	19	35	2*
NiAl-28Cr-6Mo	19	150	2
NiAl-34Cr	Induction melted and cast		

*cooling jacket used for increased thermal gradient

CHAPTER 3

MICROSTRUCTURES

Optical microscopy

Typical microstructures of the conventionally cast eutectic and the directionally solidified ingots are shown in Figures 3.3 and 3.4. The conventionally cast NiAl-34Cr alloy was characterized by a cellular structure with a coarse eutectic spacing near the cell boundaries, Figure 3.3a,b. A fibrous reinforcement morphology was observed for the directionally solidified NiAl-34Cr and NiAl-33.4Cr-0.6Mo eutectic alloys, Figures 3.3c,d and 3.3e,f, respectively. Microstructures from these alloys are characterized by an array of discontinuous chromium fibers that are aligned parallel with the growth direction and embedded within a single crystal NiAl matrix. Also evident in Figures 3.3c-f are growth faults that lie perpendicular to the growth direction.

Molybdenum additions greater than 0.6 atomic percent tended to produce a lamellar reinforcement morphology as seen in Figure 3.4. The microstructures of these NiAl-(Cr,Mo) alloys consisted of eutectic cells composed of chromium plates within a NiAl matrix. Good alignment of the reinforcing phase was produced in the NiAl-31Cr-3Mo alloy, Figure 3.4c,d. The NiAl-33Cr-1Mo and the NiAl-28Cr-6Mo alloys have similar microstructures but exhibited poor alignment of the refractory metal phase, Figure 3.4a,b and 3.6e,f, respectively. Hence, the good alignment of the NiAl-31Cr-3Mo microstructure was probably a result of the increased thermal gradient provided by the cooling jacket during processing.

A number of growth defects that consist of parallel bands running perpendicular to the growth direction exist in the directional solidified microstructures. The origin of these growth defects is presently unknown and does not appear to correlate with the

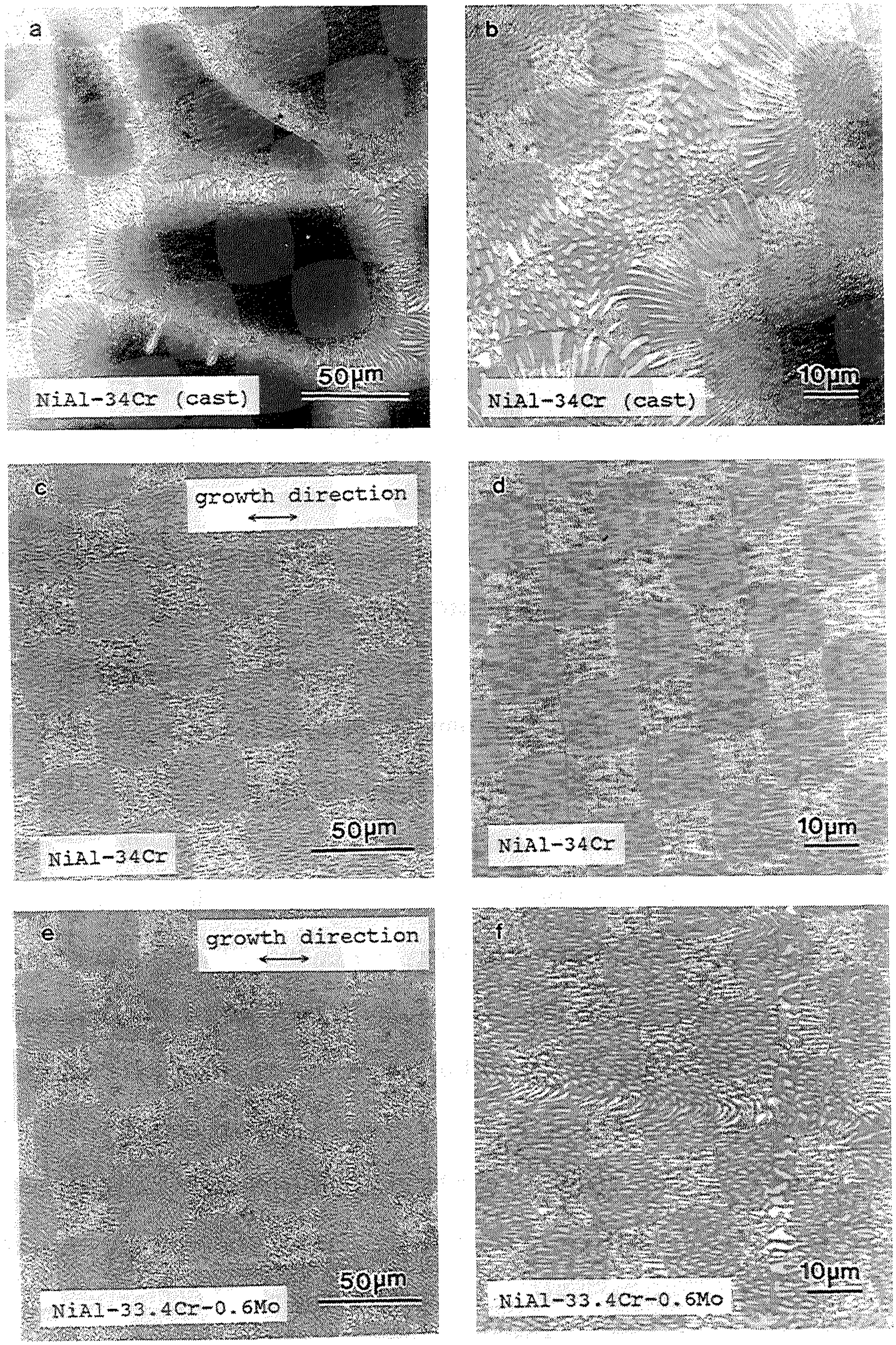

Figure 3.3: Light optical photomicrographs taken from longitudinal sections of (a,b) conventionally cast and (c-f) directionally solidified eutectics having a fibrous second phase morphology.

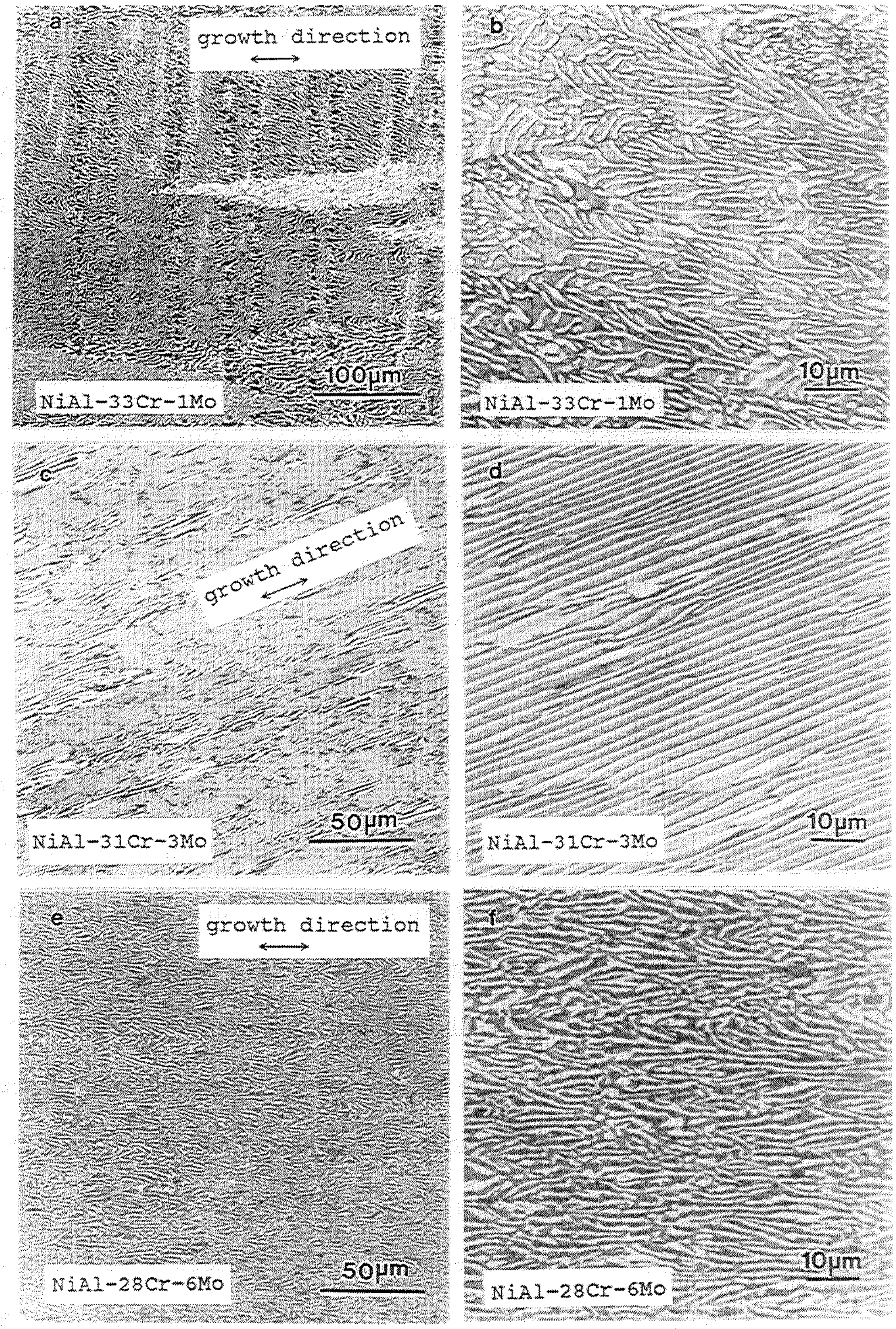

Figure 3.4: Light optical photomicrographs taken from longitudinal sections of directionally solidified NiAl-(Cr,Mo) eutectics having a lamellar second phase morphology.

different automated control schemes employed. These bands are characterized by a change in eutectic spacing or a complete interruption of the eutectic microstructure. However, some important differences between the banding morphology exist between fibrous and lamellar eutectic microstructures. When the NiAl-Cr alloys have a fibrous morphology, the banding defects can consist of uninterrupted layers of NiAl, Figure 3.3d. The unreinforced NiAl phase within the banded region is expected to have extremely deleterious effects on the mechanical properties of the eutectic during tensile loading. In contrast, the density of banding defects in the lamellar microstructures is much less, Figure 3.4. For the lamellar reinforced alloys, the banding defects are the result of different eutectic spacings but still contain the reinforcing metal phase, Figure 3.4b. Thus, the effects of banding in the lamellar microstructures are expected to be less severe than in the fibrous microstructures.

TEM results

Consistent with previous observations of the NiAl-Cr eutectic [6], TEM results confirmed a cube-on-cube crystallographic relationship between the NiAl matrix and the chromium phase as determined from selected area diffraction patterns. Also, a <100> growth direction was determined for the NiAl-34Cr eutectic while a <111> growth direction was found for the NiAl-28Cr-6Mo ingot with the lamellar morphology.

A semicoherent interface exists between the chromium-rich metal phase and the NiAl matrix due to the small lattice mismatch between the two phases [7,8]. The lattice mismatch is accommodated by a network of interface dislocations as shown in Figure 3.5. The dislocation spacing along the interface is much smaller for the NiAl-28Cr-6Mo alloy than the NiAl-34Cr eutectic. This is due to the greater mismatch in lattice parameter between NiAl and (Cr,Mo) than for NiAl and Cr [8].

In addition, arrays of fine precipitates were observed in the chromium-rich metal phase of the NiAl-28Cr-6Mo alloy, Figure 3.6. After heat treating at 1300 K, these

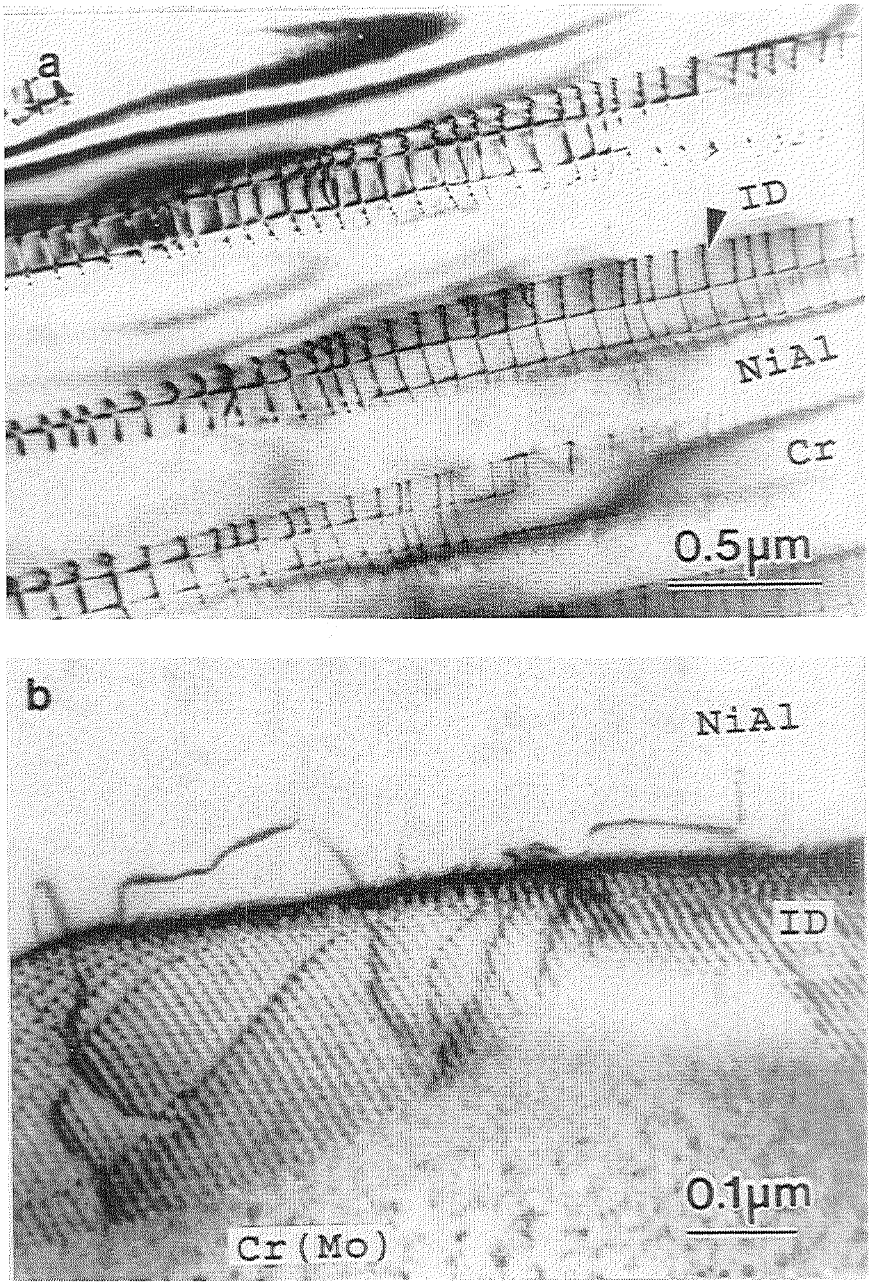

Figure 3.5: TEM photomicrograph of the interface dislocations (marked 'ID') between the NiAl matrix and the Cr-rich metal phase for (a) NiAl-34Cr eutectic and (b) NiAl-28Cr-6Mo eutectic.

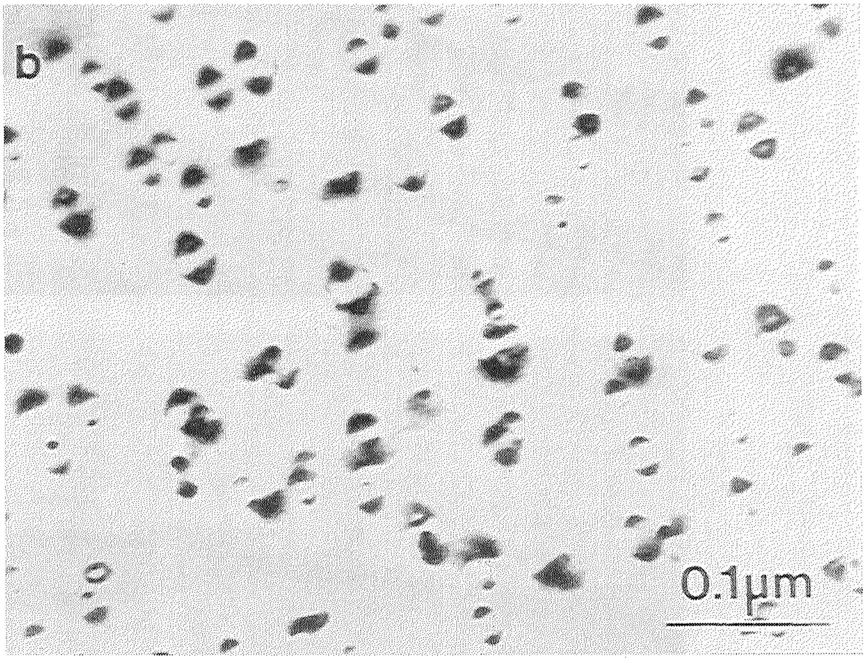

Figure 3.6: TEM photomicrograph showing fine NiAl precipitates within the Cr-rich lamella from an as-processed NiAl-28Cr-6Mo eutectic.

precipitates coarsened and were determined to be NiAl [10]. Precipitates of this nature were not observed in the chromium phase of the NiAl-34Cr eutectic before or after heat treatment.

CHAPTER 4

ELEVATED TEMPERATURE STRENGTH

Two directionally solidified ingots were selected for measurement of elevated temperature strength: the NiAl-34Cr-0.1Zr alloy with a fibrous eutectic morphology and the NiAl-28Cr-6Mo alloy consisting of a lamellar microstructure. Elevated temperature properties were determined in compression at 1300 K for both alloys. The NiAl-28Cr-6Mo alloys showed promising creep strength so additional testing was performed at 1200 and 1400 K. Zirconium was added to the NiAl-34Cr eutectic in an attempt to enhance the oxidation resistance of this alloy. Trace additions of zirconium are known to greatly improve the cyclic oxidation resistance of NiAl [11]. Compression tests were not performed on the well aligned NiAl-31Cr-3Mo alloy due to a lack of material, though this would have been an interesting alloy to test.

The flow stress and strain rate, $\dot{\varepsilon}$, data were fitted to a power law or a temperature compensated-power law equation:

$$\dot{\varepsilon} = A\sigma^n$$

or

$$\dot{\varepsilon} = B\sigma^n \exp(-Q/RT)$$

where A and B are constants, σ is the applied true stress (MPa), Q is the activation energy for deformation (kJ/mol), T is the absolute temperature, R is the gas constant (8.315×10^{-3} kJ/mol-K), and n is the stress exponent. The creep characteristics for the NiAl-34Cr and NiAl-28Cr-6Mo alloys are compared to that of single crystal NiAl in Table 3.2.

Table 3.2: Representative Creep Behavior of NiAl-Cr eutectic alloys compared to binary NiAl.

Alloy	Representative creep behavior
NiAl [001] (Ni-50Al)	1100-1300 K: $\dot{\varepsilon} = (1.48\text{x}10^{3})\sigma^{6.3}\exp(-439.3/RT)$ [12]
NiAl-Cr (Ni-33Al-34Cr-0.1Zr)	1300 K: $\dot{\varepsilon} = (3.52\text{x}10^{-23})\sigma^{7.69}$
NiAl-(Cr,Mo) (Ni-33Al-28Cr-6Mo)	1200-1400 K: $\dot{\varepsilon} = (1.99\text{x}10^{-2})\sigma^{6.37}\exp(-456.6/RT)$

In Figure 3.7 the 1300 K compressive creep behavior of the NiAl-Cr and NiAl-(Cr,Mo) alloys are compared to single crystal binary NiAl [12] and a nickel-based single crystal superalloy [13]. The creep characteristics, stress exponent and activation energy for deformation, are similar for the eutectic alloys and binary NiAl. However, the NiAl-Cr and NiAl-(Cr,Mo) alloys have significantly higher strengths compared to binary NiAl. Of the two eutectic alloys, the lamellar NiAl-(Cr,Mo) alloy displays a slightly greater strength over the strain rates tested. While the NiAl-Cr and NiAl-(Cr,Mo) alloys are much stronger then binary NiAl, they are still weaker than a single crystal nickel-based superalloy. The elevated temperature strength of the NiAl-28Cr-6Mo ingot over the temperature range of 1200 - 1400 K is shown in Figure 3.8. Except for the fastest strain rates at 1200K where power-law breakdown behavior has occurred, the NiAl-28Cr-6Mo eutectic exhibits a very consistent power law behavior over the strain rates and temperatures investigated.

Generally, the strength of a directionally solidified eutectic is controlled by the strength of the second phase. Since the refractory metal phase in the NiAl-28Cr-6Mo eutectic is precipitation hardened by fine NiAl precipitates, this material would be expected to have better strength than the simple ternary NiAl-Cr alloy. In addition, the greater strength of the NiAl-28Cr-6Mo may be due to strengthening by the dislocation networks at the semicoherent interface between the chromium-rich phase and NiAl. Cline et al. suggested that the strengthening should be proportional to the lattice mismatch and hence the dislocation density along the interface [8]. From their data, the mismatch for the NiAl-28Cr-6Mo eutectic should be greater than the NiAl-34Cr eutectic for all temperatures up to the melting point. However, the actual difference in strength between the two eutectic alloys, especially at lower strain rates, is not as large as the previous arguments may suggest. While the network of interface dislocations is immobile and constrained to lie along the interface, it may act as a source or sink for

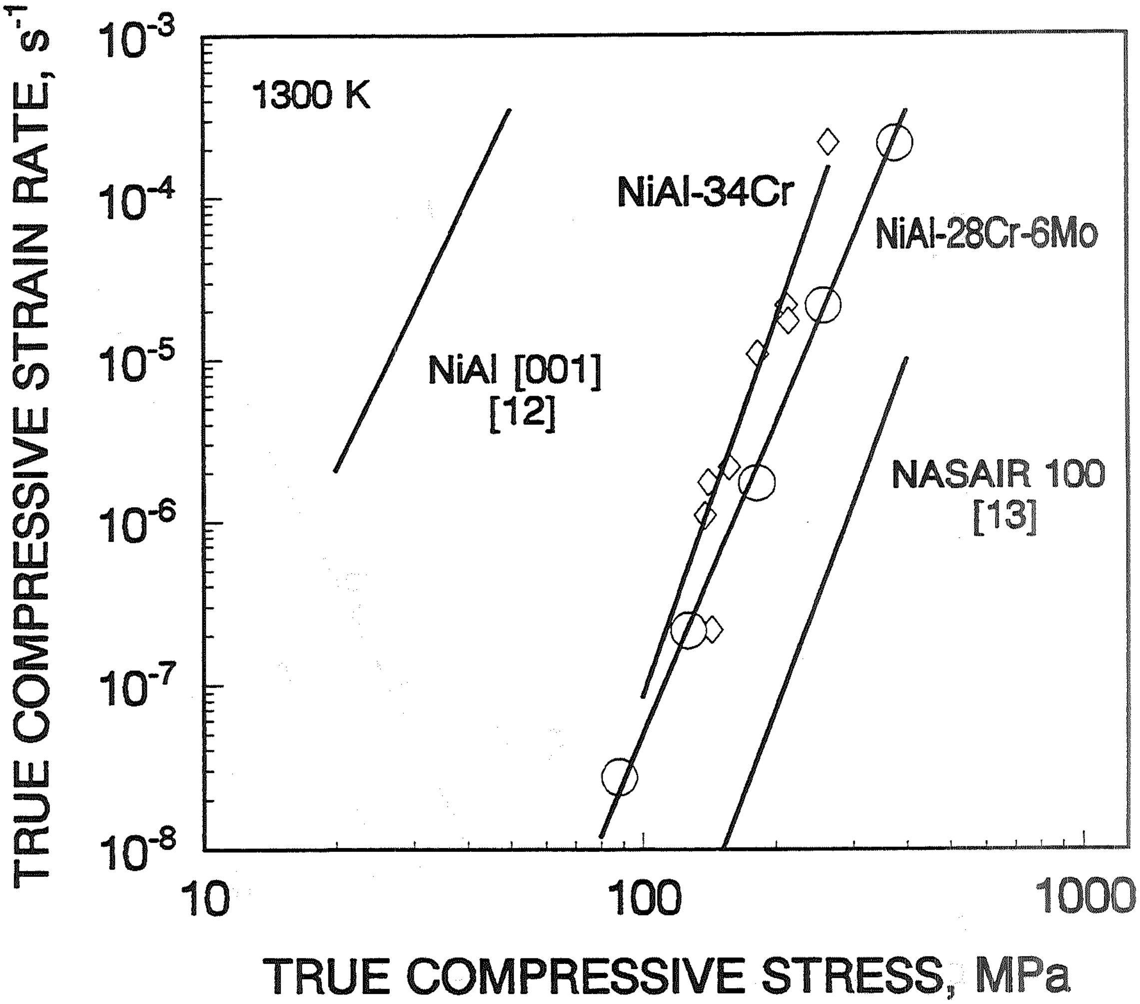

Figure 3.7: 1300 K compressive flow stress-strain rate behavior for the NiAl-34Cr and NiAl-28Cr-6Mo eutectics compared to NiAl and a single crystal superalloy.

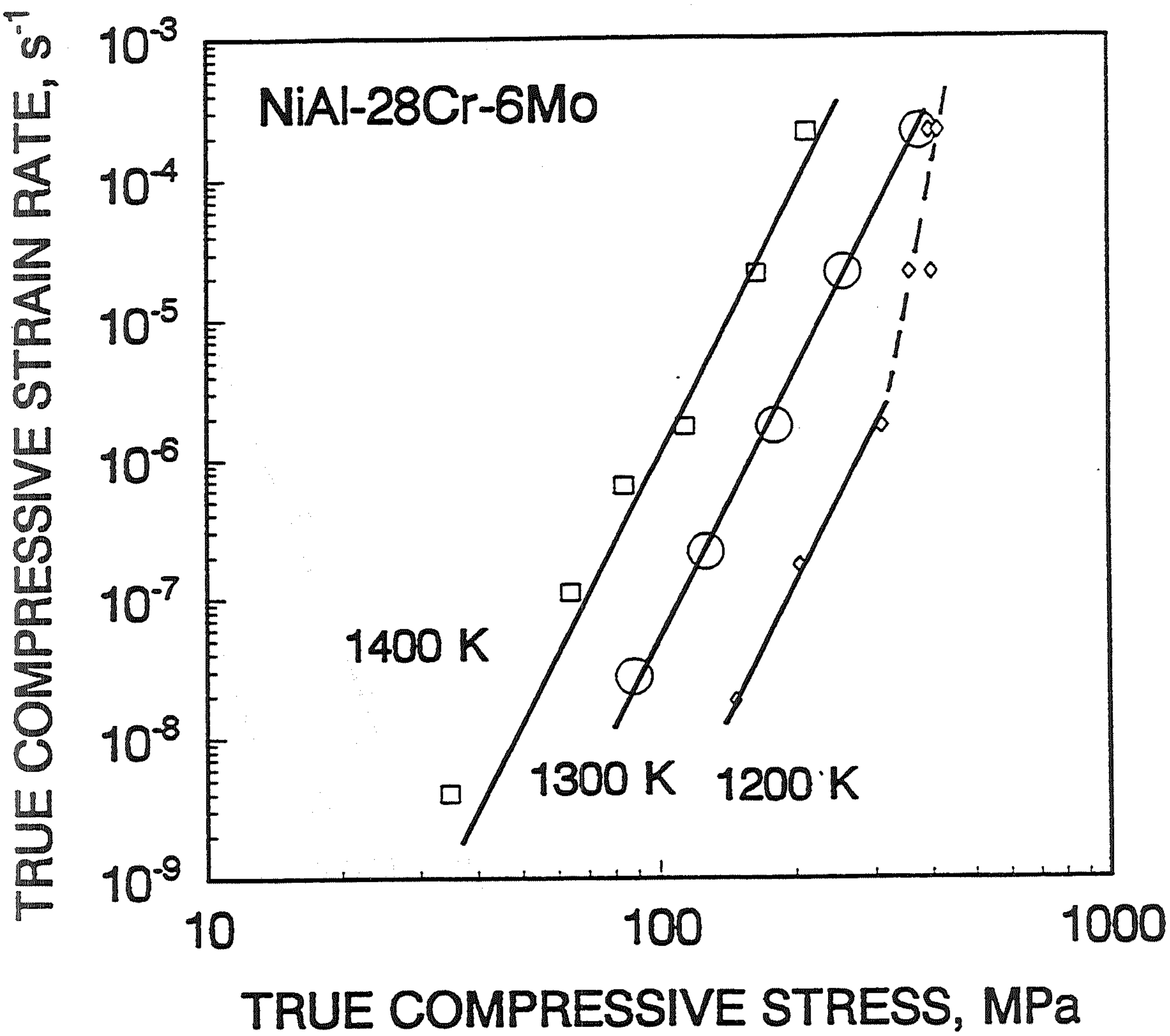

Figure 3.8: Compressive flow stress-strain rate behavior for the NiAl-28Cr-6Mo eutectic as a function of temperature.

vacancies and other dislocations. Therefore, a larger lattice mismatch may not provide strengthening at low deformation rates such as those in the creep regime.

CHAPTER 5

ROOM TEMPERATURE TOUGHNESS

The room temperature fracture toughness data for the eutectic alloys are listed in Table 3.3. The fracture toughness of the directionally solidified NiAl-Cr and the NiAl-(Cr,Mo) eutectics are much higher than that of binary NiAl. The directionally solidified eutectic alloys have a fracture toughness of around 20 - 22 MPa$\sqrt{}$m as opposed to 6 MPa$\sqrt{}$m [14] for polycrystalline NiAl or even 11 MPa$\sqrt{}$m [16] for zone-refined single crystal NiAl. However, the improvement in toughness is only maintained for aligned, directionally solidified microstructures since the conventionally cast NiAl-34Cr alloy had a fracture toughness of only 6 MPa$\sqrt{}$m.

For the directionally solidified materials, the addition of molybdenum to the NiAl-Cr eutectic, while not having a significant effect on the measured fracture toughness, did have other advantages. For a number of the NiAl-34Cr bend specimens, fracture did not initiate at the notch, invalidating the test. Instead fracture occurred at the banded growth defects described previously. In contrast, fracture initiated at the notch for all the NiAl-(Cr,Mo) alloys since any growth faults in these alloys were not composed of eutectic free zones. Moreover, two of the NiAl-31Cr-3Mo specimens did not break into two separate halves after fracture initiation but instead exhibited a strong crack arrest behavior. These specimens could be handled quite easily without further propagation of the crack. The crack arrest behavior displayed by the NiAl-31Cr-3Mo bend specimens is due to the well-aligned microstructure. The NiAl-28Cr-6Mo specimens, having a cellular microstructure, did not display this behavior.

Heat treating the bend specimens at 1300 K did not change the fracture toughness significantly (Table 3.4). The toughness of both the NiAl-Cr and NiAl-(Cr,Mo) alloys

Table 3.3: Room temperature fracture toughness of directionally solidified NiAl-(Cr,Mo) and induction melted and conventionally cast NiAl-34Cr eutectic alloys.

Alloy	K_1 (MPa√m)	Alloy	K_1 (MPa√m)
NiAl-34Cr-0.1Zr	19.2	NiAl-31.4Cr-0.6Mo	22.2
		NiAl-31.4Cr-0.6Mo	16.7
NiAl-34Cr	20.4	NiAl-31.4Cr-0.6Mo	19.6
NiAl-34Cr	18.5		
NiAl-34Cr	21.5	NiAl-31Cr-3Mo	21.1
NiAl-34Cr	20.7	NiAl-31Cr-3Mo	22.2
NiAl-34Cr	20.8	NiAl-31Cr-3Mo	22.0
NiAl-34Cr (cast)	6.0	NiAl-28Cr-6Mo	22.6
NiAl-34Cr (cast)	5.8	NiAl-28Cr-6Mo	24.1
NiAl-34Cr (cast)	5.6	NiAl-28Cr-6Mo	17.5
NiAl-34Cr (cast)	5.6	NiAl-28Cr-6Mo	22.2

Table 3.4: Room temperature fracture toughness of directionally solidified alloys heat treated at 1300 K for 1.8x106 s (500 hours) and air cooled.

Alloy	K1 (MPa√m)
NiAl-34Cr	21.8
NiAl-34Cr	20.4
NiAl-34Cr	21.7
NiAl-31Cr-3Mo	19.8
NiAl-31Cr-3Mo	21.3
NiAl-28Cr-6Mo	19.6

after heat treatment were similar to those in the as-processed condition. Consistent with the fracture toughness values, no major changes in eutectic morphology were observed after heat treatment. These results indicate that the eutectic morphologies are stable under isothermal conditions.

CHAPTER 6

ROOM TEMPERATURE FRACTURE CHARACTERISTICS

In general, ductile phase toughening is an effective method for increasing the toughness of NiAl [1]. Heredia et al. recently reviewed the different toughening mechanisms they observed in the NiAl-refractory metal eutectics [15]. The improved fracture toughness and the fracture characteristics of NiAl-based eutectics originate from both initiation toughness and subsequent crack growth toughness processes. These toughening mechanisms include crack trapping, crack renucleation, and crack bridging.

The initiation toughness depends upon the ductile phase morphology. For a fibrous microstructure, such as the NiAl-Cr eutectic, a crack trapping mechanism controls the initiation toughness. The crack front in this process is trapped (or hindered) by tough second phase particles whose fracture toughness value exceeds the local stress intensity [17,18]. For a lamellar microstructure, such as the NiAl-(Cr,Mo) eutectic, the crack front cannot surround the tough second phase particles and must renucleate in the adjacent material [15,19,20]. With both toughening mechanisms, the crack may also be blunted or deflected by the ductile phase.

Once a crack has initiated, unbroken second phase fibers or lamellae may lag behind the crack front. The plastic work expended upon stretching these second phase particles during crack propagation provides a resistance to crack growth and is referred to as crack bridging [21,22]. The amount of toughening provided by crack bridging depends upon the volume fraction and flow characteristics of the second phase and the amount of debonding present at the ductile phase/matrix interface. Partial debonding at the interface enhances the toughening effect of the ductile phase [21].

Examination of microcracking near the notched region of broken bend specimens may offer some insight to the operative fracture mechanisms. The fracture behavior of the NiAl-34Cr and the NiAl-31Cr-3Mo bend specimens is shown in Figure 3.9. These photomicrographs were taken along the side of the bend specimen perpendicular to the fracture surface. The volume fraction of the chromium-rich metal phase at 34 percent is essentially the same in both microstructures. However, the morphology and growth orientation are different. For the NiAl-34Cr microstructure, the angle between the crack and the <100> growth direction is nominally 45 degrees. This observation is consistent with a {110} type cleavage plane for NiAl [23].

Crack bridging by the refractory metal phase is evident in both microstructures. In addition, crack renucleation and crack deflection mechanisms are visible in the lamellar microstructure, Figure 3.9b. Additional examples of crack bridging for the two different eutectic morphologies are shown in Figure 3.10. Partial debonding along the phase boundary and necking of the metal phase are visible. In all the specimens tested, a crack bridging mechanism was observed. Therefore, the amount of toughening provided by a crack bridging mechanism was estimated to determine the percentage of the toughness increase due to this particular mechanism.

Crack bridging

The increase in fracture energy, ΔG, due to a crack bridging mechanism has been described by Mataga [21] and Flinn et al. [22] and can be written as:

$$\Delta G = G - G_m = f \int_0^{u^*} \sigma du - fG_m$$

where G_m is the fracture energy for the matrix, f is the volume fraction of the ductile phase, and u^* is the crack opening displacement needed to rupture the ductile phase.

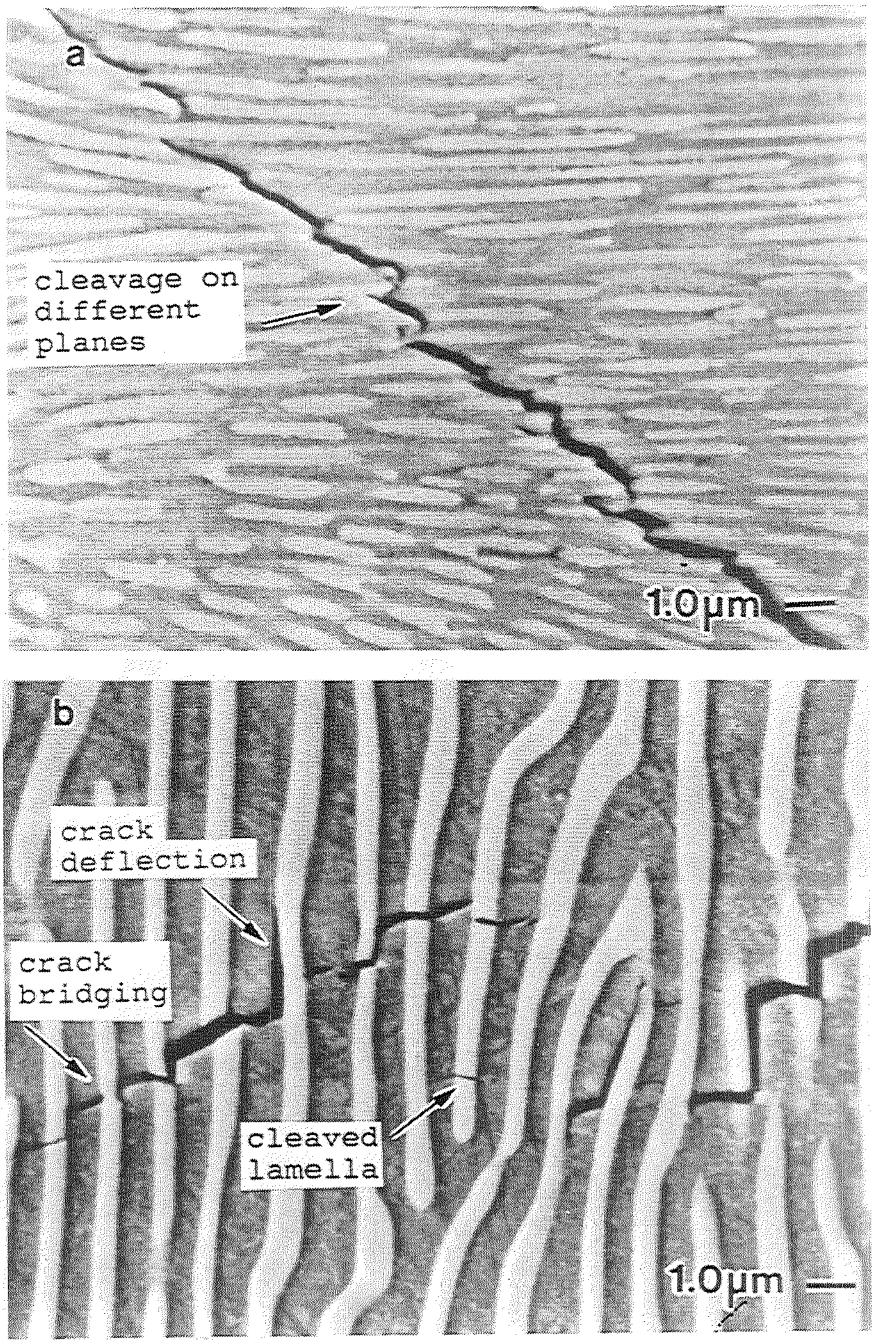

Figure 3.9: SEM backscattered electron photomicrographs of microcracking in (a) NiAl-34Cr bend specimen and (b) NiAl-31Cr-3Mo bend specimen.

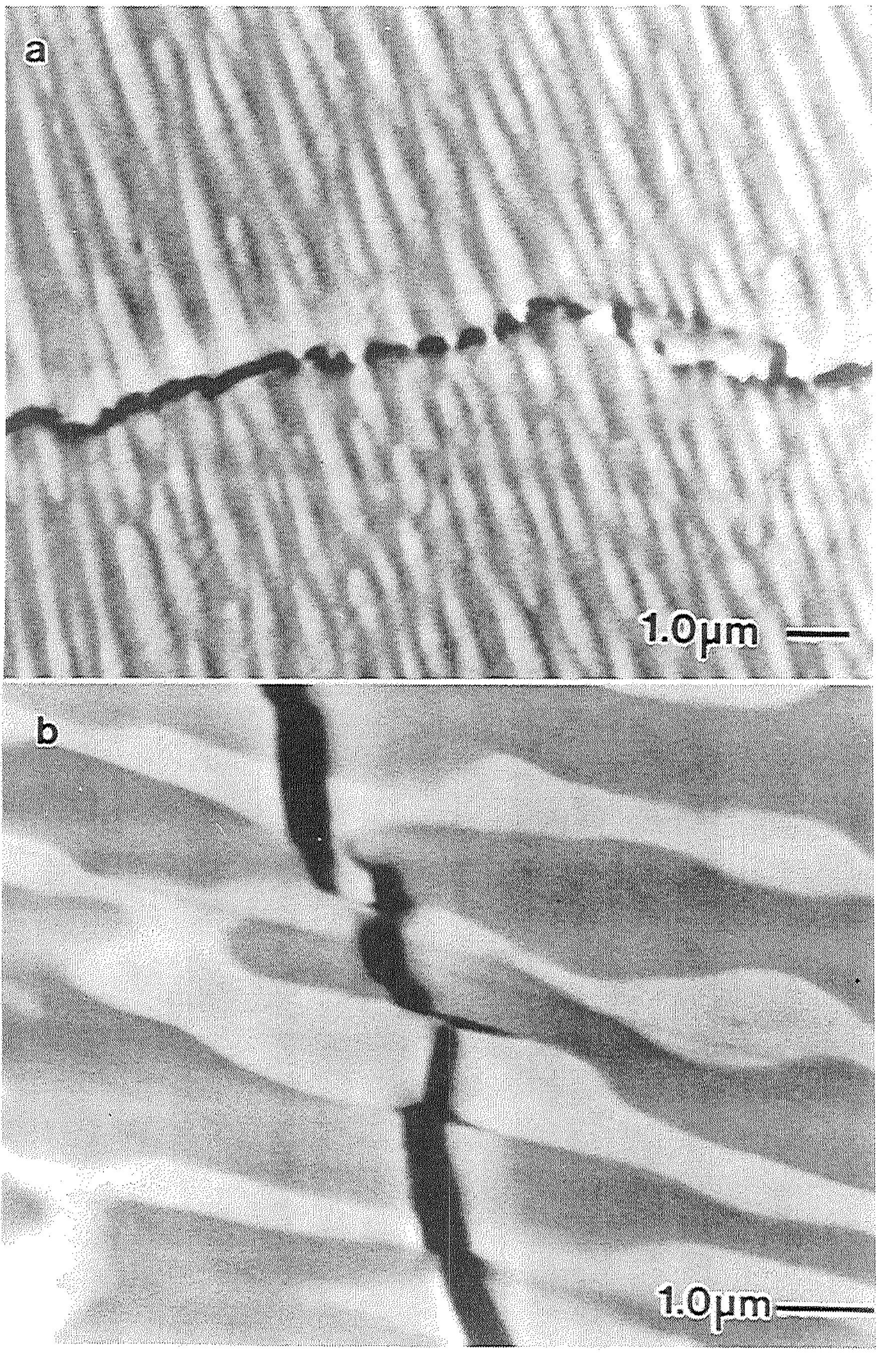

Figure 3.10: SEM backscattered electron photomicrographs of crack bridging in (a) NiAl-34Cr eutectic and (b) NiAl-28Cr-6Mo eutectic.

Rearranging,

$$G = (1\text{-}f)\, G_m + f \int_0^{u^*} \sigma du$$

or

$$G = G_m(1\text{-}f) + f\sigma_o a_o \chi$$

where σ_o is the yield stress of the ductile phase, a_o is the radius of the ductile phase, and χ is the work of rupture parameter [22] which depends on the flow characteristics of the ductile phase and the amount of plastic constraint present. The amount of plastic constraint is controlled by the interfacial strength and the amount of decohesion between the ductile phase and the matrix. The work of rupture parameter, χ, is approximately the ratio between the work needed to fracture the constrained ductile phase to that of the unconstrained case. Experimental studies of lead wires or sheets constrained within a glass matrix have shown that χ can vary from 1 (unconstrained) to about 6 when partial decohesion is present [24,25]. Converting the energy for fracture to the stress intensity factor in plane strain by $K^2(1\text{-}\nu^2)=GE$ where ν is Poisson's ratio and E is the elastic modulus gives [26]:

$$K_{Ic} = \sqrt{\frac{K_m^{\,2}(1\text{-}\nu_m^{\,2})(1\text{-}f)E_c}{E_m(1\text{-}\nu_c^{\,2})} + \frac{fE_c\sigma_o a_o \chi}{(1\text{-}\nu_c^{\,2})}} \qquad \text{(equation 1).}$$

(subscripts: m=matrix, c=composite)

Ravichandran used such a model to predict the fracture toughness of a wide range of ductile phase composites with good results with an assumption that χ=4 [26].

To apply this model to the NiAl-Cr and NiAl-(Cr,Mo) eutectics, the elastic and plastic properties of the composite and constituent phases must be estimated. The elastic properties of NiAl and chromium for <100> and <111> oriented crystals [27,28] are listed in Table 3.5. The rule of mixtures was used to estimate the elastic properties of

Table 3.5: Elastic modulus for <100> and <111> oriented crystals of NiAl and Cr.

Material	orientation	E (GPa)	Poisson's ratio
NiAl	[100]	95.9	0.404
Cr	[100]	325	0.159
NiAl	[111]	277	0.222
Cr	[111]	248	0.239
rule of mixtures			
NiAl-34Cr	[100]	174	0.321
NiAl-Cr,Mo	[111]	263	0.228

Table 3.6: Vickers microhardness and estimated or measured strength data for NiAl,Cr and various NiAl-Cr alloys.

Material	Vickers microharndess (kg/mm^2)	Yield stress (MPa)
Arc-melted NiAl-Cr alloys heat treated at 1100 K, for 9000 s (2.5 hours) and furnace cooled.		
NiAl (high purity)	276	---
NiAl,Cr (NiAl-10Cr)	431	560 [29]
Eutectic (NiAl-34Cr)	481	700
Cr,NiAl (NiAl-90Cr)	589	990*
Cr (high purity)	189	---
Compressive yield strength values for [100] oriented crystals of a directionally solidified NiAl-34Cr eutectic and a NiAl single crystal.		
NiAl [100]	---	1400 [4]
NiAl-34Cr [100]	370	1240 [4]
Cr-rich solid solution	---	930*

---

*rule of mixtures

the eutectic alloys. The yield strength of the eutectic and the constituent phases was estimated from compressive yield strength data [4] and from microhardness measurements. These data are listed in Table 3.6. Due to the fineness of the eutectic microstructure, the microhardness values for the constituent phases were determined from arc-melted ingots.

Microhardness data were generated with a standardized Vickers indenter using 1 kg load and a dwell time of 15 seconds. To ensure similar thermal histories, all arc-melted ingots were heat treated at 1100 K for 9000 s (2.5 hours) and furnace cooled. The resulting microhardness data had a standard deviation less than ±15 HV. The ratio of the hardness data from the directionally solidified and arc-melted NiAl-34Cr eutectic ingots was used to scale the hardness values listed in Table 3.6. The scaled hardness values were then used to estimate the yield strength of the NiAl,Cr solid solution based on the relationship between hardness and yield strength determined by Cotton et al. for NiAl alloys containing up to 5 at.% chromium [29]. Since the microhardness data for the eutectic alloys follows the rule of mixtures behavior, the yield strength for the chromium-rich solid solution was also estimated by the rule of mixtures. Data from both the arc-melted and the directionally solidified ingots gave similar values for the yield strength of the chromium-rich solid solution, Table 3.6.

Substituting the data from Tables 3.5 and 3.6 into the crack bridging model along with the following data, a_o = 0.3 m from SEM photomicrographs, K_{Ic} = 11 MPa$\sqrt{}$m for NiAl having <100> crystal orientation [16], K_{Ic} = 9 MPa$\sqrt{}$m for NiAl having a non-<100> crystal orientation [30], and $\chi=4$ (first approximation) gives the follow results:

For the NiAl-Cr eutectic with a <100> growth direction,

$$K_{Ic} = \sqrt{1.12K_m^2 + 19.6\chi} \quad \text{or} \quad K_{Ic} = 15 \qquad \text{(equation 2)}$$

for the NiAl-(Cr,Mo) eutectic with a <111> growth direction;

$$K_{Ic} = \sqrt{0.628K_m^2 + 28.1\chi} \quad \text{or} \quad K_{Ic} = 13 \qquad \text{(equation 3).}$$

These values underestimate the measured values (Table 3.3) indicating that crack bridging is not the only toughening mechanism in these microstructures.

Crack initiation toughness

Given the increase in fracture toughness due to crack bridging alone, it is evident that other toughening mechanisms must also be responsible for the measured toughness of the NiAl-Cr and NiAl-(Cr,Mo) alloys. The initiation toughness of these alloys can be described by a crack trapping mechanism for fibrous microstructures or by a crack renucleation mechanism for lamellar microstructures. Evidence for each of these mechanisms can be found in the fracture surfaces of these alloys as demonstrated in Figure 3.11. A crack trapping mechanism is clearly visible for the fibrous NiAl-34Cr eutectic, Figure 3.11a. Consistent with a crack renucleation event, the lamellar morphology of the metal phase is visible on the fracture surface of the NiAl-31Cr-3Mo alloy, Figure 3.11b. Plastic stretching of the chromium-rich metal phase is also evident for the lamellar NiAl-31Cr-3Mo eutectic.

Heredia et al. [15] measured the initiation toughness of a lamellar NiAl-(Cr,Mo) eutectic at 17 MPa√m. Using this value instead of 9 MPa√m for the initiation toughness, a value of $\chi=11$ in equation (3) is still needed for the work of rupture parameter to account for the measured toughness of the NiAl-(Cr,Mo) specimens. Since extensive plastic deformation of the chromium-rich metal phase is not observed, such a

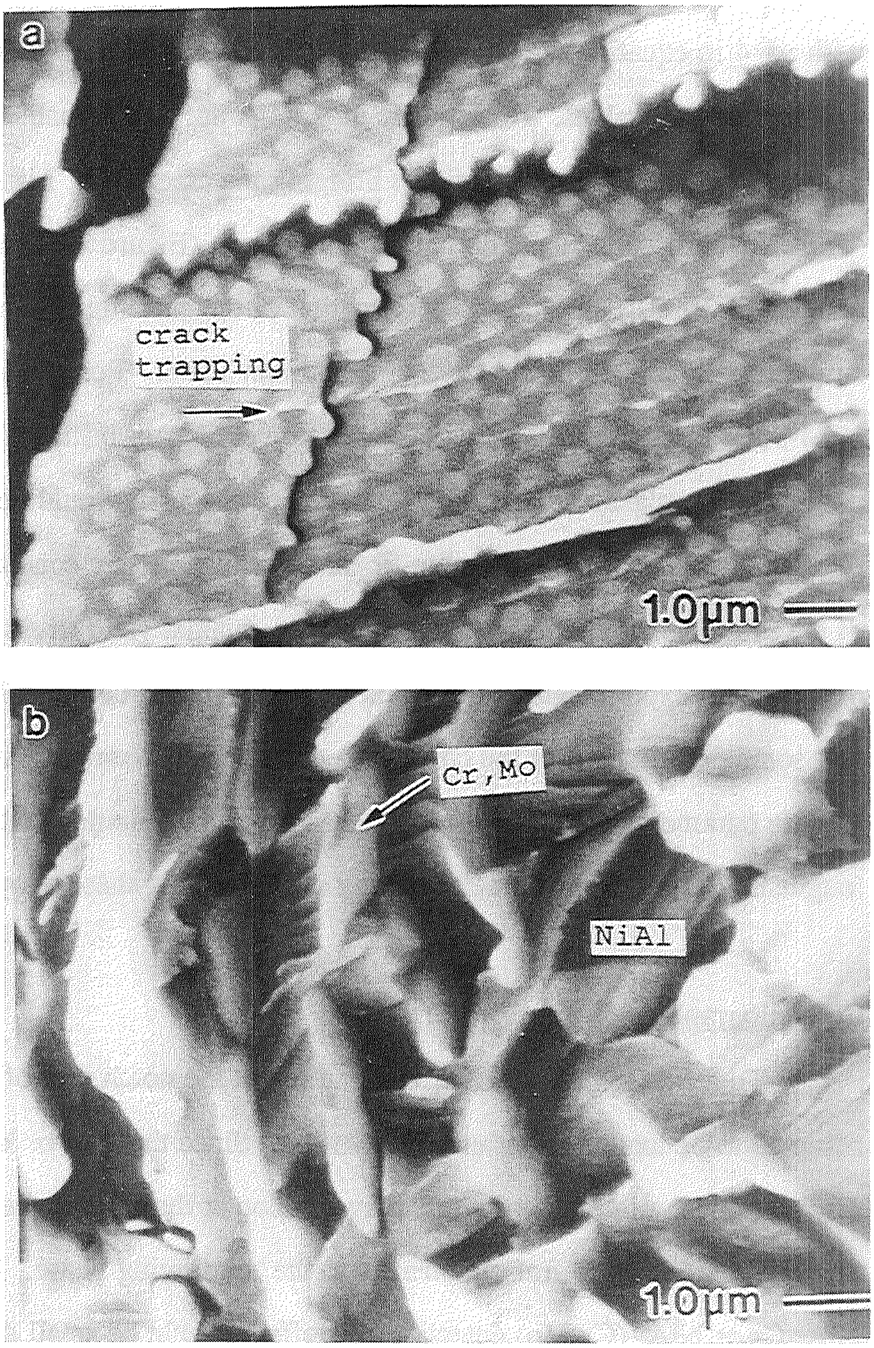

Figure 3.11: SEM photomicrograph showing the fracture surface from (a) NiAl-34Cr eutectic and (b) NiAl-31Cr-3Mo eutectic.

high value for the work of rupture parameter is unreasonable. Hence, still other toughening mechanisms must be operative, at least in the NiAl-(Cr,Mo) alloys.

For the fibrous NiAl-Cr eutectic, using an initiation toughness of 17 MPa$\sqrt{}$m with $\chi=4$ in equation (2) gives a fracture toughness of 20 MPa$\sqrt{}$m which is much closer to the measured values. An estimate of $\chi=4$ is not unreasonable based on the plastic deformation of the chromium fibers bridging the crack path, Figures 3.9 and 3.10. While the chromium fibers do not neck to a point (Figure 3.11) as in the NiAl-Mo eutectic [4,15,30], any plastic deformation of the chromium-rich phase is somewhat surprising given the brittle nature of chromium alloys. For example, the arc-melted NiAl-90Cr ingot (Table 3.6) was found to be extremely brittle. However, even with practically no plastic deformation, a value nearing $\chi=2$ would be expected due to the plastic constraint of the chromium fibers. For plane strain conditions, the average value of the effective yield stress is larger than the uniaxial yield stress by a calculated factor of 1.68 with experimentally determined values ranging between 1.5 and 2 [31]. The fact that some deformation of the chromium-rich phase is observed, suggests that the work of rupture parameter should be greater than $\chi=2$, which demonstrates the potent toughening effect from a crack bridging mechanism in these alloys.

Crystallographic effects

To a first approximation, the material at the notch root of a bend specimen is assumed to be loaded under uniaxial tension. Since the rods or lamellae are discontinuous, a large shear stress may develop at the ends of the fibers or lamellae as the load is transferred from the matrix to the reinforcing phase. However, for the NiAl-Cr or NiAl-(Cr,Mo) eutectics, this effect should be small due to the small difference between elastic moduli of NiAl and chromium (Table 3.5). Consistent with this observation, the fracture path does not follow the ends of the refractory metal rods or lamellae.

Small changes in orientation between eutectic grains or cells with the loading axis may effect the fracture behavior. Figures 3.12 and 3.13 show how the resolved normal stress on {110} type cleavage planes may change in NiAl as the load axis is rotated away from the <100> or <111> growth direction. For a loading orientation along the growth direction, there is a high resolved normal stress on more than one cleavage plane, Figures 3.12a and 3.13a. The angle between these cleavage planes can be 90° or 60° apart. However, as the loading axis is rotated from the growth direction, only one cleavage plane is favored. If a shear stress is added to the stress tensor, again only one cleavage plane is favored but it may be different than the one for the uniaxial case.

Changing the preferred cleavage plane may generate crack branching or crack deflection. For example in Figure 3.12a, a $(\bar{1}10)$ type cleavage plane is preferred for a loading axis rotated -5° or so from the [100] growth direction. If the propagating crack is stopped by the metal phase, then the fractured NiAl phase cannot support a tensile stress and a shear stress must develop along the NiAl/Cr phase boundary. For such a stress state, a (110) type cleavage plane would be favored, Figures 3.12b,c. The alternating change of preferred cleavage planes may increase the energy needed for fracture. A torturous crack path that may have developed from such a mechanism is shown in Figure 3.9a.

The induced shear stress along the NiAl/Cr phase boundary may also cause the crack to deflect. Consider the lamellar morphology of the NiAl-(Cr,Mo) eutectic shown in Figure 3.9b. Again, if the propagating crack is stopped by the metal phase, a shear stress would develop along the NiAl/(Cr,Mo) phase boundary. Depending on the loading orientation, a normal stress may also develop at the NiAl/(Cr,Mo) phase boundary. Consider a $(11\bar{2})$ facet plane for the chromium-rich phase. A loading axis rotated -5° or so from the [111] growth direction would result in a change of the preferred cleavage plane from (110) to (011), as the stress state changes from tension to shear, Figures 3.13a-c. In addition, there is a compressive stress acting on the $(11\bar{2})$

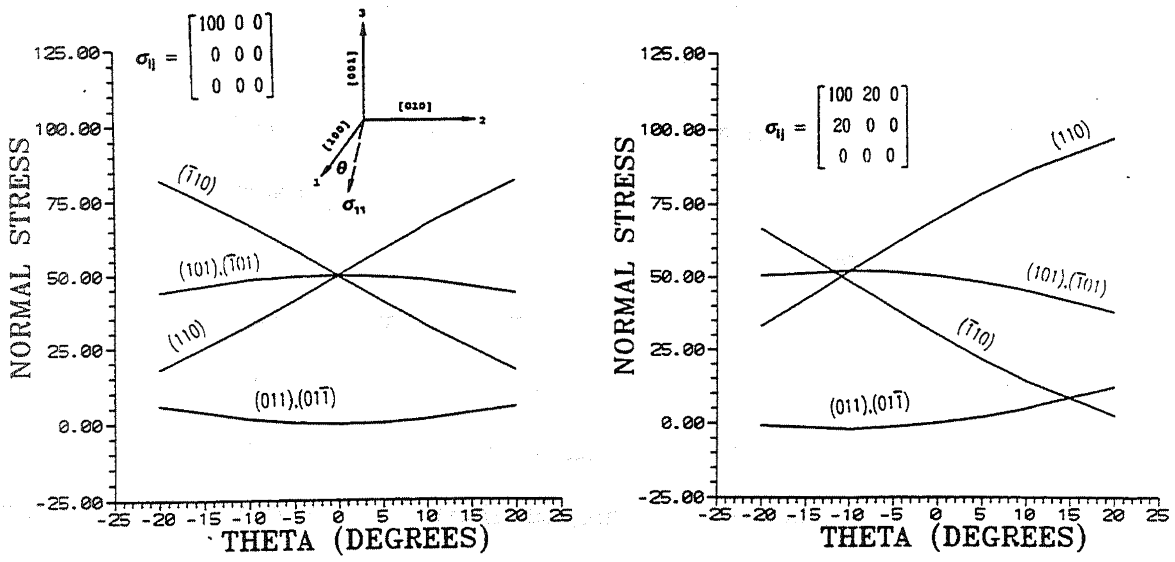

(a) tensile loading

(b) tensile and shear loading

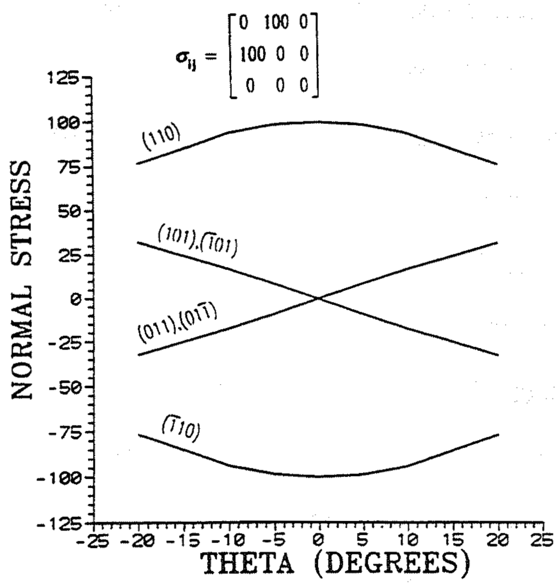

(c) shear loading

Figure 3.12: Resolved normal stress on {110} type cleavage planes for (a) tensile, (b) tensile and shear, and (c) shear loading orientation relative to the [100] direction.

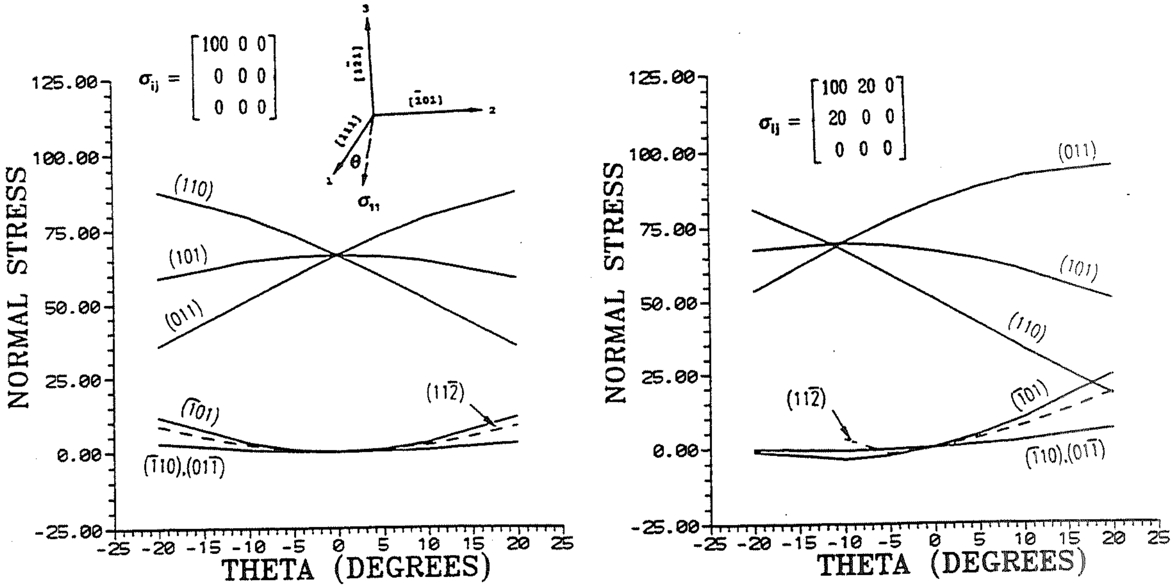

(a) tensile loading

(b) tensile and shear loading

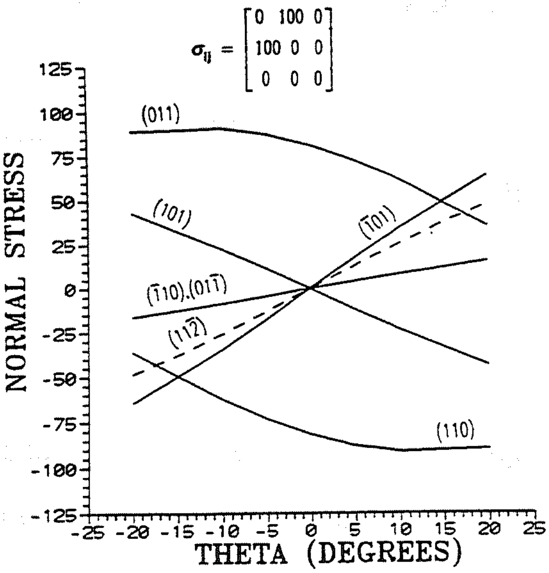

(c) shear loading

Figure 3.13: Resolved normal stress on a (11$\bar{2}$) plane and on {110} type cleavage planes for (a) tensile, (b) tensile and shear, and (c) shear loading conditions relative to the [111] direction.

facet plane, see Figure 3.13c. However, for a loading axis rotated +5° or so from the growth direction, a tensile stress develops on the $(11\bar{2})$ facet plane. Also, there is no change in the preferred cleavage plane. Such conditions are favorable for crack deflection along the NiAl/(Cr,Mo) phase boundary as shown in Figure 3.9b. Consequently, the combination of crack deflection and crack renucleation due to orientation effects contribute to the high toughness of the NiAl-(Cr,Mo) alloys.

Linkage of microcracks

A toughening mechanism similar to that of shear ligament toughening described by Chan [32] for two phase TiAl alloys is also observed in the NiAl-Cr and NiAl-(Cr,Mo) alloys. Crack deflection and renucleation caused by the tough second phase reinforcement may result in a series of microcracks. The material between the microcracks should fracture by shear as the microcracks connect with the main crack. Linkage of these microcracks with the main crack may then provide further resistance to crack growth.

The fracture surface of a NiAl-34Cr bend specimen is shown in Figure 3.14. Characteristic to this type of fracture mechanism, 'strips' of material, containing both the chromium rods and the NiAl matrix, have separated from the fracture surface due to the linkage of microcracks. Often these 'strips' have peeled away from the fracture surface and appear to be plastically deformed. As evident in Figure 3.14a, a shear strain has displaced the 'strips' of material normal to the fracture surface. Formation of these 'strips' can be visualized in Figure 3.14b, which shows the linkage of a series of microcracks in the NiAl-34Cr bend specimen. A similar mechanism is observed in the lamellar NiAl-(Cr,Mo) alloys as shown in Figure 3.15. While the amount of toughening due to this mechanism is not known, it was widely observed on the fracture surfaces of the directionally solidified bend specimens.

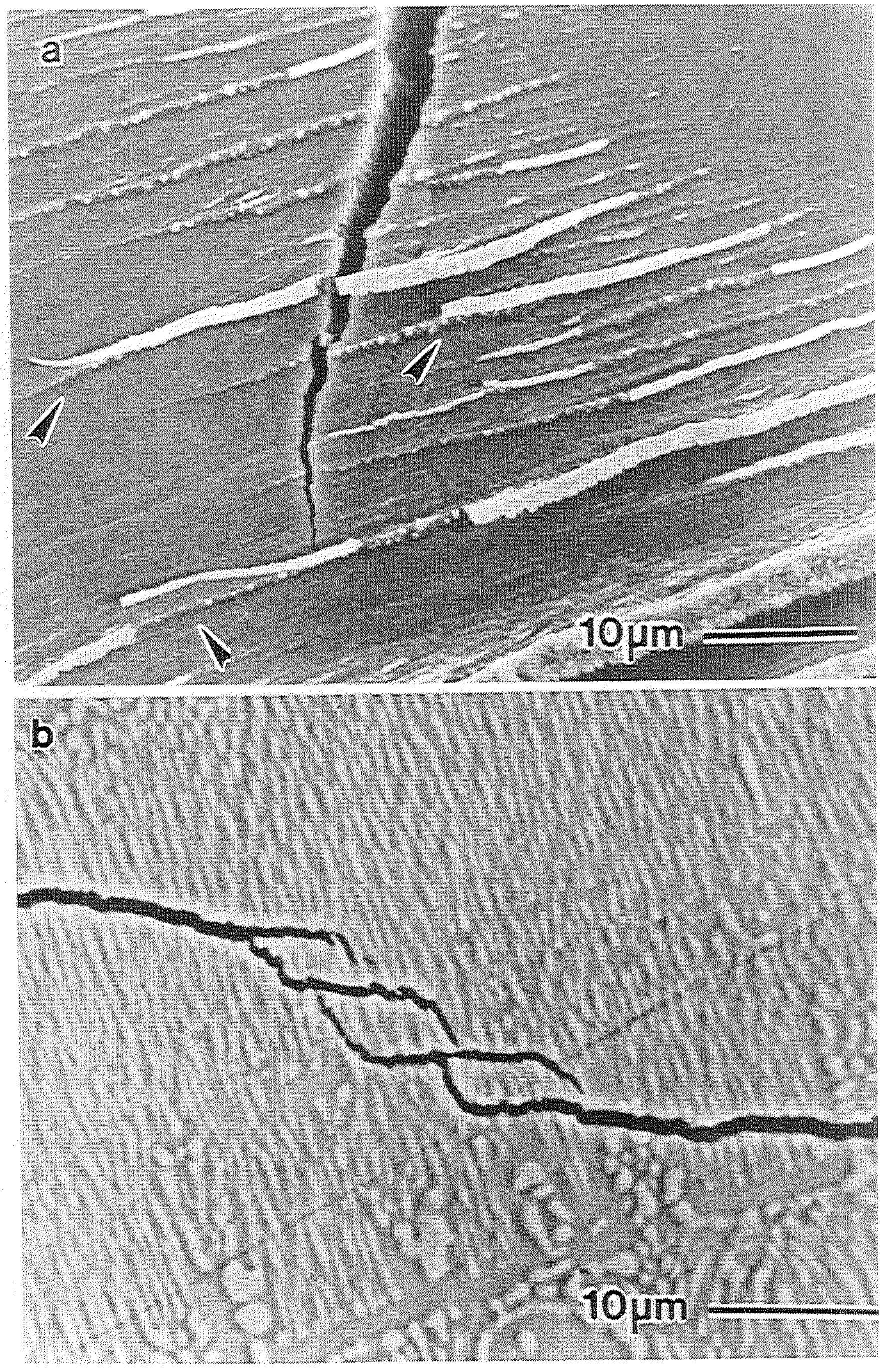

Figure 3.14: Linkage of microcracks by shear deformation in a NiAl-34Cr eutectic showing (a) "strips" of material displaced from fracture surface by a shear strain (marked with arrows) and (b) microcracking along the side of the bend specimen.

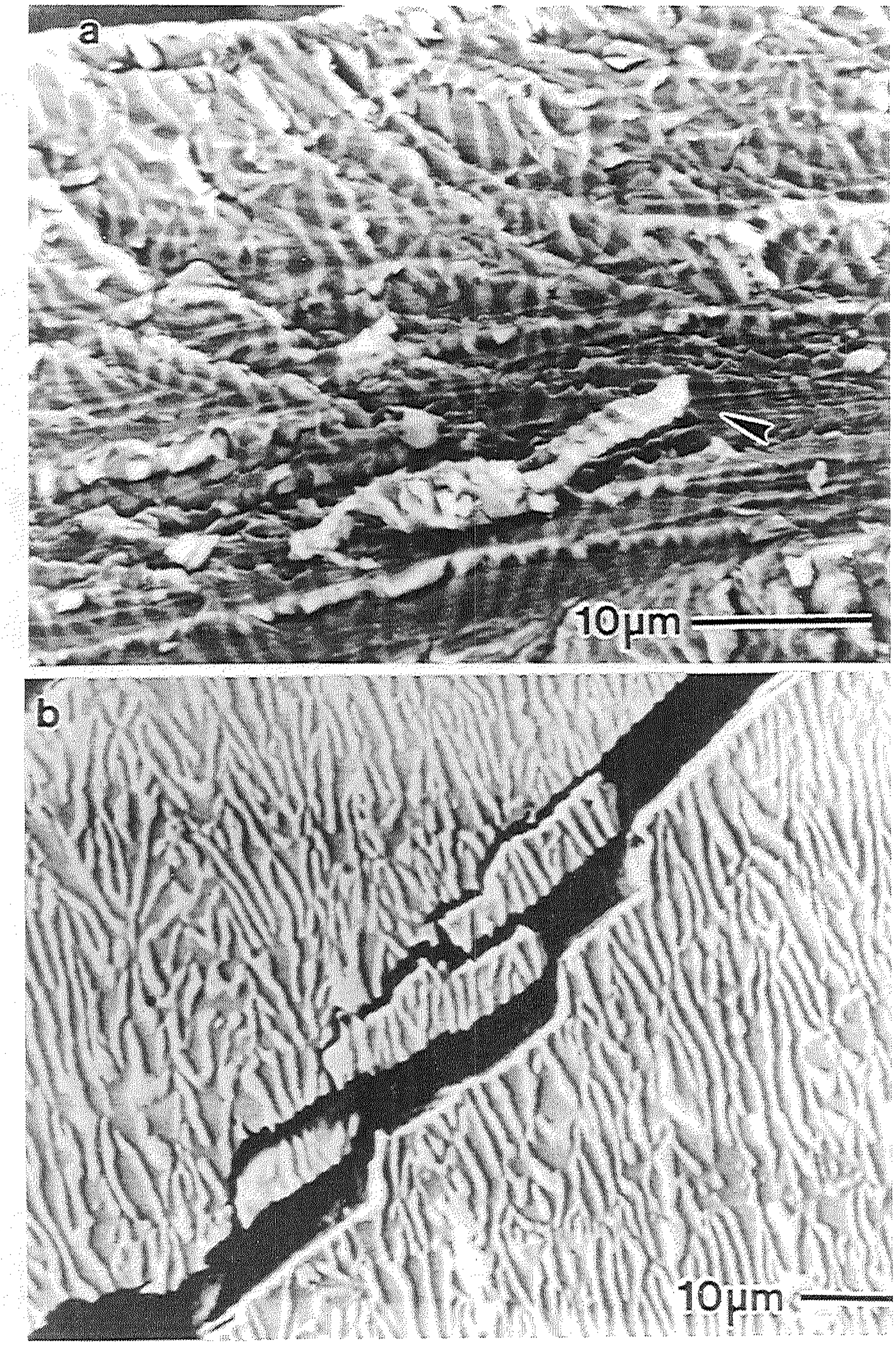

Figure 3.15: Linkage of microcracks by shear deformation in a NiAl-28Cr-6Mo eutectic showing (a) "strips" of material displaced from fracture surface by a shear strain (marked with arrows) and (b) microcracking along the side of the bend specimen.

TEM observations

For material taken very near the fracture surface, localized regions of deformation are evident by the strain contrast produced by slip band formation, Figure 3.16. In all the specimens examined, the dislocation density found in the NiAl phase was much greater than that of the chromium-rich metal phase as shown in Figure 3.17. The low number of dislocations found in the chromium-rich metal phase is attributed to the greater yield strength of the chromium solid solution compared to the yield strength of non-<100> oriented crystals of NiAl, Table 3.6. However, plastic deformation of the metal phase by a crack bridging mechanism is clearly evident in Figure 3.10. Hence, to account for the low dislocation density observed in the chromium phase, NiAl must deform and fracture before the yield strength of the chromium-rich phase is exceeded. The bridging chromium-rich phase then deforms in the crack wake. Specimens for TEM studies were taken below the fracture surface and thus away from the necked regions of the refractory metal phase.

Cotton et al. have shown that the slip system in NiAl is not altered by chromium additions and is predominantly <100>{011} at room temperature [33]. To see if the molybdenum additions had any affect on the slip behavior of the NiAl,Cr solid solution, the Burgers vector was measured for dislocations observed near the fracture surface of a NiAl-28Cr-6Mo bend specimen [10]. Consistent with other NiAl alloys, only a <100> Burgers vector was measured for dislocations in the matrix phase.

As shown in Figure 3.5, a dislocation network exists along the phase boundary between the eutectic phases. This network is constrained to lie along the metal/NiAl interface, strengthening the alloy. During deformation, new dislocations are generated from the interface network. These dislocations can then move into the NiAl matrix as shown in Figure 3.17. However, due to the fineness of the eutectic microstructure, these dislocations are often pinned by neighboring interfaces, Figure 3.18, providing further strengthening.

C-2

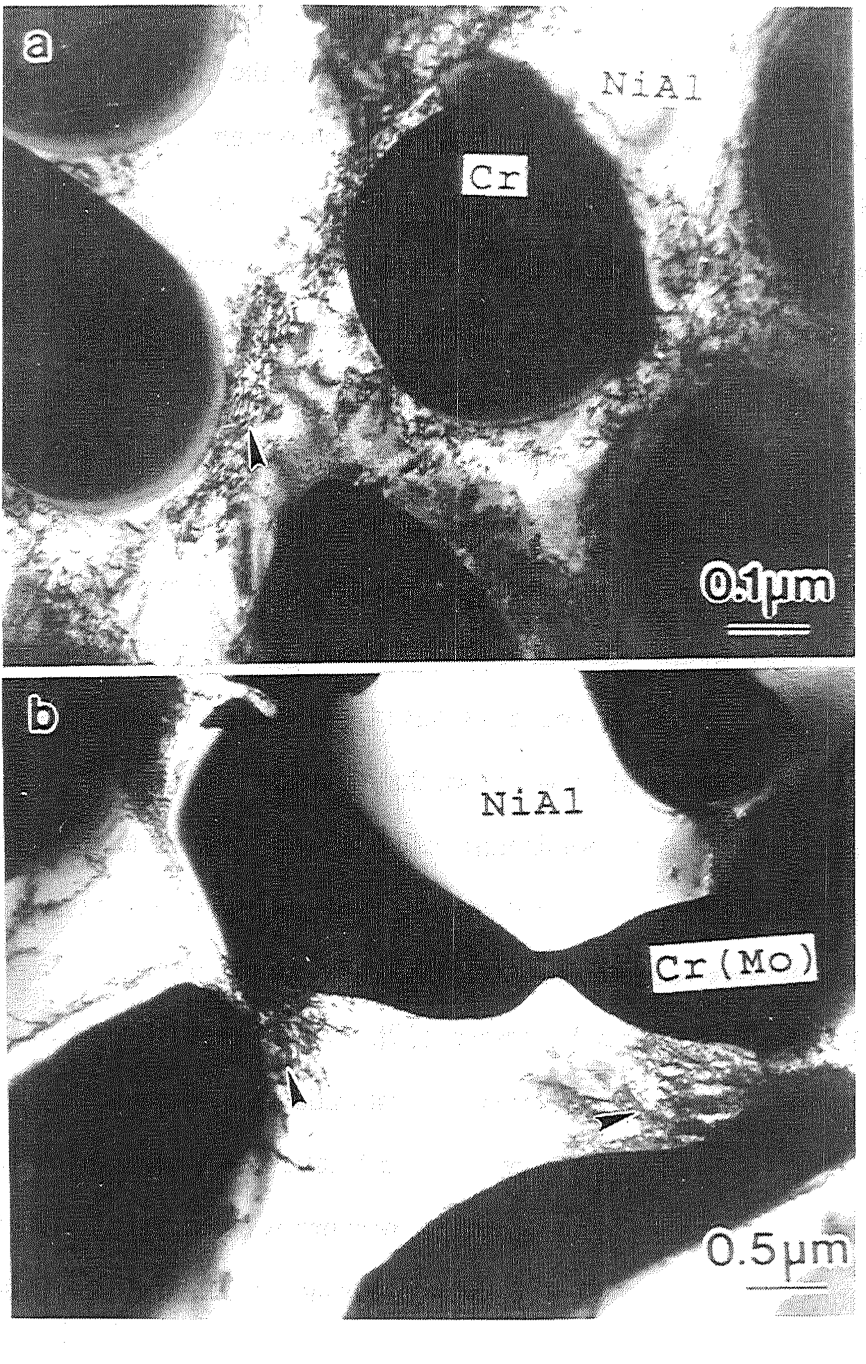

Figure 3.16: TEM photomicrographs from samples taken very near the fracture surface showing slip activity (marked with arrows) for (a) NiAl-34Cr eutectic and (b) NiAl-28Cr-6 Mo eutectic.

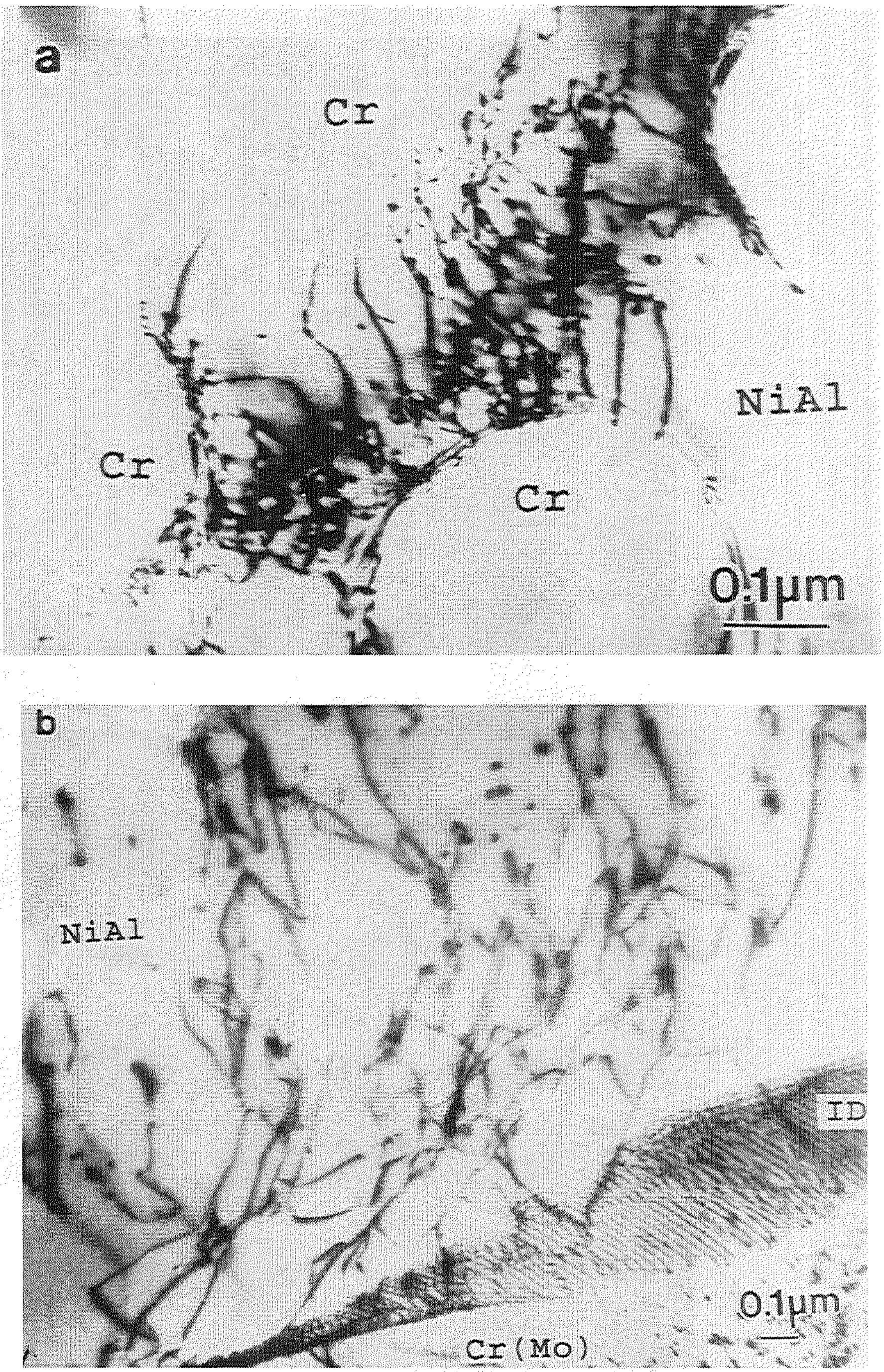

Figure 3.17: TEM photomicrographs of the dislocation structure in failed bend specimens of (a) NiAl-34Cr eutectic and (b) NiAl-28Cr-6Mo eutectic.

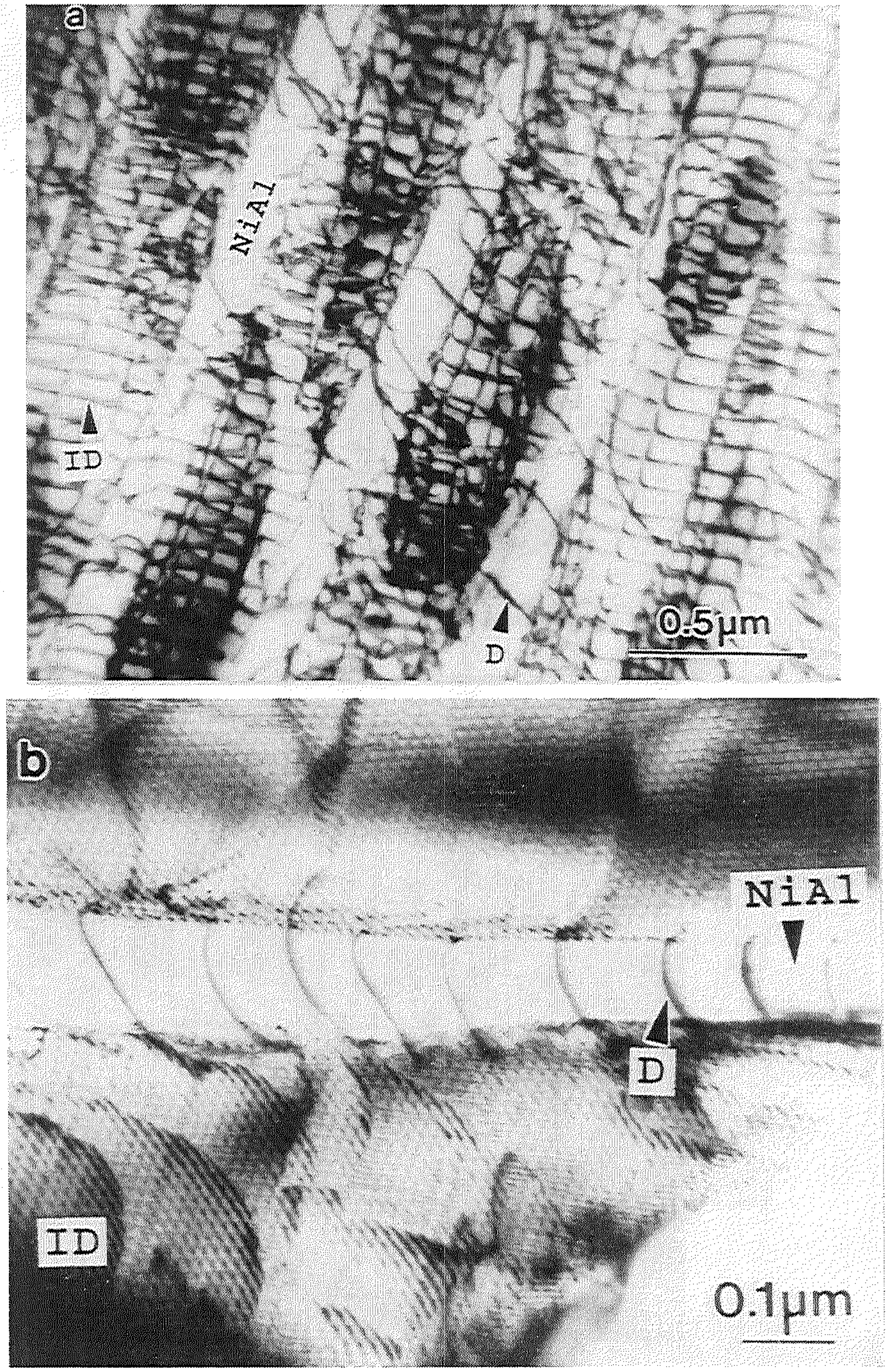

Figure 3.18: TEM photomicrographs showing dislocations (marked 'D') in NiAl that are generated and pinned by the interface dislocation network (marked 'ID') in (a) NiAl-34Cr eutectic and (b) NiAl-28Cr-6Mo eutectic.

CHAPTER 7

DISCUSSION

The most notable changes due to alloying with molybdenum were the changes in morphology, growth direction, and the degree of lattice mismatch between the matrix and refractory metal phase. However, the room temperature fracture resistance and the elevated temperature strength of the NiAl-Cr eutectic were moderately improved by molybdenum additions. The improved 1300 K compressive strength of the NiAl-28Cr-6Mo alloy is likely due to a strengthening of the refractory metal phase due to the presence of fine NiAl precipitates and to the greater lattice mismatch between the eutectic phases. An increased lattice mismatch results in an increased number of immobile dislocations constrained to lie at the phase boundaries, creating additional obstacles for mobile dislocations. Solid solution hardening of the NiAl matrix phase by molybdenum additions may provide some additional strengthening. However, at very low strain rates such as those in the creep regime, the advantage of solid solution strengthening in NiAl is reduced or eliminated [34].

For NiAl, the change in growth direction from the 'hard' <100> orientation to a 'soft' <111> orientation cannot account for the increase in strength of the NiAl-(Cr,Mo) eutectic. In fact, the opposite effect would be expected [34]. In addition, the change from a fibrous microstructure to a lamellar one will not greatly change the amount of interfacial area between the eutectic phases. From the Jackson and Hunt solution [35], the rod to lamellar transition occurs at a volume fraction of $1/\pi$ (0.32), assuming isotropic surface energies. Thus, the NiAl-Cr eutectic, having a second phase volume fraction of about 0.34, is a borderline case with both morphologies having about the same energy.

The room temperature toughness of the NiAl-Cr and NiAl-(Cr,Mo) alloys is controlled by crack front interactions with the reinforcing metal phase, with a number of different specific mechanisms all contributing to the enhanced toughness of the eutectics. However, the orientation of NiAl matrix has little effect on the measured toughness values of the eutectic. Typically, the room temperature fracture toughness of NiAl tested with the notch perpendicular to the <100> direction is between 8-11 MPa$\sqrt{m}$ [16,23]. For softer orientations, like the <111>, the fracture toughness of NiAl is between 4-6 MPa$\sqrt{m}$ [23]. The fracture toughness of the eutectics changed very little when tested in these orientations. However, changing the morphology of the reinforcing metal phase did have some affect on the fracture toughness with the well aligned lamellar microstructure having the highest toughness.

Optimization of the microstructure may provide further improvements in properties. For example, the lamellar microstructure of the NiAl-(Cr,Mo) eutectic resulted in improved properties compared to the fibrous NiAl-Cr eutectic. Better aligned and finer eutectic microstructures should produce further improvements in fracture toughness and creep strength. Well aligned microstructures can be produced from these eutectics, such as the NiAl-31Cr-3Mo eutectic grown in a large thermal gradient. In addition, further alloying may provide increases in creep strength. Alloying approaches to strengthen the NiAl matrix and the chromium-rich metal phase need to be investigated. For example, hafnium additions may further increase the creep strength of NiAl-(Cr,Mo) alloys by strengthening the NiAl phase. The effects of changing the (Cr,Mo)/NiAl phase boundary strength by alloying with interstitial elements should also be examined.

REFERENCES

1. R.D. Noebe, F.J. Ritzert, A. Misra, and R. Gibala, Prospects for Ductility and Toughness Enhancement of NiAl by Ductile Phase Reinforcement, NASA TM-103796, 1991.
2. J.L. Walter and H.E. Cline, Met. Trans., 1 (1970), 1221-1229.
3. R. Darolia, D.F. Lahrman, R.D. Field, J.R. Dobbs, K.M. Chan, E.H. Goldman, and D.G. Konitzer, in Ordered Intermetallics-Physical Metallurgy and Mechanical Behavior, C. T. Liu, et. al., eds., Kluwer Academic Publishers, The Netherlands (1991), 679-698.
4. D.R. Johnson, S.M. Joslin, B.F. Oliver, R.D. Noebe, and J.D. Whittenberger, in Intermetallic Matrix Composites II, D. Miracle et. al., eds., MRS Symp. Proc. Vol. 273, Pittsburgh PA, (1992), 87-92.
5. J.L. Walter and H.E. Cline, Met Trans., 4 (1973), 33-38.
6. H.E. Cline and J.L. Walter, Met Trans., 1 (1970), 29007-2917.
7. J.L. Walter, H.E. Cline, and E.F. Koch, Trans. AIME, 245 (1969), 2073-2079.
8. H.E. Cline, J.L. Walter, E.F. Koch, and L.M. Osika, Acta Met., 19 (1971), 405-414.
9. S.M. Merchant and M.R. Notis, Mat. Sci. and Engr., 66 (1984), 47-60.
10. X.F. Chen, D.R. Johnson, B.F. Oliver, and R.D. Noebe, to be submitted to Mat. Characterization.
11. J.A. Nesbitt and C.A. Barrett, in Structural Intermetallics, R. Darolia et al. eds, TMS, Warrendale, PA (1993), 601-610.
12. J.D. Whittenberger and R.D. Noebe, unpublished data, 1991
13. M.V. Nathal and L.J. Ebert, Metall. Trans. A, 16A (1985), 427-439.
14. K.S. Kumar, S.K. Mannan, and R.K. Viswanadham, Acta Metal. Mater., 40 (1992), 1201-1222.
15. F.E. Heredia, M.Y. He, G.E. Lugas, A.G. Evans, H.E. Deve, and D. Konitzer, Acta Metall. Mater., 41 (1993), 505-511.
16. D.R. Johnson, S.M. Joslin, B.F. Oliver, R.D. Noebe, and J.D. Whittenberger., in First International Conference on Processing Materials for Properties, H. Henein and T. Oki eds., TMS, Warrendale PA (1993), 865-870.
17. N. Fares, J. Appl. Mech., 56 (1989), 837-843.
18. H. Gao and J. Rice, J. Appl. Mech., 56 (1989), 828-836.
19. K.S. Chan, JOM, 44[5] (1992), 30-38.
20. K.S. Chan, Metall. Trans. A, 23A (1992), 183-199.
21. P.A. Mataga, Acta Metall. 37 (1989) 3349-3359.
22. B.D. Flinn, M. Rhle, and A.G. Evens, Acta Metall. 37 (1989), 3001-3006.
23. K.M. Chang, R. Darolia, and H.A. Lipsitt, Acta Metall. Mater., 40 (1992), 2727-2737.
24. M.F. Ashby, F.J. Blunt, and M. Bannister, Acta Metall. 37 (1989), 1847-1857.
25. M. Bannister and M.F. Ashby, Acta Metall. Mater., 39 (1991) 2575-2582.
26. K.S. Ravichandran, Scripta Metall. Mater., 26 (1992), 1389-1393.
27. R.J. Wasilewski, Trans AIME, 236 (1966), 455-457.
28. Smithells Metals Reference Book 6th ed., E. A. Brandes ed., Butterworths, London (1983), 15-5.
29. J.D. Cotton, R.D. Noebe, and M.J. Kaufman, Intermetallics, 1 (1993), 117-126.
30. S.M. Joslin, Ph.D. Thesis, University of Tennessee (in progress).
31. D. Broek, Elementary Engineering Fracture Mechanics, Martinus Nijhoff Publishers, Boston, MA (1986), 115
32. K.S. Chan, Met. Trans. A, 22A (1991), 2021-2029.
33. J.D. Cotton, R.D. Noebe, and M.J. Kaufman, Intermetallics, 1 (1993), 3-20.
34. R.D. Noebe, R.R. Bowman, and M.V. Nathal, Int. Mat. Rev., 38 (1993), 193-232.
35. K.A. Jackson and J.D. Hunt, Trans AIME, 236 (1966), 1129-1142.

PART 4: DIRECTIONAL SOLIDIFICATION AND MECHANICAL PROPERTIES OF NiAl-NiAlTa ALLOYS

CHAPTER 1

INTRODUCTION

The intermetallic compound NiAl has potential for structural applications at elevated temperature due to its superior oxidation resistance, high melting point, and high thermal conductivity [1,2]. However, improvements in both the room temperature fracture toughness and elevated temperature strength are necessary before NiAl can be used in load bearing applications. Considerable research to improve the room temperature ductility of NiAl has been conducted with promising results [1-4]. For example, a tensile ductility of five percent has been measured for both high purity [5] and iron-doped single crystals of NiAl [6]. In addition, room temperature fracture toughness values nearing 24 $MPa\sqrt{m}$ have been measured for in-situ composites containing a refractory metal phase such as the NiAl-(Cr,Mo) eutectic [7].

While improving the elevated temperature strength of NiAl based materials may not be considered as challenging, approaches to strengthen NiAl to date have not produced materials competitive with the nickel-based superalloys. Conventional strengthening techniques such as precipitation, solid solution, and dispersion strengthening have all been applied with varying success [2,3]. Precipitates of the Heusler phases as a strengthening agent have shown the most promise [2,3,8,9]. The Heusler phases, such as Ni_2AlTi or Ni_2AlHf, have a $L2_1$ crystal structure. Polvani et al. have shown that the creep resistance of the two phase microstructure $NiAl+Ni_2AlTi$ is much greater than that of the individual phases [10]. While impressive yield strength values have been measured for NiAl containing Heusler precipitates [3,9], the improved strengths from solid solution and precipitation strengthening are diminished at low strain rates such as those in the creep regime [2,3].

Another approach to strengthening NiAl consists of developing composite materials containing phases much stronger than the Heusler phase, for example the NiAl-Laves phase alloys [11]. Sauthoff has shown that the C14 Laves phases NiAlNb and NiAlTa can be used to strengthen NiAl [11,12,13]. These phases are very brittle. They have a hexagonal $MgZn_2$ type crystal structure and can be denoted by $Ta(Ni,Al)_2$. In general, the improvement in strength of the NiAl+Laves phase alloys increases with the greater volume fraction of Laves phase present. Compressive yield strengths surpassing that of an advanced nickel-based superalloy have been measured for the NiAl-NiAlTa alloys [13].

However, eutectic microstructures are possible within the NiAl-NiAlNb and NiAl-NiAlTa systems allowing for in-situ composite studies. Whittenberger et al. have found that the creep strength of the NiAl-NiAlNb eutectic is extremely sensitive to microstructure and processing conditions [14]. By directional solidification of this eutectic, an order of magnitude increase in creep resistance was measured when compared to materials processed using a casting and extrusion procedure. Unfortunately, the creep strength of the NiAl-NiAlNb alloys is still less than that of the nickel-based superalloys.

While the phase equilibria in the NiAl-NiAlTa system are not well known [15,16], directionally solidified alloys from this system may display better strengths than the NiAl-NiAlNb alloys. The purpose of this study was to characterize the effects of containerless processing on the microstructure and subsequently the elevated temperature strength and room temperature fracture toughness of in-situ composite based on the NiAl-NiAlTa system.

CHAPTER 2

EXPERIMENTAL PROCEDURES

Arc-melted ingots

As a first approach to locating promising microstructures for in-situ composites studies, alloys containing high purity Ni, Al, and Ta were arc-melted with a non-consumable tungsten electrode into approximately 12 gram buttons. Each button was melted at least five times and flipped between each melting to promote homogeneity. Arc-melted ingots were then metallographically examined. From this survey study, a near eutectic alloy of NiAl-14.5Ta (atomic percent) was chosen for further study.

Directional solidification

Near-eutectic alloys were directional solidified to produce in-situ composites for mechanical testing. Precursor ingots consisting of the NiAl-NiAlTa eutectic were provided by NASA Lewis Research Center. These ingots were produced by induction melting of elemental Ni, Al, and Ni-Ta master alloys. The 1 kg charges were then chill cast into a copper mold. After removal of the hot-top, precursor ingots were nominally 25 mm in diameter and 300 mm in length. These ingots were then directionally solidified in the containerless mode by the electromagnetically-levitated zone process in ultra-pure helium atmospheres.

An as-processed NiAl-14.5Ta ingot is shown in Figure 4.1. The unusually rough surface of the ingot was created by a series of very small spills where a portion of the molten zone would spill-over the edge of the solid-liquid interface. The melt record for this ingot is shown in Figure 4.2. Note that the liquid diameter was held

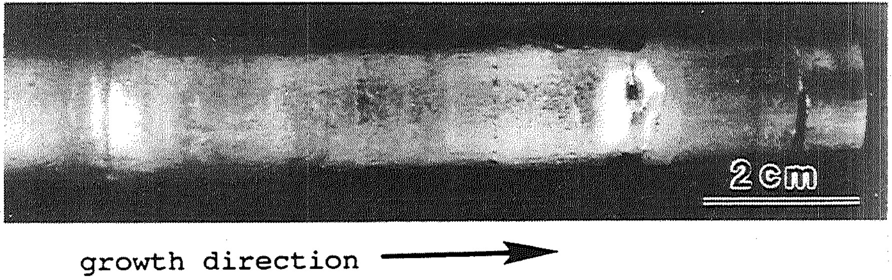

Figure 4.1: As-processed NiAl-14.5Ta ingot.

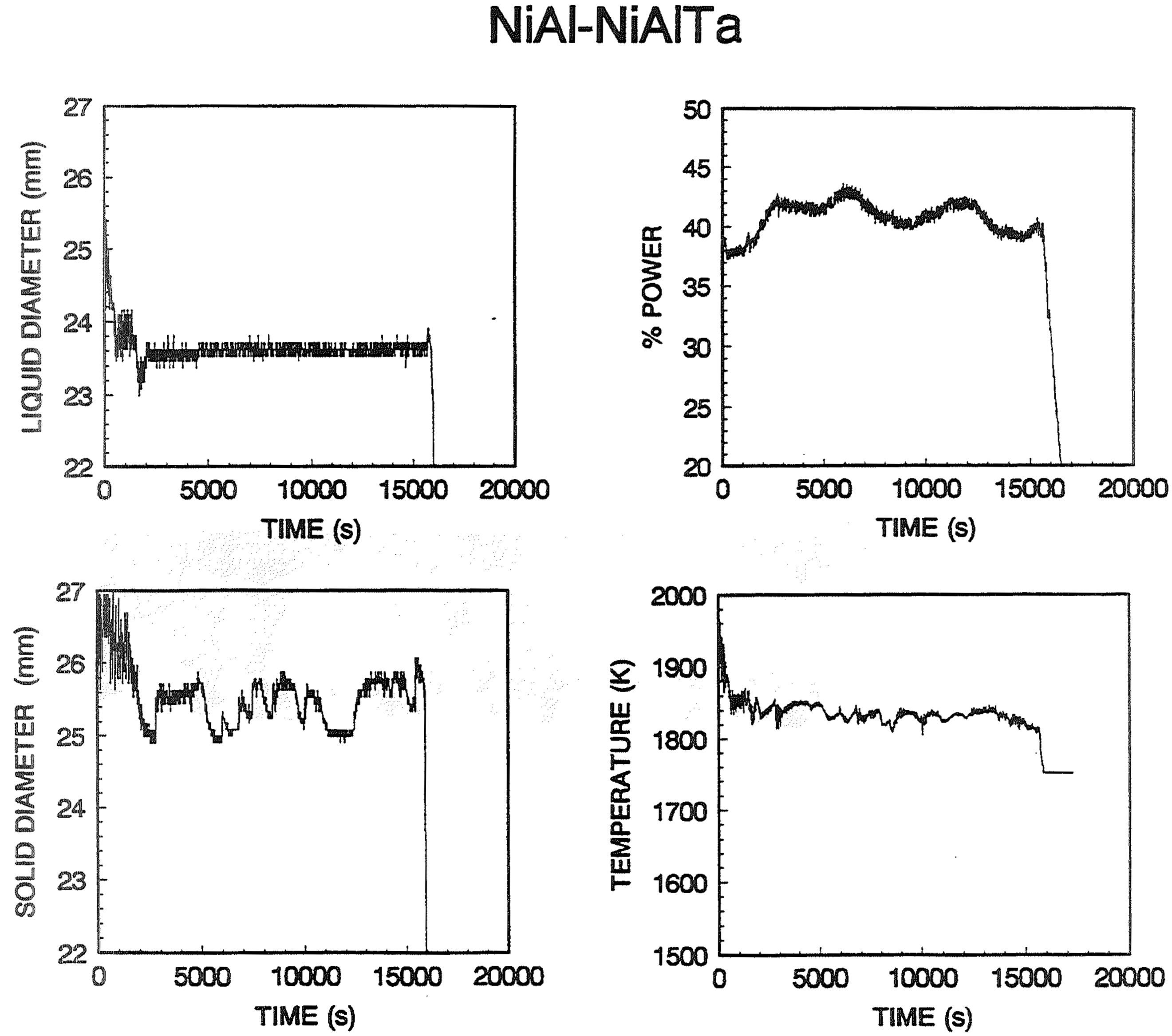

Figure 4.2: Processing record for a NiAl-14.5Ta ingot.

constant but that a variation of 2 mm resulted in the diameter of the solidified ingot. Without automated process control of the solidification process, the freezing diameter of the NiAl-NiAlTa alloys would tend to increase with time causing the processing run to finally be terminated.

CHAPTER 3

MICROSTRUCTURES

NiAl-NiAlTa eutectic

Fully coupled microstructures consisting of NiAl and NiAlTa were found in arc-melted ingots containing 14 to 16 atomic percent tantalum. These microstructures consisted of the eutectic NiAl-NiAlTa microconstituent and contained no single phase dendrites. Since alloy compositions that contain lower percentages of tantalum are expected to have better oxidation resistance, an NiAl-14.5Ta (at.%) alloy was chosen for further study. Induction melted and drop cast ingots of this composition were directionally solidified for mechanical property testing.

Microstructures of the NiAl-NiAlTa eutectic are shown in Figure 4.3. This eutectic is characterized by a lamellar microstructure and has a melting point near 1815 K as determined by differential thermal analysis (DTA), see Appendix B. The volume fractions were estimated as 53% NiAl and 47% NiAlTa from SEM photomicrographs at 4000x. A $<100>$ growth direction was found for the NiAl phase by selected area diffraction patterns. However, no definite crystallographic relationship was determined for the NiAlTa phase.

The microstructure of the directionally solidified NiAl-14.5Ta ingot consisted of NiAl dendrites and eutectic colonies, Figure 4.3b. Since the directionally solidified ingot was processed at near equilibrium conditions, the dendritic microstructure represents an off-eutectic composition. To better determine the eutectic composition, another NiAl-14.5Ta ingot was directionally solidified with a small amount of tantalum added to the initial molten zone. The added tantalum produced a well aligned microstructure for the beginning section of the ingot,

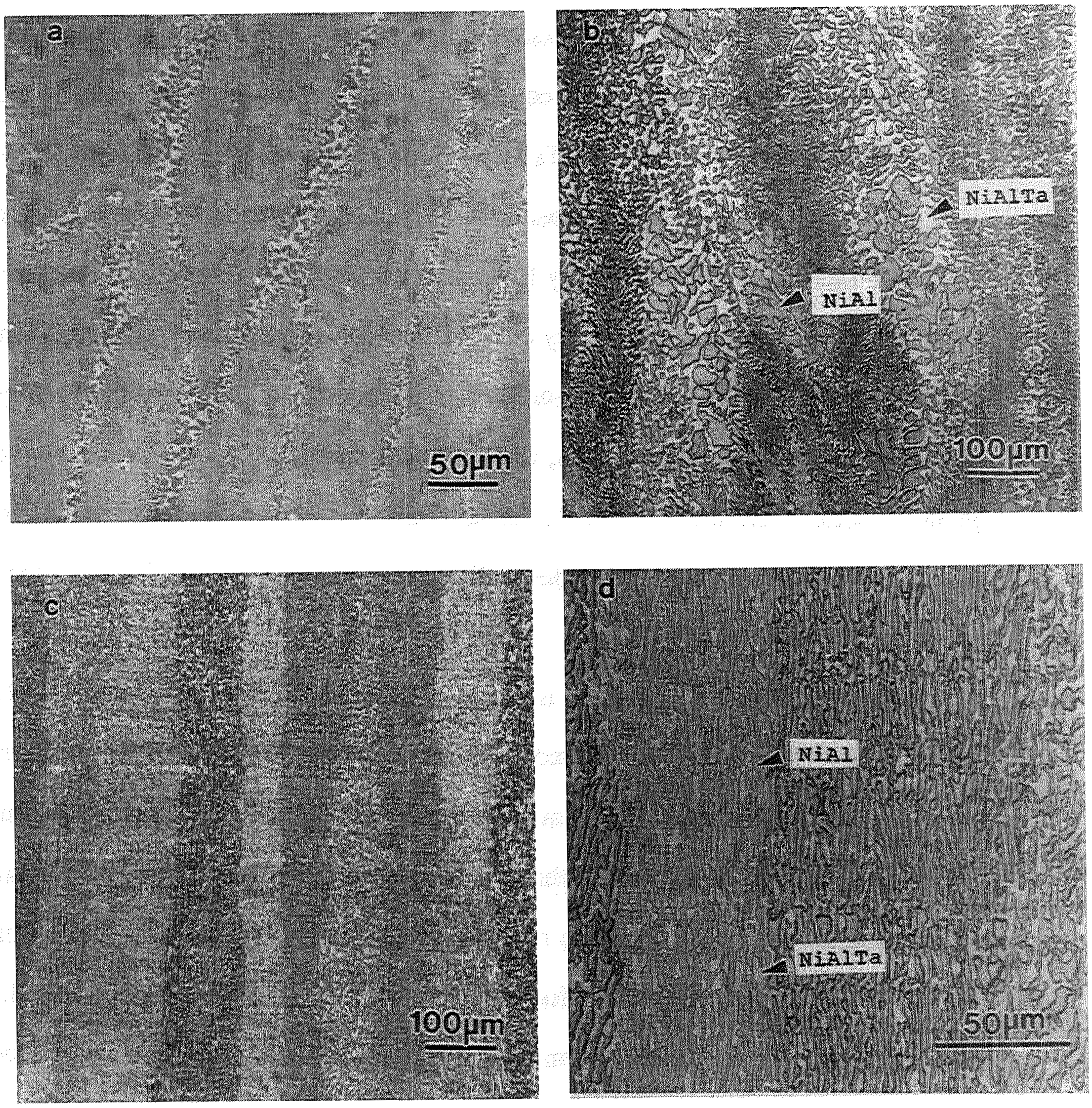

Figure 4.3: Light optical photomicrographs of arc-melted and directionally solidified NiAl-NiAlTa alloys showing (a) NiAl-14.5Ta arc-melted ingot, (b) directionally solidified NiAl-14.5Ta ingot (19mm/h) and (c) and (d) directionally solidified NiAl-15.5Ta ingot (15mm/h).

Figures 4.3c. An eutectic composition of NiAl-15.5Ta (at%) was determined for this region by inductively coupled plasma atomic emission spectroscopy. Another NiAl-14.5Ta ingot processed in a similar manner (with additional tantalum) also produced a well aligned, fully eutectic microstructure. This ingot was used for elevated temperature testing. The composition and processing conditions of the directionally solidified NiAl-NiAlTa alloys used in this study are listed in Table 4.1.

The arc-melted and directionally solidified microstructures were different for the NiAl-14.5Ta alloy as shown by Figures 4.3a and 4.3b. The microstructure for the arc-melted ingot was essentially eutectic while the directionally solidified ingot contained dendrites of NiAl. The difference in the arc-melted and directionally solidified microstructures suggests, that for rapid solidification rates, the coupled growth region is skewed towards lower tantalum contents at moderate undercoolings. Higher solidification rates and undercoolings are produced by the water cooled hearth during arc-melting.

In an attempt to produce a more aligned microstructure for the NiAl-14.5Ta ingot, a cooling jacket was mounted below the upward moving molten zone during one processing run. This was an attempt to increase the thermal gradient through the solid-liquid interface. Such a cooling jacket was previously used to produce aligned microstructures from alloys in the NiAl-(Cr,Mo) eutectic system [7]. However, there was no change in microstructure for the NiAl-14.5Ta alloy when so processed. This indicates that a much greater thermal gradient may be needed for coupled growth at this composition.

NiAl-Ni_2AlTa-NiAlTa liquidus regions

The shape of the liquidus surface for the NiAl, NiAlTa (Laves), and Ni_2AlTa (Heusler) phases was estimated from the cast microstructures of arc-melted ingots. A cast microstructure consisting mostly of the NiAl-NiAlTa eutectic is shown in

Table 4.1: Compositions and processing conditions for NiAl-NiAlTa alloys.

Nominal Composition (at.%)	growth velocity (mm/h)	Rotational velocity (rpm)	Number of passes
NiAl-14.5Ta	19	75	2
NiAl-14.5Ta*	19	75	2
NiAl-15.5Ta	15	75	1

*cooling jacket used for increased thermal gradient

Figure 4.4. Another phase identified as Ni_2AlTa was found in the interdendritic region between the eutectic cells. The Heusler phase Ni_2AlTa contacts both eutectic phases, NiAl and NiAlTa, indicating the following ternary peritectic reaction, Figure 4.4:

$$\mathrm{NiAl} + \mathrm{NiAlTa} + \mathrm{Liquid} = \mathrm{Ni_2AlTa}.$$

The following binary invariant reactions are consistent with the above reaction:

Liquid = NiAl + NiAlTa (eutectic),
NiAl + Liquid = Ni_2AlTa (peritectic), and
NiAlTa + Liquid = Ni_2AlTa (peritectic).

The eutectic reaction has already been described and its composition located. Additional arc-melted ingots were made to examine the existence of the two peritectic reactions. A partial 1753 K isotherm for the Ni-Ta-Al ternary system [16] is shown in Figure 4.5 along with a schematic of the projected liquidus troughs. Two arc-melted ingots with compositions marked melt-1 and melt-2 in Figure 4.5 were produced for further study. A section from each of these arc-melted ingots was then heat treated at 1373 or 1473 K for 43.2×10^3 s (12 hours).

The cast microstructure of the incomplete peritectic reaction:

$$\mathrm{NiAl} + \mathrm{Liquid} \rightarrow \mathrm{Ni_2AlTa}\ (\text{melt-1})$$

is shown in Figure 4.6. This microstructure consists of primary NiAl dendrites surrounded by Ni_2AlTa formed from the binary peritectic reaction. Since the Heusler phase encases NiAl, the remaining liquid cannot react with the primary NiAl phase and the last phase to solidify from the tantalum rich liquid is the Laves phase NiAlTa.

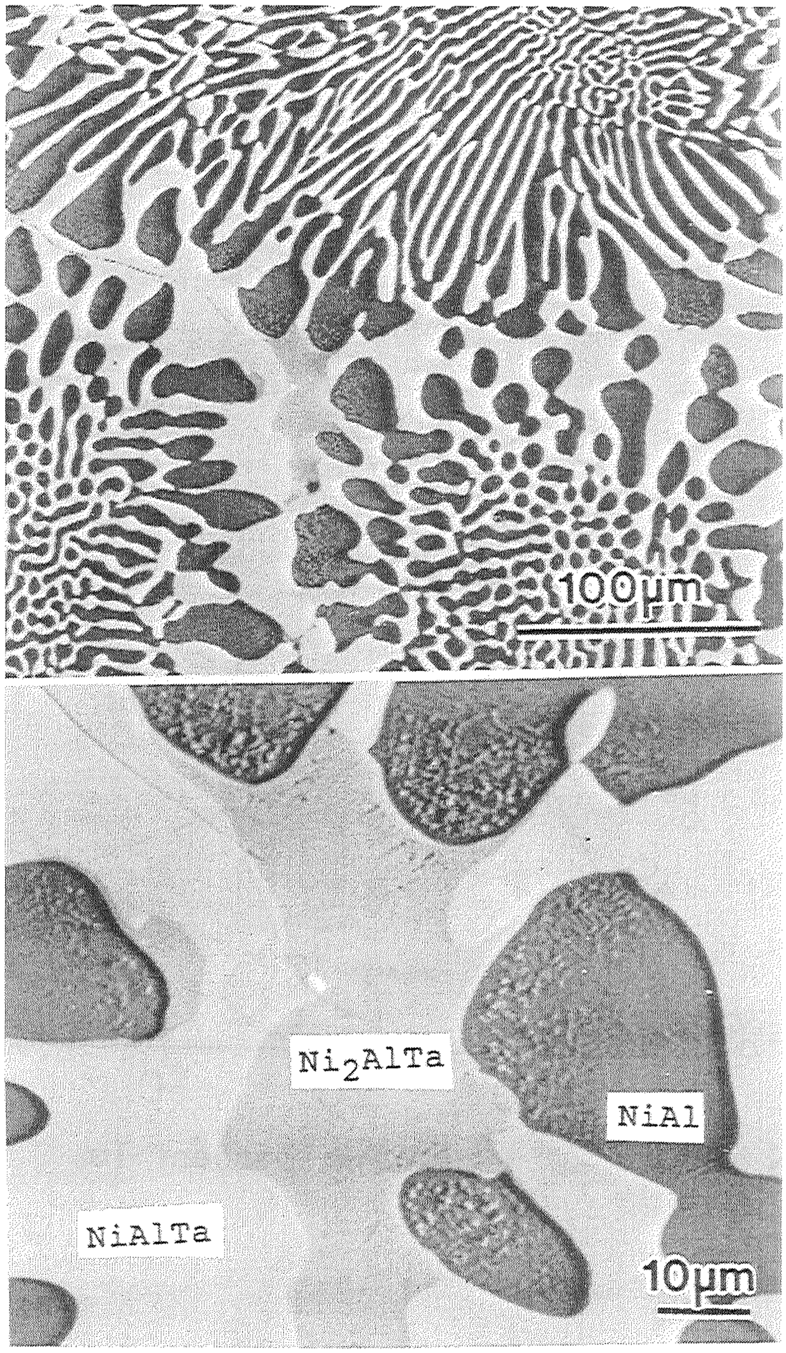

Figure 4.4: SEM backscattered electron photomicrographs showing the interdendritic Heusler phase Ni_2AlTa in an arc-melted NiAl-15Ta alloy.

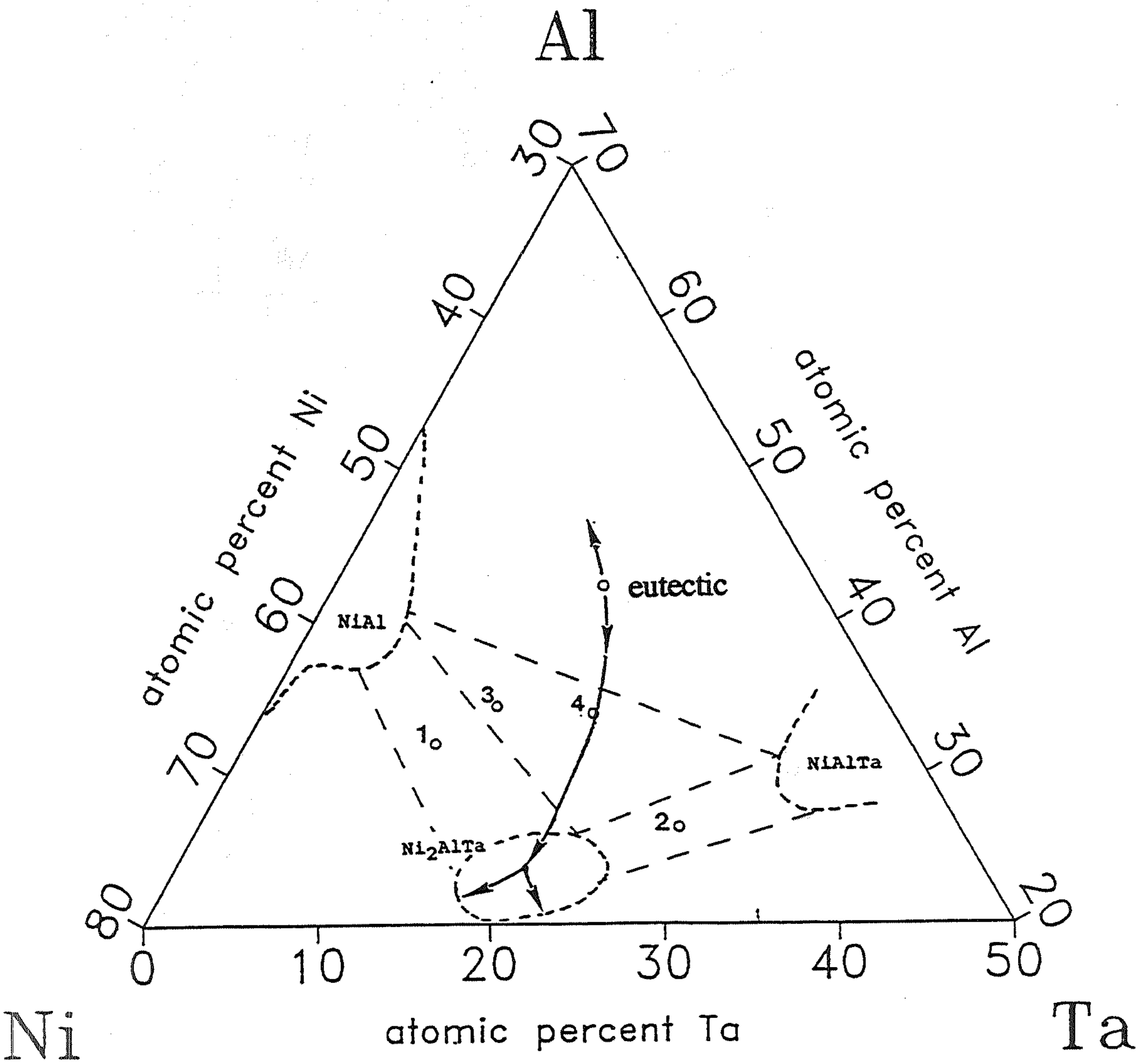

Figure 4.5: A 1753 K isotherm from the Ni-Al-Ta system [16] combined with a schematic of the liquidus surface.

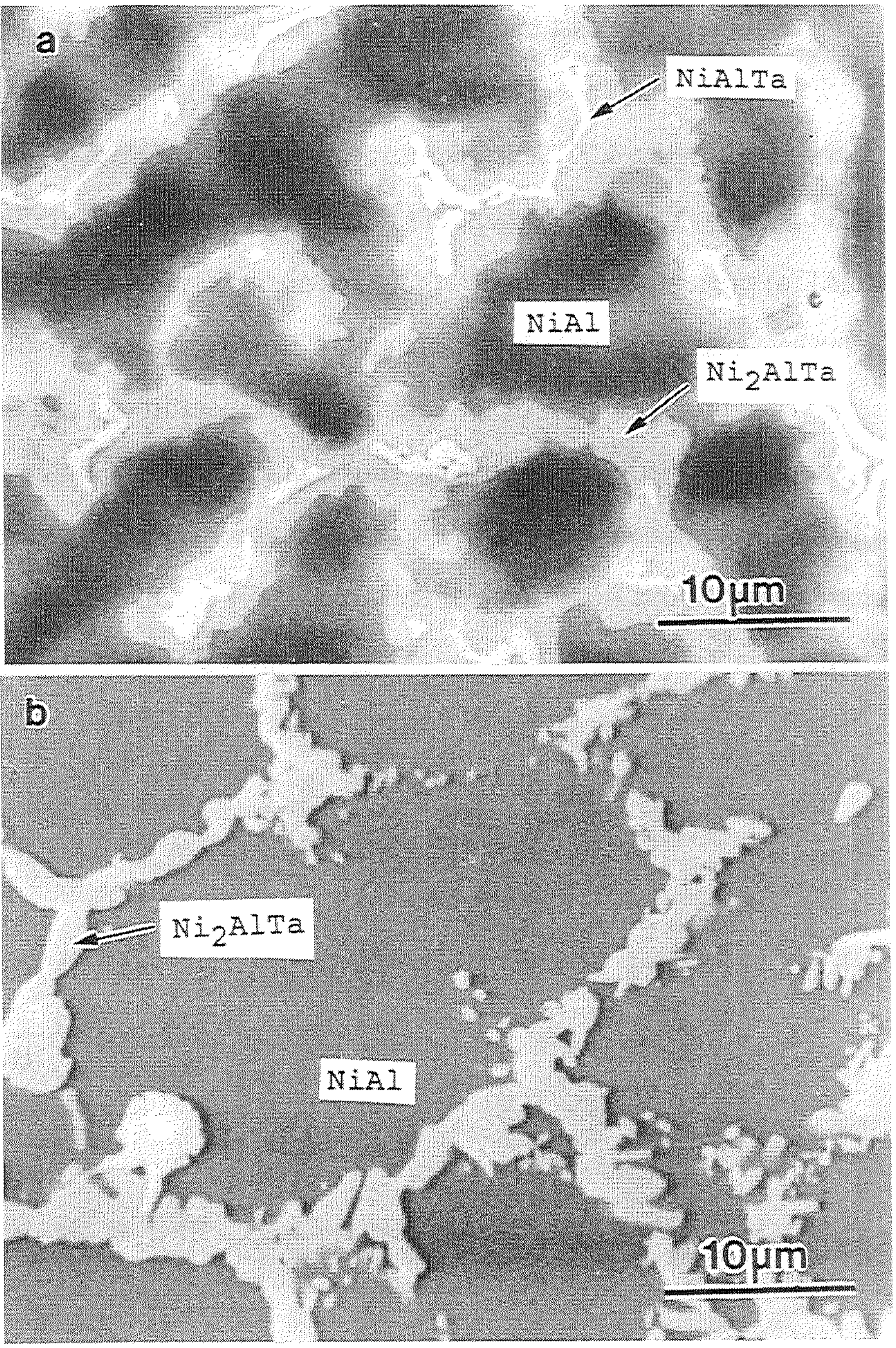

Figure 4.6: SEM backscattered electron photomicrographs of an arc-melted Ni-32Al-11Ta alloy (melt-1) in the (a) as-cast condition and (b) after heat treating at 1373 K for 43.2x10^3 s (12 hours).

After heat treating at 1373 K, the amount of Laves phase decreased as expected and additional Heusler phase precipitates are observed in the NiAl.

Similarly, the cast microstructure of the incomplete peritectic reaction:

$$\text{NiAlTa} + \text{Liquid} \rightarrow \text{Ni}_2\text{AlTa} \text{ (melt-2)}$$

is shown in Figure 4.7. This microstructure consists of primary NiAlTa dendrites surrounded by Ni_2AlTa. Again, the Heusler phase encases the primary phase (NiAlTa) preventing a reaction with the remaining liquid that solidifies as NiAl. After heat treating at 1473 K, the amount of NiAl decreases as expected.

The projected view of the eutectic monovariant trough and the approximate location of the peritectic regions are shown in Figure 4.5. While this data represents a first approximation, it provides a starting point for further alloying studies. The phase compositions from some of the directionally solidified and arc-melted alloys are listed in Table 4.2.

Table 4.2: Quantitative X-ray analysis for Ni-Al-Ta alloys.

Nominal composition	Processing technique		Phase composition (at. %)		
			Al	Ni	Ta
NiAl-14.5Ta+Ta (NiAl-15.5Ta)	directionally solidified, 19mm/h	NiAl:	50.5	48.5	1.0
		NiAlTa:	34.0	36.0	30.0
Ni-42.5Al-15.0Ta (near eutectic)	arc-melted	NiAl:	52.5	45.0	2.5
		NiAlTa:	33.0	33.5	33.5
		Ni_2AlTa:	28.0	52.0	20.0
Ni-26.4Al-27.7Ta (melt-2, Figure 4.5)	arc-melted	NiAl:	40.0	54.0	6.0
		NiAlTa:	26.0	42.0	32.0
		Ni_2AlTa:	26.5	54.5	19.0
Ni-34.5Al-13.3Ta (melt-3, Figure 4.5)	arc-melted	NiAl:	45.0	52.0	3.0
		NiAlTa:	22.0	48.0	30.0
		Ni_2AlTa:	26.5	55.5	18.0

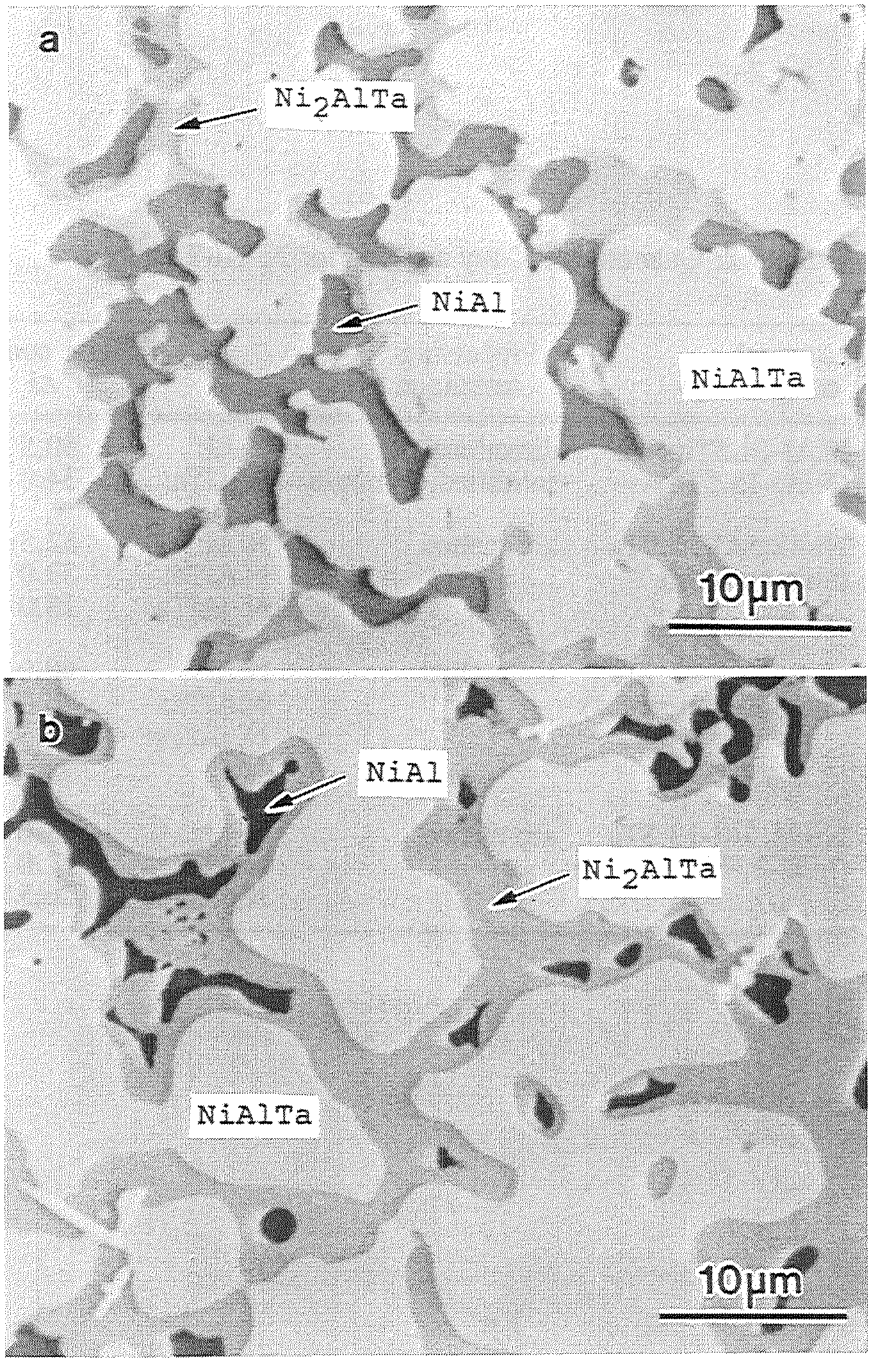

Figure 4.7: SEM backscattered electron photomicrographs of an arc-melted Ni-26.4Al-27.7Ta alloy (melt-2) in the (a) as-cast condition and (b) after heat treating at 1473 K for 43.2×10^3 s (12 hours).

CHAPTER 4

ELEVATED TEMPERATURE STRENGTH

The directionally solidified NiAl-NiAlTa alloys have a very good compressive creep strength when compared to binary NiAl. Most of the compression tests were performed on an off-eutectic NiAl-14.5Ta directionally solidified ingot. However, a limited number of tests were performed on the fully eutectic microstructure (NiAl-15.5Ta). The flow stress and strain rate, $\dot{\varepsilon}$, data for these alloys were fitted to a temperature compensated-power law equation:

$$\dot{\varepsilon} = A\sigma^{n}\exp(-Q/RT)$$

where A is a constant, σ is the applied true stress (MPa), Q is the activation energy for deformation (kJ/mol), T is the absolute temperature, R is the gas constant (kJ/mol-K), and n is the stress exponent. The creep characteristics for NiAl-Laves alloys are compared to single crystal NiAl in Table 4.3.

The elevated temperature strength of the off-eutectic NiAl-14.5Ta alloy over the temperature range of 1200-1400 K is shown in Figure 4.8. Except for the fastest strain rates at 1200 K where power-law breakdown behavior has occurred, the NiAl-14.5Ta alloy exhibits a very consistent power law behavior over the strain rates and temperatures investigated.

In Figure 4.9, the 1300 K compressive creep behavior of the NiAl-Laves alloys are compared to single crystal binary NiAl [17] and a nickel-based single crystal superalloy [18]. The NiAl-Laves alloys have significantly higher strengths compared to binary NiAl. Moreover, the strength of the NiAl-NiAlTa alloys are

Table 4.3: Representative Creep Behavior for NiAl-Laves alloys compared to binary NiAl.

Nominal Composition (at.%)	Representative creep behavior
NiAl [001] (Ni-50Al)	1100-1300K [17]: $\dot{\varepsilon}=(1.48\text{x}10^{3})\sigma^{6.3}\exp(-439.3/RT)$
NiAl-NiAlNb (NiAl-16.5Nb)	1200-1300 K [14]: $\dot{\varepsilon}=(40.0)\sigma^{4.17}\exp(-414.5/RT)$
NiAl-NiAlTa (NiAl-14.5Ta)	1200-1400 K: $\dot{\varepsilon}=(4.55\text{x}10^{3})\sigma^{4.91}\exp(-521.6/RT)$

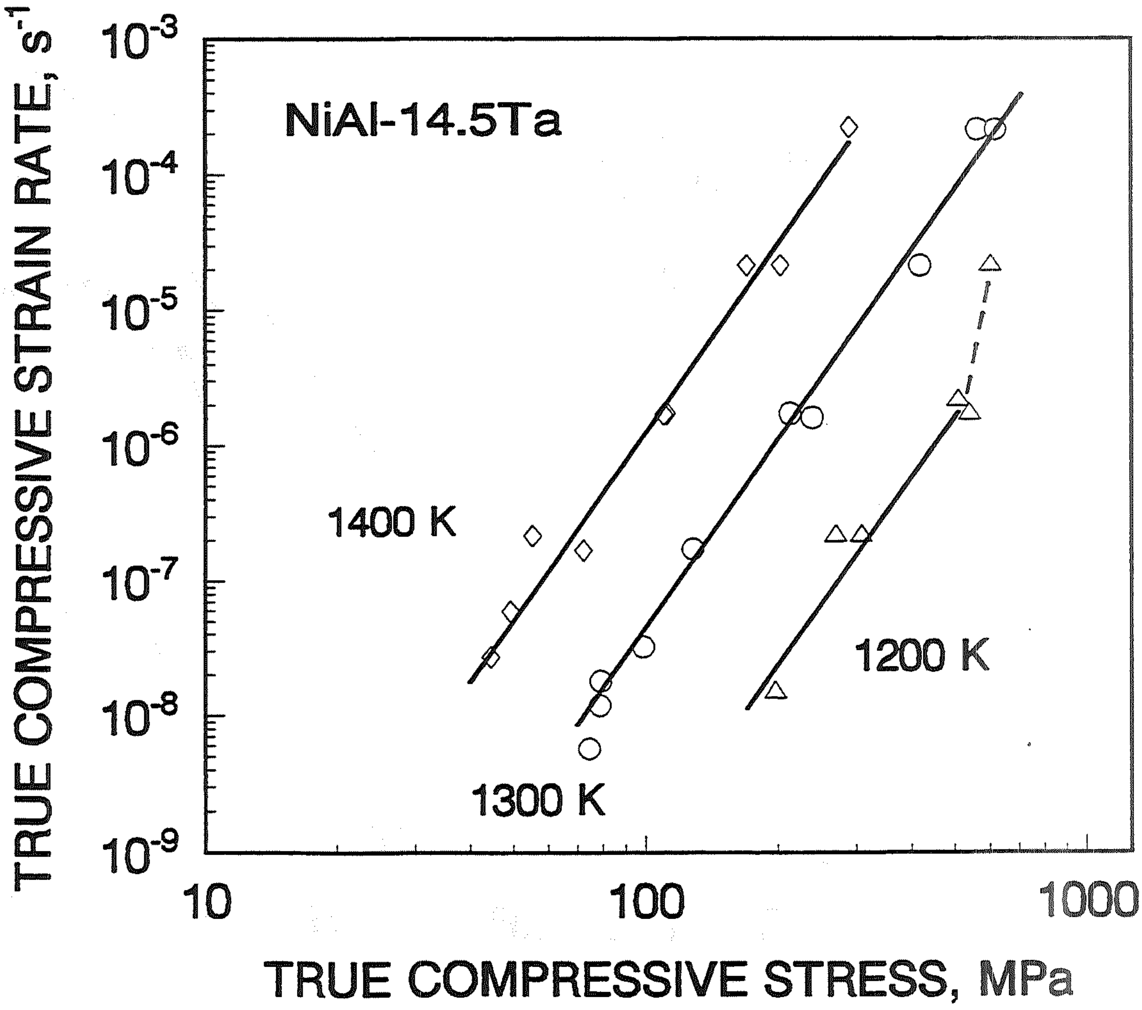

Figure 4.8: 1300 K compressive flow stress-strain rate behavior for the NiAl-14.5Ta alloy as a function of temperature.

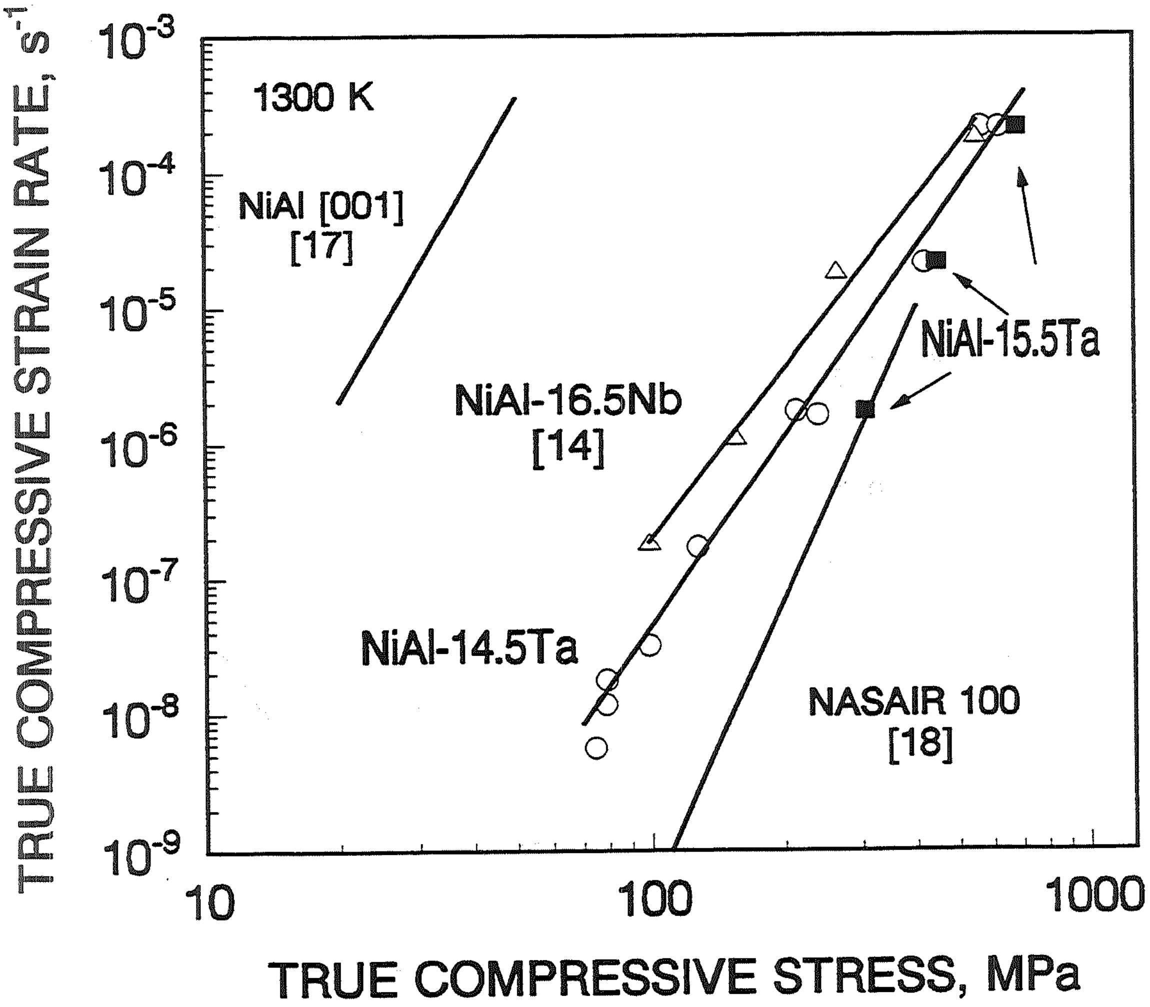

Figure 4.9: 1300 K compressive flow stress-strain rate behavior for the NiAl-Laves alloys compared to NiAl and a single crystal superalloy.

greater than that of the NiAl-NiAlNb eutectic. However, the NiAl-14.5Ta alloy is weaker than the single crystal nickel-based superalloy.

Conversely, the 1300 K compressive strength of the NiAl-15.5Ta eutectic alloy matches that of the nickel-based superalloy as shown in Figure 4.9. While the strength of the NiAl-15.5Ta alloy was found at only three strain rate values, the data does represent a modest improvement of the creep resistance. The improvement in strength is likely due to a refinement in microstructure for the fully eutectic alloy. The lamellar spacing of the eutectic microstructure was measured as 2-3 μm from SEM and TEM photomicrographs. This is much finer than the phase distribution found in the NiAl-14.5Ta alloy, Figure 4.3b.

CHAPTER 5

ROOM TEMPERATURE TOUGHNESS

The NiAl-NiAlTa alloys are brittle at room temperature with a fracture toughness of approximately 5 MPa√m. A total of nine bend specimens were tested. Three bend specimens were tested in the as-processed conditions. The remaining bend specimens were heat treated at 1000 K for 7200 s (2 hours) then either air cooled, oil quenched, or water quenched. Hack et al. [19] have shown improvements in the fracture toughness of NiAl when rapidly cooled through the temperature range of 673 to 300 K. Their results suggest that NiAl may be susceptible to strain-aging embrittlement. However, the post-processing heat treatments used in this study provided no improvement in toughness of the NiAl-NiAlTa alloys and a fracture toughness of approximately 5 MPa√m was measured from all samples.

In Table 4.4, the fracture toughness of the NiAl-14.5Ta alloy after the various heat treatments are compared to NiAl and the NiAl-NiAlNb eutectic. The fracture toughness of the NiAl-NiAlTa alloy is comparable to that of polycrystalline NiAl [20]. Hence, the large increase in creep strength is not gained at the expense of fracture toughness. However, the fracture toughness of the NiAl-NiAlTa eutectic is less than that of single crystal NiAl having a [001] notch plane. Furthermore, if a fracture toughness of 2 MPa√m is assumed for the Laves phase NiAlTa, then the fracture toughness of the eutectic is close to that predicted by the rule of mixtures.

On the other hand, materials containing a large volume fraction of the extremely brittle Laves phase can be reliably produced, handled, and tested by processing alloys near the eutectic composition. The fracture surface of a NiAl-NiAlTa bend specimen is shown in Figure 4.10. The eutectic microstructure is

Table 4.4: Room temperature fracture toughness of alloys containing NiAl, and Laves phases.

Material	Morphology	K_I (MPa$\sqrt{m}$)
NiAl	polycrystalline (HIP)	6 [20]
NiAl [001]	single crystal (DS)	11 [5]
NiAlNb	single phase (HIP)	2 [25]
NiAl-NiAlNb	eutectic (cast)	4 [25]
NiAl-14.5Ta	near eutectic (DS)	5.1 ±0.8

HIP = hot isostatically pressed powder metallurgy
DS = directionally solidified

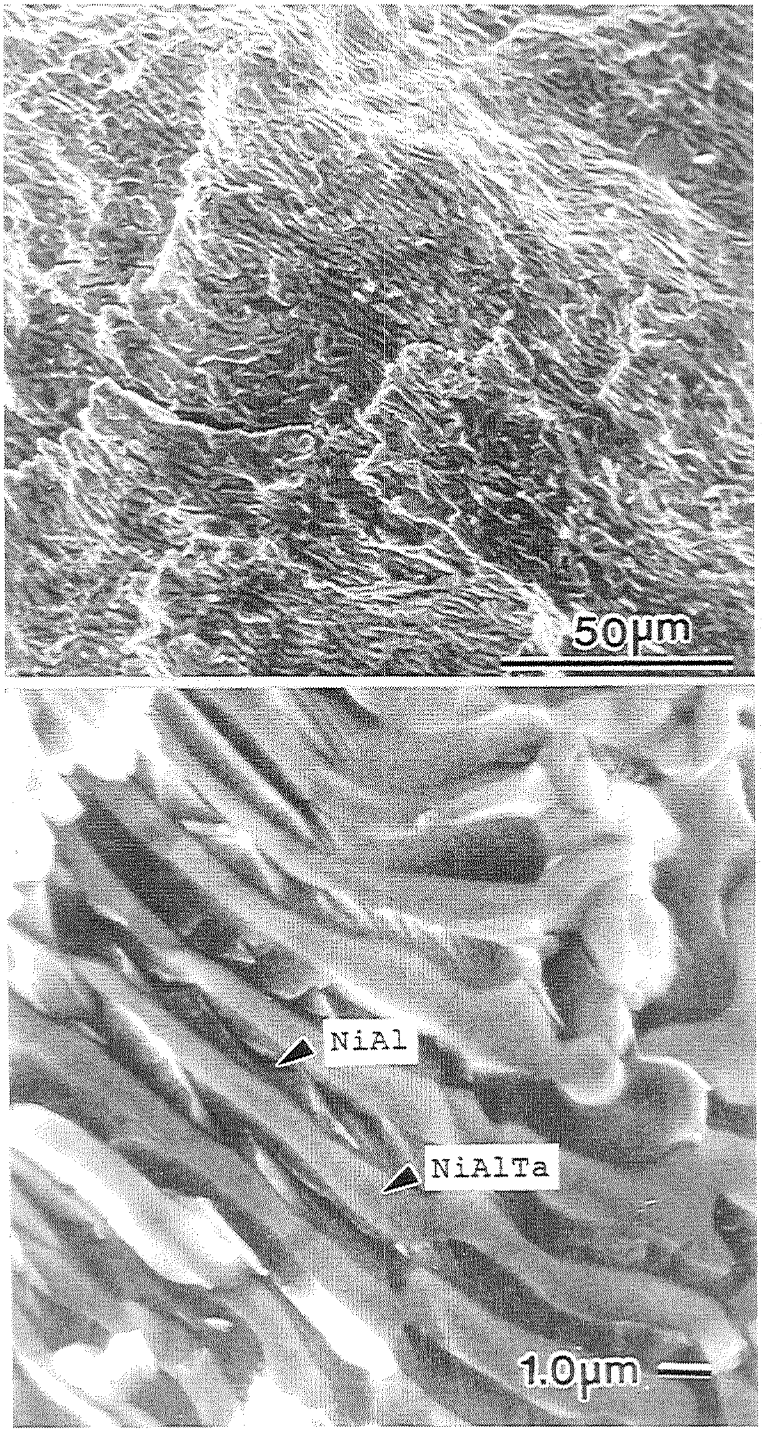

Figure 4.10: SEM photomicrographs of fracture surfaces from a NiAl-14.5Ta bend specimen.

remarkably visible from the fracture surface as a result of partial debonding between phases during fracture. Further evidence of this fracture behavior is shown in Figure 4.11. A section of the directionally solidified NiAl-14.5Ta ingot was polished and then broken with the polished surface in tension. The resulting fracture profile reveals a series of microcracks in the Laves phase with the NiAl phase bridging the crack path. In addition, cracking is also visible along the NiAl/NiAlTa phase boundary.

A high dislocation density was found in NiAl from material taken near the fracture surface of the broken bend specimen as shown in Figure 4.12. The microstructure of NiAl consists of coarse dislocation tangles with the dislocation density greatest in the sections where the NiAl lamella are the thinnest. No precipitates were found in the NiAl phase for all the imaging conditions used. The above data suggest that the NiAl phase provides most of the fracture toughness in these brittle alloys.

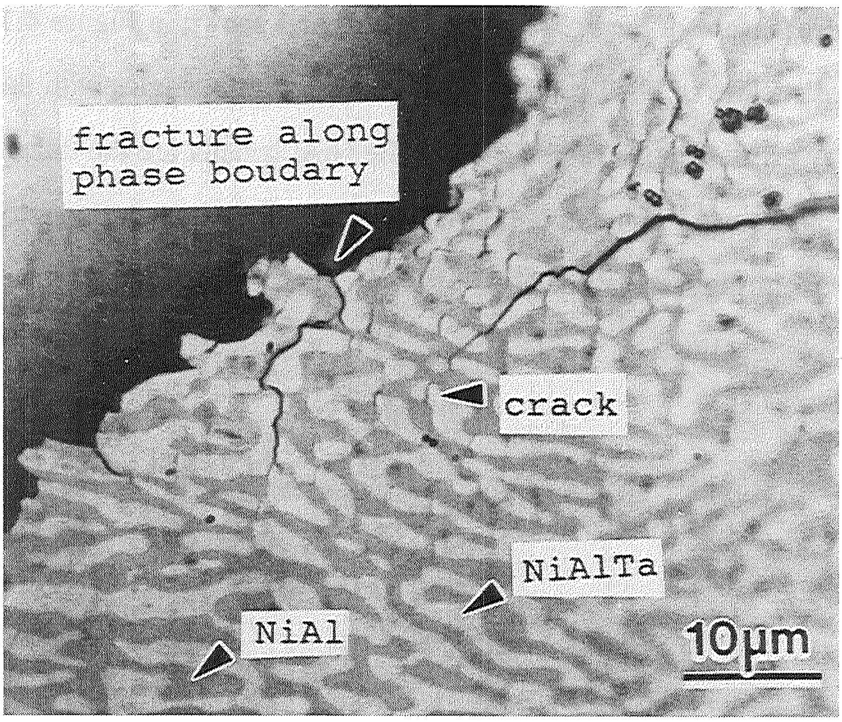

Figure 4.11: Light optical photomicrograph of the fracture region from a directionally solidified NiAl-14.5Ta alloy.

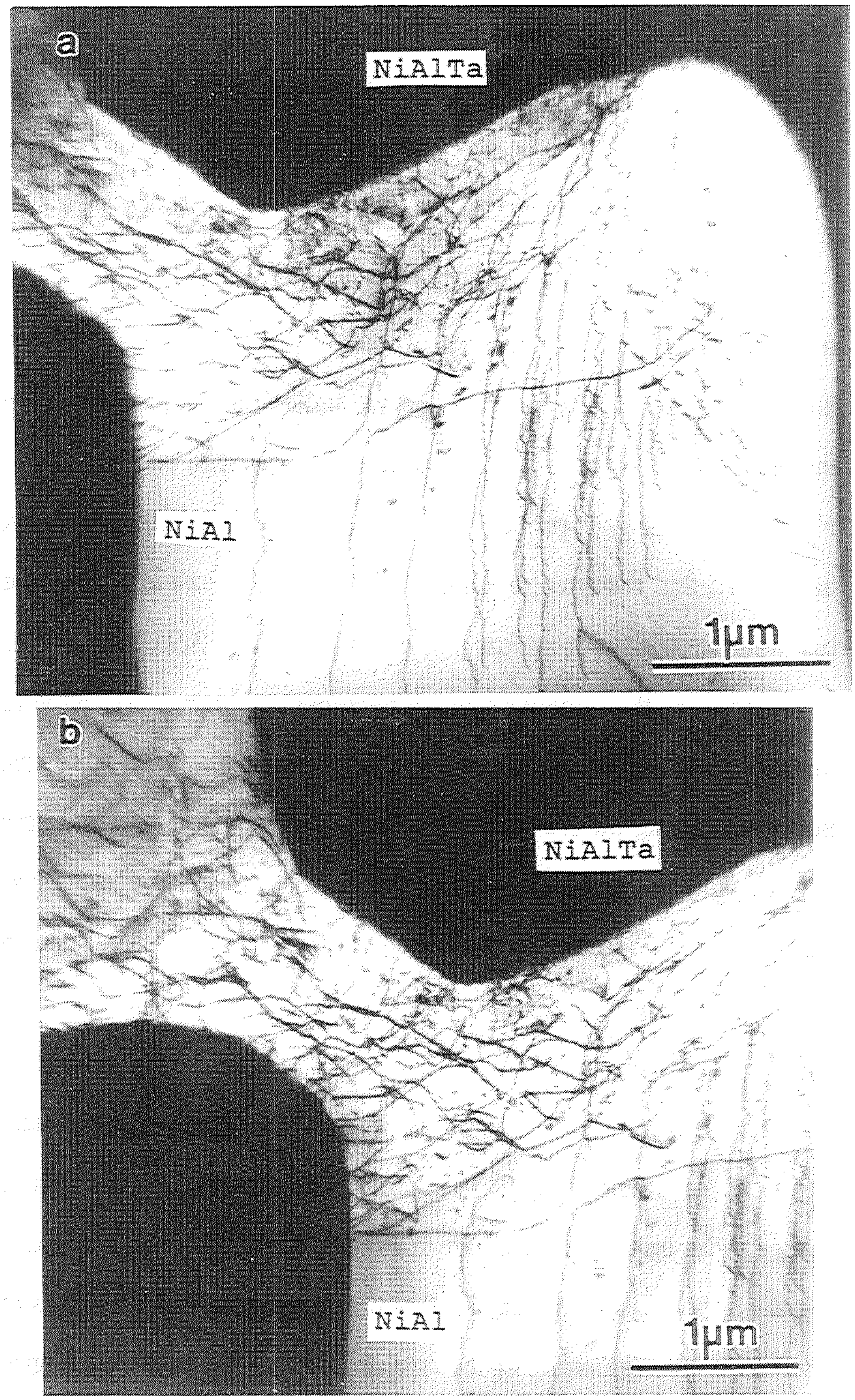

Figure 4.12: TEM photomicrographs of samples taken near the fracture surface of a NiAl-14.5Ta bend specimen.

CHAPTER 6

DISCUSSION

The directionally solidified NiAl-NiAlTa alloys have a very good creep resistance. In fact the 1300 K compressive strength of the fully eutectic NiAl-15.5Ta alloy approaches that of a single crystal nickel-base superalloy, Figure 4.9. The modest improvement in strength of the NiAl-NiAlTa eutectic alloy compared to the NiAl-14.5Ta alloy is probably due to a refinement of the microstructure. Sauthoff has shown that the strength NiAl-Laves alloys follows a simple rule of mixtures behavior except for very fine phase distributions [13,21]. Additional strengthening is provided once the lamellar spacing becomes less than a critical value corresponding to the mean free dislocation path [21]. Klower and Sauthoff have studied the effects of lamellar spacing on the creep behavior for Ni-Al-Fe alloys and have calculated a critical lamellar spacing of 8 μm for additional phase boundary strengthening [22]. The preliminary results for the creep resistance of the NiAl-NiAlTa eutectic with a lamellar spacing of 2-3 μm are consistent with their argument.

However, the directionally solidified NiAl-NiAlTa eutectic has a coarse eutectic spacing when compared to the NiAl-refractory metal eutectics such as the NiAl-(Cr,Mo) eutectic [7]. In addition, the eutectic spacing was relatively coarse even for the quickly cooled, arc-melted NiAl-NiAlTa alloy, Figure 4.3a. Hence, lamellar spacing is not a strong function of processing conditions and further significant strengthening of the eutectic alloy is not expected at greater solidification rates.

One method to further improve the strength of the NiAl-NiAlTa alloys may simply be to improve the strength of the NiAl phase. Promising strengths have been found for two phase material consisting of NiAl and the Heusler precipitate Ni_2AlTa [9]. Hence, alloys heat treated in the three phase region shown in Figure 4.5 may show improved strengths. For example, an arc-melted ingot with the composition near the NiAl-NiAlTa liquidus trough (melt-4 in Figure 4.5) lies well within the NiAl-Ni_2AlTa-NiAlTa region on the 1753 K isotherm. The cast microstructure of this alloy (Figure 4.13) consists mainly of NiAl-NiAlTa dendrites surrounded by an interdendritic Heusler phase, Ni_2AlTa. Post-processing heat treatments of this alloy should produce precipitates of the Heusler phase within the NiAl phase. Alloys with compositions closer to the NiAl-NiAlTa eutectic should contain smaller percentages of the interdendritic Heusler phase. Hence, it may by possible to produce aligned NiAl-NiAlTa microstructures with NiAl strengthened by the precipitates of the Ni_2AlTa phase.

While the NiAl-NiAlTa alloys show promising creep strengths, the room temperature fracture toughness of these alloys is very poor. One scheme for improving the toughness is to include a metallic phase within the NiAl-NiAlTa microstructure as described in Part 5.

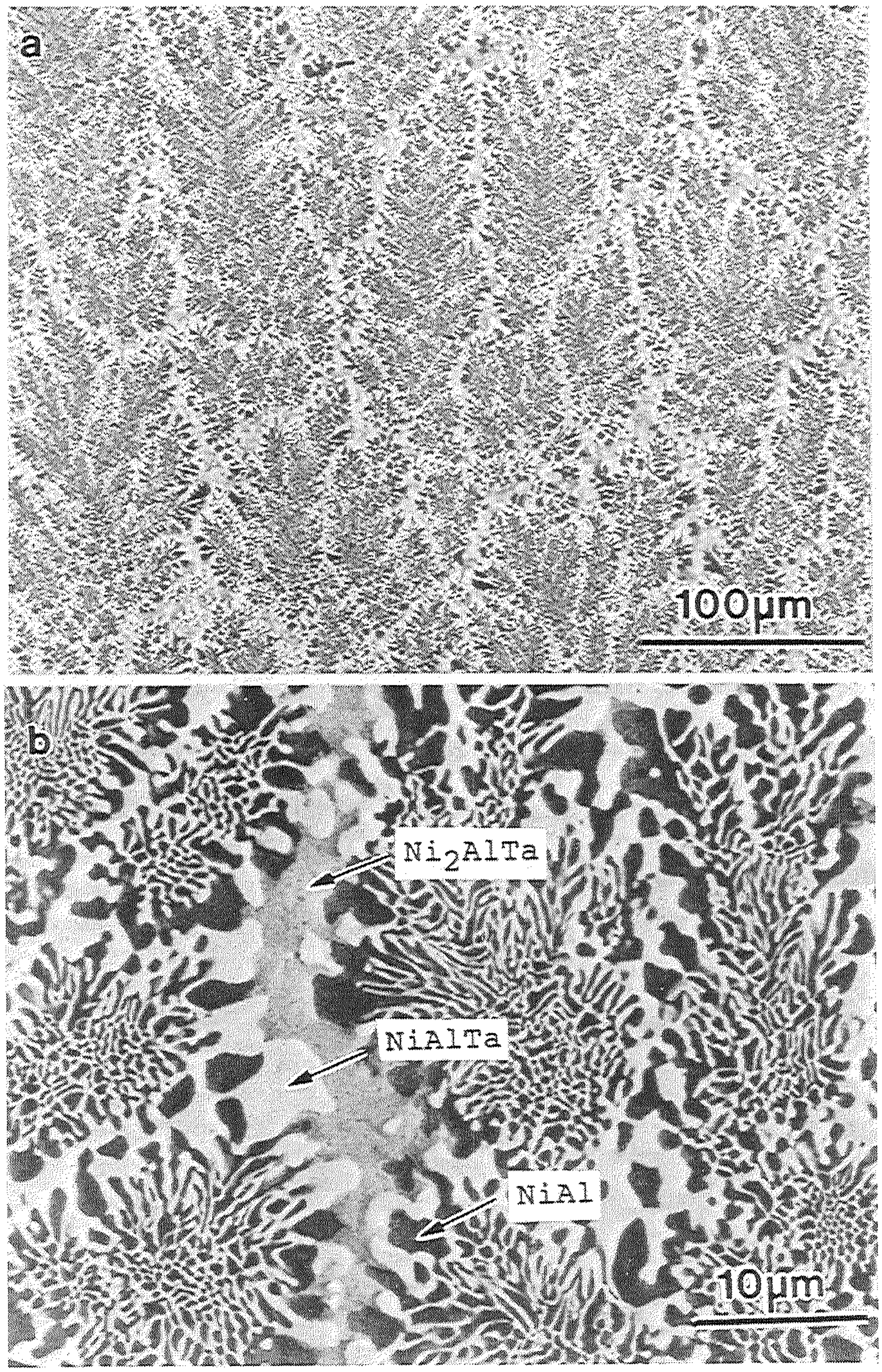

Figure 4.13: SEM backscattered electron photomicrographs of an arc-melted Ni-34Al-19Ta alloy (melt-4) in the as-cast condition.

REFERENCES

1. R. Darolia, JOM 43[3], (1991) 44-49.
2. R.D. Noebe, R.R. Bowman, and M.V. Nathal, Int. Mat. Rev., 38 (1993), 192-232
3. R. Darolia, in Structural Intermetallics, R. Darolia, et al., eds., TMS, Warrendale PA (1993), 495-502.
4. C.T. Liu, JOM 45[5] (1993) 38
5. D.R. Johnson, S.M. Joslin, B.F. Oliver, R.D. Noebe, and J.D. Whittenberger, in First International Conference on Processing Materials For Properties, H. Henein and T. Oki eds., TMS, Warrendale PA (1993), 865-870.
6. R. Darolia, D. Lahrman, and R. Field, Scripta Metall. Mater., 26 (1992), 1007-1012.
7. D.R. Johnson, X.F. Chen, B.F. Oliver, R.D. Noebe, and J.D. Whittenberger, submitted to Intermetallics (1994).
8. W.S. Walston, R.D. Field, J.R. Dobbs, D.F. Lahrman, and R. Darolia, in Structural Intermetallics, R. Darolia, et al., eds., TMS, Warrendale PA (1993),523-531.
9. M. Igarashi and H. Senba, in Structural Intermetallics, R. Darolia, et al., eds., TMS, Warrendale PA (1993), 533-542.
10. R.S. Polvani, Wen-Shian Tzeng, and P.R. Strutt, Met. Trans., 7A (1976), 33-40.
11. G. Sauthoff, Z. Metallkde., 81 (1990), 855-861.
12. G. Sauthoff, in Intermetallic Compounds - Structure and Mechanical Properties, O. Izumi, ed., Japan Institute of Metals, Sendai, Japan (1991), 371-378.
13. G. Sauthoff, in Structural Intermetallics, R. Darolia, et al., eds., TMS, Warrendale PA (1993), 371-378.
14. J.D. Whittenberger, R. Reviere, R.D. Noebe, and B.F. Oliver, Scripta Metall. Mater., 26 (1992), 987-992.
15. P. Nash and D.R.F. West, Met. Sci., 12 (1979), 670-676.
16. J.R. Dobbs, R.D. Field, and D.G. Konitzer, TMS Fall Meeting, Detroit, MI (Oct. 7-11, 1990).
17. J.D. Whittenberger and R.D. Noebe, unpublished data, 1991.
18. M.V. Nathal and L.J. Ebert, Met. Trans., 16A (1985), 427-439.
19. J.E. Hack, J.M. Brzeski, and R. Darolia, Scripta Metall. Mater., 27 (1992), 1259-1263.
20. K.S. Kumar, S.K. Mannan, and R.K. Viswanadham, Acta Metal. Mater., 40 (1992), 1201-1222.
21. Jutta Klower and Gerhard Sauthoff, Z. Metallkde., 82 (1991), 510-518.
22. Jutta Klower and Gerhard Sauthoff, Z. Metallkde., 83 (1992), 699-704.
23. S. Reuss, and H. Vehoff, Scripta Met., 23 (1990), 1021-1026.

PART 5: POLYPHASE IN-SITU COMPOSITES

CHAPTER 1

INTRODUCTION

Polyphase in-situ composites are defined here as directionally solidified eutectics resulting in three or more phases. The basic idea is to include a metal phase for improved room temperature toughness with a number of intermetallic phases for good high temperature properties. For example the NiAl-Cr eutectic described in PART 3 has a promising room temperature fracture toughness while the NiAl-NiAlTa eutectic described in PART 4 has a very good creep strength. Thus, it may be possible to blend the properties of each system in a directionally solidified three phase eutectic, provided such systems thermodynamically exist.

The systems studied were the Ni-Al-Ta-X (X=refractory metal) alloys. In addition to chromium, NiAl undergoes a eutectic reaction with the refractory metals Mo, V, W, and Re [1]. The volume fractions of Re and W are very small in the quasi-binary eutectics. In addition, the oxidation resistance of vanadium is extremely poor. Since the NiAl-V eutectic has a room temperature fracture toughness near 40 $\mathrm{MPa}\sqrt{\mathrm{m}}$ [2], the Ni-Al-Ta-V alloys were studied as a model system. Thus, only the Ni-Al-Ta-X (X=Cr, Mo, or V) systems were considered. Unfortunately, much of the alloying work to date on these systems has considered only the nickel rich alloys [3-6].

CHAPTER 2

EXPERIMENTAL PROCEDURES

As a first approach to locating promising microstructures for in-situ composites studied, exploratory arc-melts containing high purity Ni, Al, Ta, Cr, Mo, and V were made. These ingots were metallographically examined for evidence of eutectic-like microstructures. Alloy compositions were then varied to increase the eutectic volume fraction.

Since the arc-melted ingots had an extremely fine microstructure, a coarsening heat treatment was performed to better characterize the microstructure. Heat treatments were performed in an induction furnace using a helium atmosphere. Specimens were wrapped in tantalum foil and placed in an alumina crucible that was surrounded by a graphite susceptor. Temperature measurements were made with an optical pyrometer assuming black body conditions at the gap between the alumina crucible and the graphite susceptor.

Small inductions melts (25 grams) were also made from promising alloy compositions to better characterize the solidification microstructure. The induction melts were allowed to cool within the alumina crucible providing a much slower cooling rate and coarser microstructure than the arc-melted ingots. Lastly, selectively chosen alloys were directionally solidified at 19 mm/h to produce near-equilibrium microstructures. Preliminary mechanical property testing and microstructural characterization as described in PART 2 were performed on these directionally solidified alloys.

CHAPTER 3

MICROSTRUCTURES

Ternary eutectic microstructures consisting of NiAl, a Laves phase, and a metal phase were found in all three of the Ni-Al-Ta-X (X=Cr,Mo,V) systems. The eutectic microstructure from each system is shown in Figure 5.1. The approximate eutectic composition, melting point of each eutectic and the volume fraction of each phase are all listed in Table 5.1. Identification of each phase was determined from X-ray diffractometer scans performed at NASA Lewis Research Center. The Laves phase in all three alloys was found to have the hexagonal C14 crystal structure with lattice parameter values near a=0.49 and c=0.80 nm. The melting point of each alloy was determined by differential thermal analysis (DTA) and these results are listed in Appendix B. The volume fraction of each phase was measured from SEM backscattered electron photomicrographs and was also calculated by the lever rule using the phase compositions from energy dipersive x-ray analysis (EDS) results.

Substantial solid solutions are possible in the Laves phase and the body centered refractory metals. However, for convenience the C14 Laves phase is denoted by "NiAlTa" in the following photomicrographs. The body centered solid solutions are denoted by the element present in the greatest atomic fraction.

Ni-Al-Ta-Mo system

Alloys examined in this system are plotted on the NiAl-Ta-Mo composition triangle as shown in Figure 5.2. The large undercooling provided by the water cooled hearth during arc-melting produced microstructures that were difficult to characterize. Over a wide composition range, the material that solidified adjacent to the water cooled hearth consisted of an eutectic-like microstructure whereas the rest of

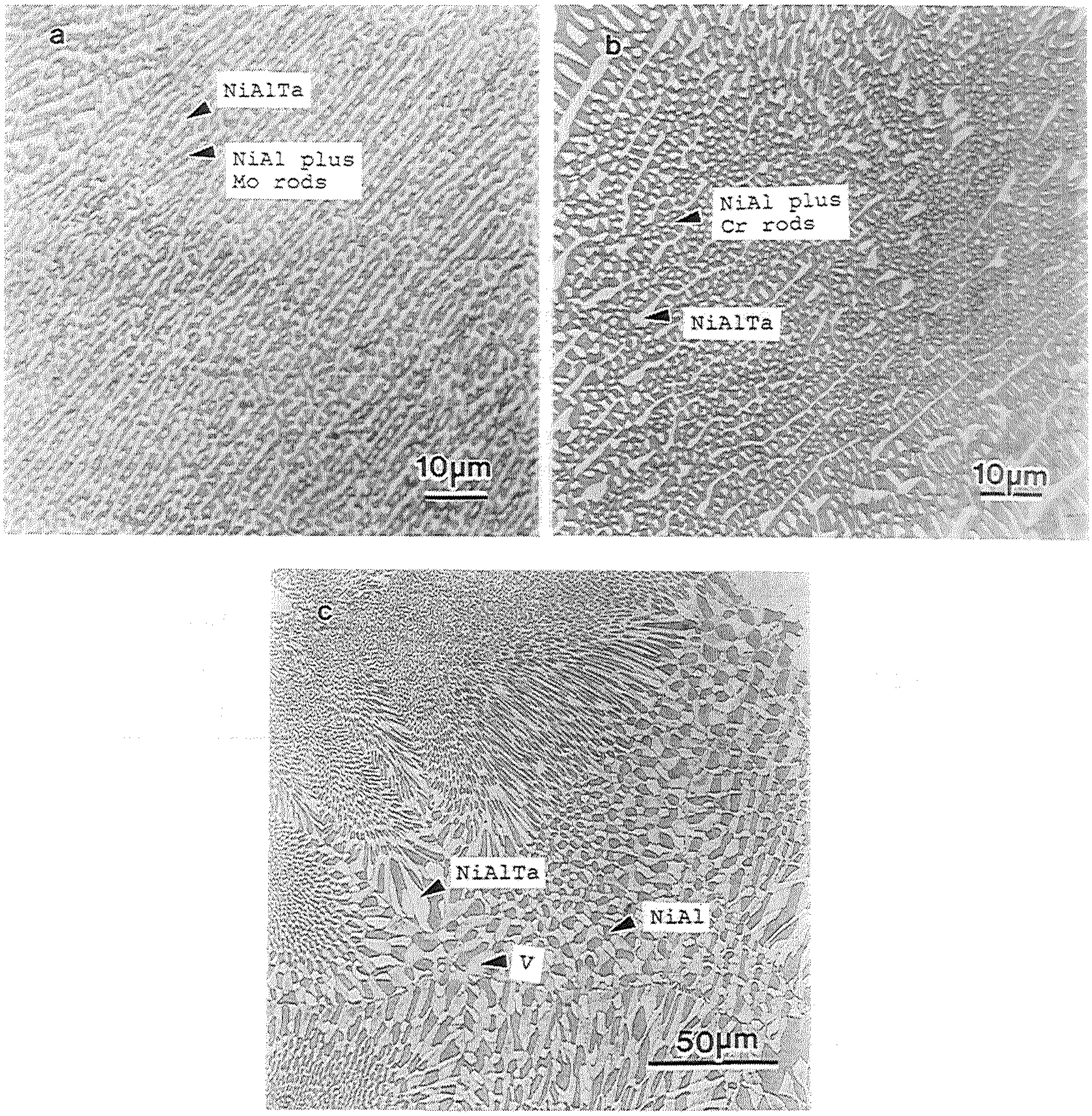

Figure 5.1: Light optical photomicrograph of ternary eutectics consisting of NiAl, a Laves phase, and a refractory metal.
(a) NiAl-NiAlTa-(Mo,Ta)
(b) NiAl-(Cr,Al)NiTa-Cr
(c) NiAl-NiAlTa-V

Table 5.1: Melting point and volume fraction of each phase for ternary eutectics in the NiAl-NiAlTa-refactory metal systems. Values for the volume fraction calculated by the lever rule are enclosed by parentheses.

		Volume Fraction		
Alloy (at%)	Melting point (K)	NiAl	Laves	Metal
Ni-42Al-12.5Ta-7Mo	1800	57 (60)	33 (29)	10 (11)
Ni-30.5Al-6Ta-33Cr	1700	40 (53)	25 (17)	35 (30)
Ni-28.5Al-10Ta-33V	1615	24 (26)	32 (29)	44 (45)

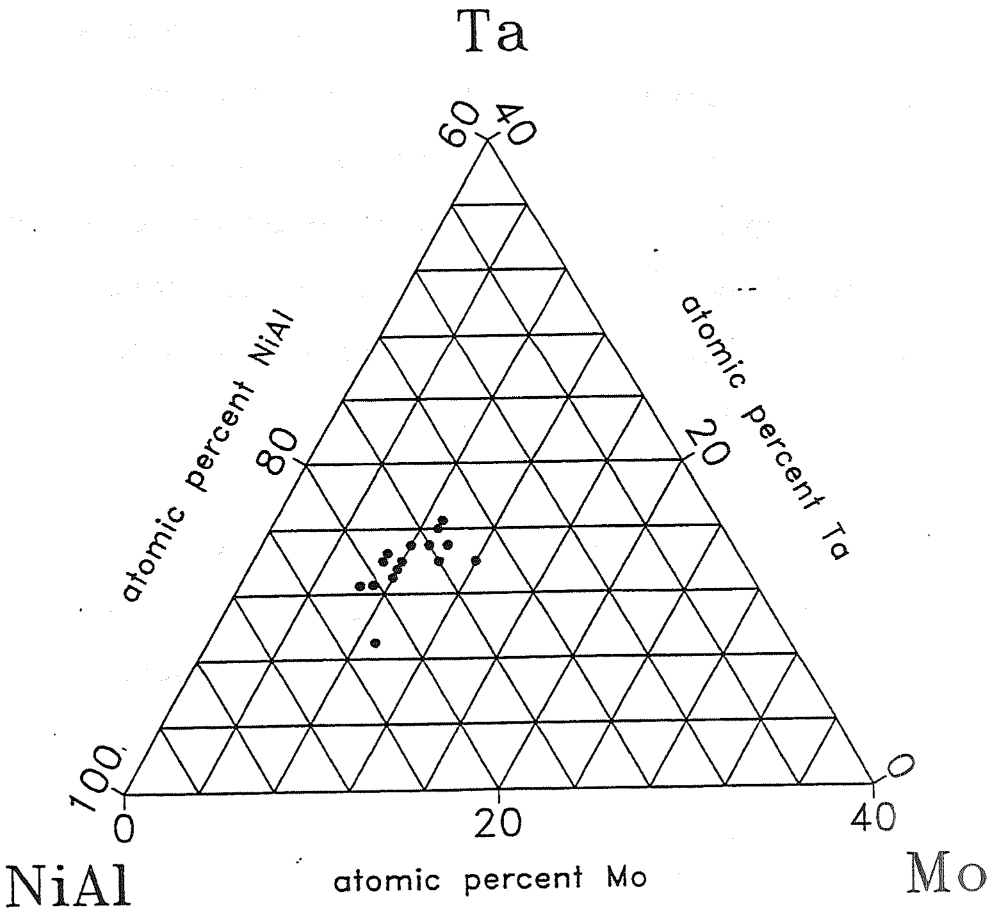

Figure 5.2: Compositions of arc-melted ingots made in the NiAl-Mo-Ta system.

the ingot was dendritic in nature. A composition of Ni-42Al-12.5Ta-7.0Mo (at.%) resulted in the largest volume fraction of eutectic material in either the arc-melted or induction melted ingots. However, the melting temperature (1800 K) of this alloy was greater than that of the NiAl-Mo eutectic (1778 K), indicating an off-eutectic composition. Ingots of this composition were directionally solidified at 19, 25, and 100 mm/h for mechanical property testing.

The longitudinal microstructure from a directionally solidified ingot is shown in Figure 5.3. The NiAl-NiAlTa-(Mo,Ta) ternary eutectic consists of a lamellar microstructure between NiAl and NiAlTa. A fibrous morphology is found for the molybdenum-rich solid solution that is surrounded completely by NiAl. The slow processing speed of 19 mm/h produced the best aligned microstructure. The directionally solidified microstructure consisted of some regions of well aligned three phase material while other areas contained NiAl+(Mo,Ta) two phase dendrites and the two phase NiAl-NiAlTa eutectic microstructure.

The phase compositions were determined for an arc-melted ingot heat treated at 1673 K for 14.4×10^3 s (4 hours). These results along with a schematic of the projected liquidus troughs are shown in Figure 5.4. The relative amounts of each phase determined by lever rule calculations and by the area fractions measurements are comparable, Table 5.1.

Ni-Al-Ta-Cr system

Alloys examined in the Ni-Al-Ta-Cr systems are plotted in the composition triangle shown in Figure 5.5. Arc-melted ingots in this system were much easier to produce than the Ni-Al-Ta-Mo systems since no abrupt changes in microstructure were observed. An ingot with a composition of Ni-33Al-28Cr-6Ta (at.%) was directionally solidified at 19 mm/h for further study.

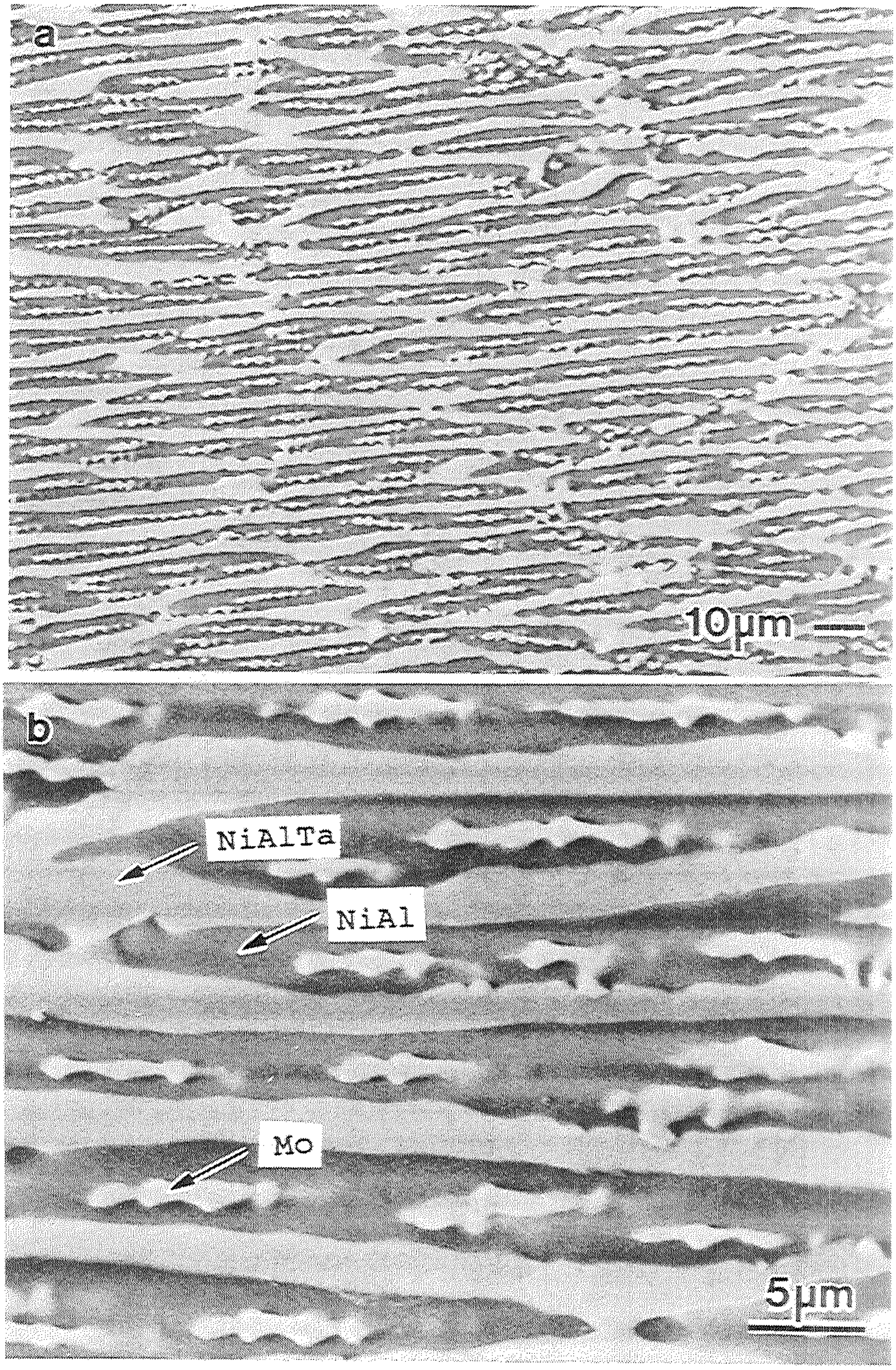

Figure 5.3: Longitudinal SEM photomicrographs of the directionally solidified NiAl-NiAlTa-(Mo,Ta) eutectic.

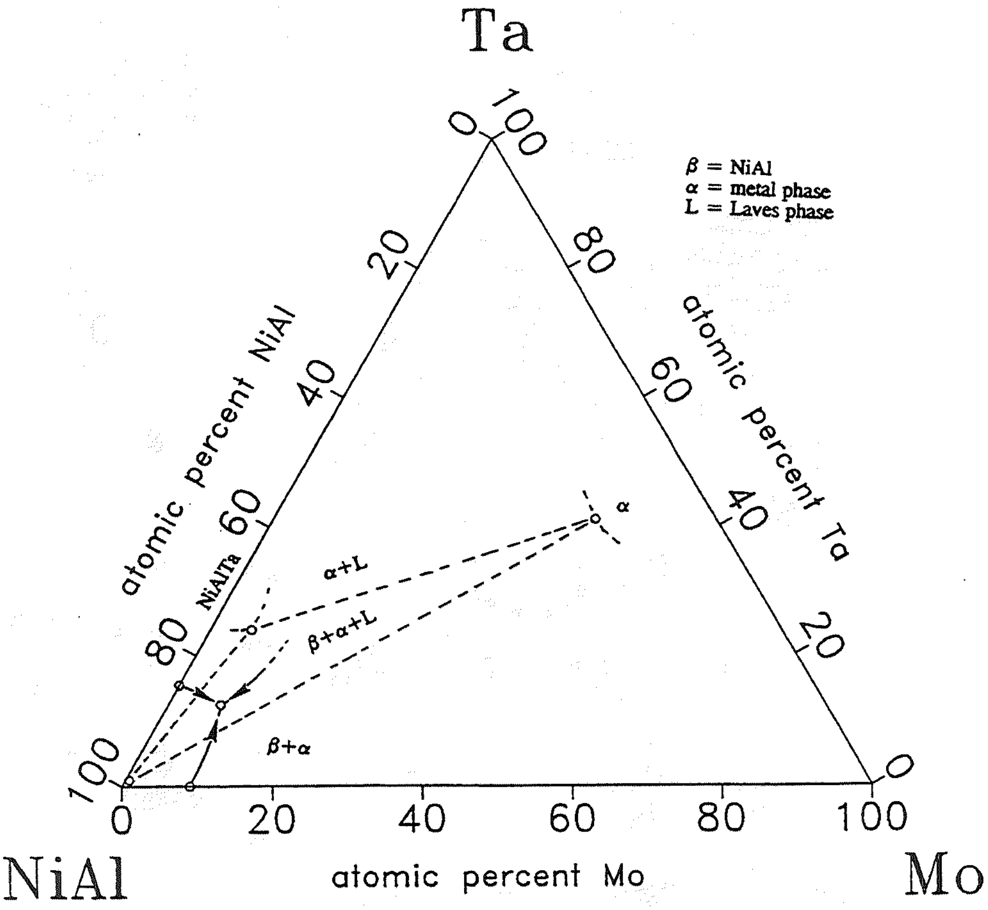

Figure 5.4: Compositions of the eutectic phases at 1673 K and a schematic of the projected liquidus troughs in the NiAl-Mo-Ta system.

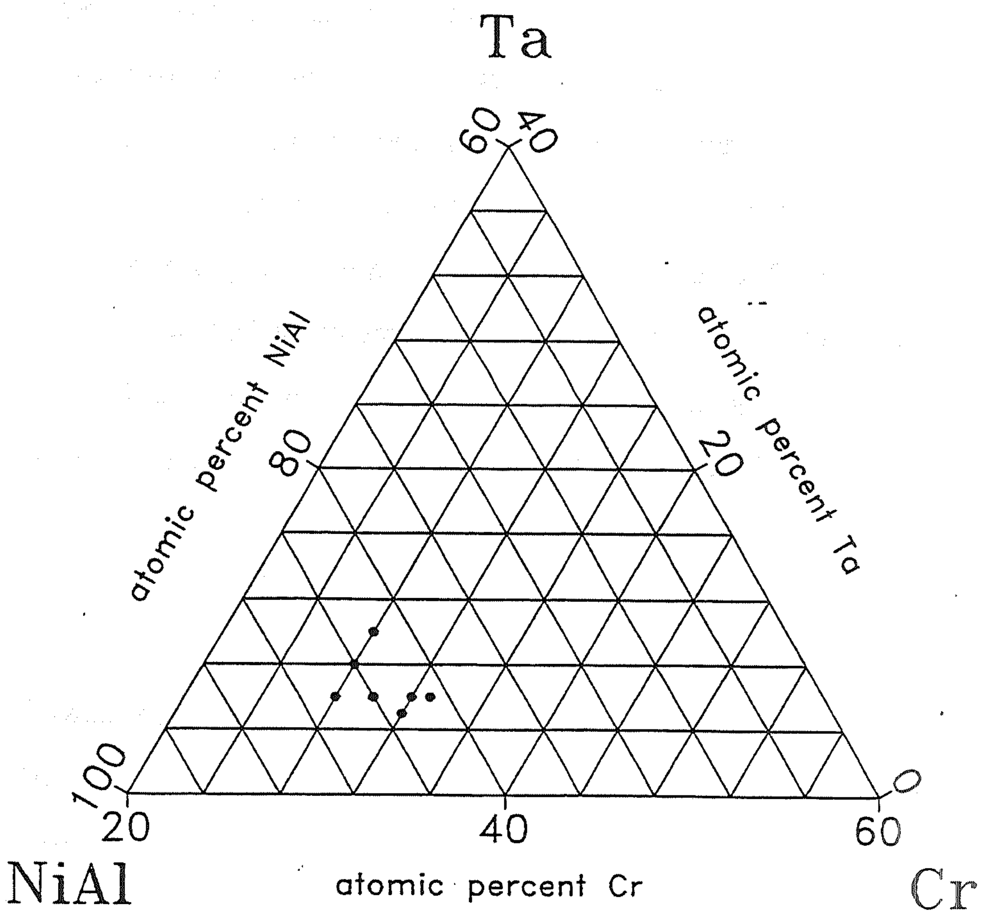

Figure 5.5: Compositions of arc-melted ingots made in the NiAl-Cr-Ta system.

The longitudinal microstructure from the directionally solidified ingot is shown in Figure 5.6. The microstructure of this ingot was essentially all eutectic. The NiAl-(Cr,Al)NiTa-Cr ternary eutectic consists of an NiAl matrix containing chromium rods and laths of the Laves phase. The morphology of this eutectic is more clearly shown in Figure 5.7. The greater resolution of the TEM image more clearly shows the fine structure.

The phase compositions were determined for an arc-melted ingot heat treated at 1673 K for 14.4×10^3 s (4 hours). These results along with a schematic of the projected liquidus troughs are shown in Figure 5.8. The relative amounts of each phase determined by the lever rule differed from those determined from the area fractions. The difference in these values are probably due to errors in measuring the area fractions. The atomic number contrast of the NiAl and chromium phases were similar making an accurate determination from the SEM backscattered electron image difficult. As indicated in Figure 5.8, a possible continuous solid solution between the NiAlTa and the Ta_2Cr Laves phases exists.

Ni-Al-Ta-V system

Compositions studied in the Ni-Al-Ta-V systems are shown in Figure 5.9. Based on the survey study, a near eutectic composition of Ni-28.5Al-10Ta-33V was directionally solidified at 19 mm/h for further study. The microstructure of the directionally solidified ingot consisted of vanadium-rich dendrites surrounded by cells or colonies of the three phase eutectic. The eutectic cells were not aligned along the growth axis of the ingot. The eutectic microstructure is shown in Figure 5.10. This eutectic is different than the previous two in that the Laves phase contacts both the NiAl and the metal phase. The eutectic microstructure is characterized by a lamellar morphology between the between NiAl and vanadium-rich metal phase with the Laves phase having an faceted rod type morphology. Figure 5.10 consists of longitudinal

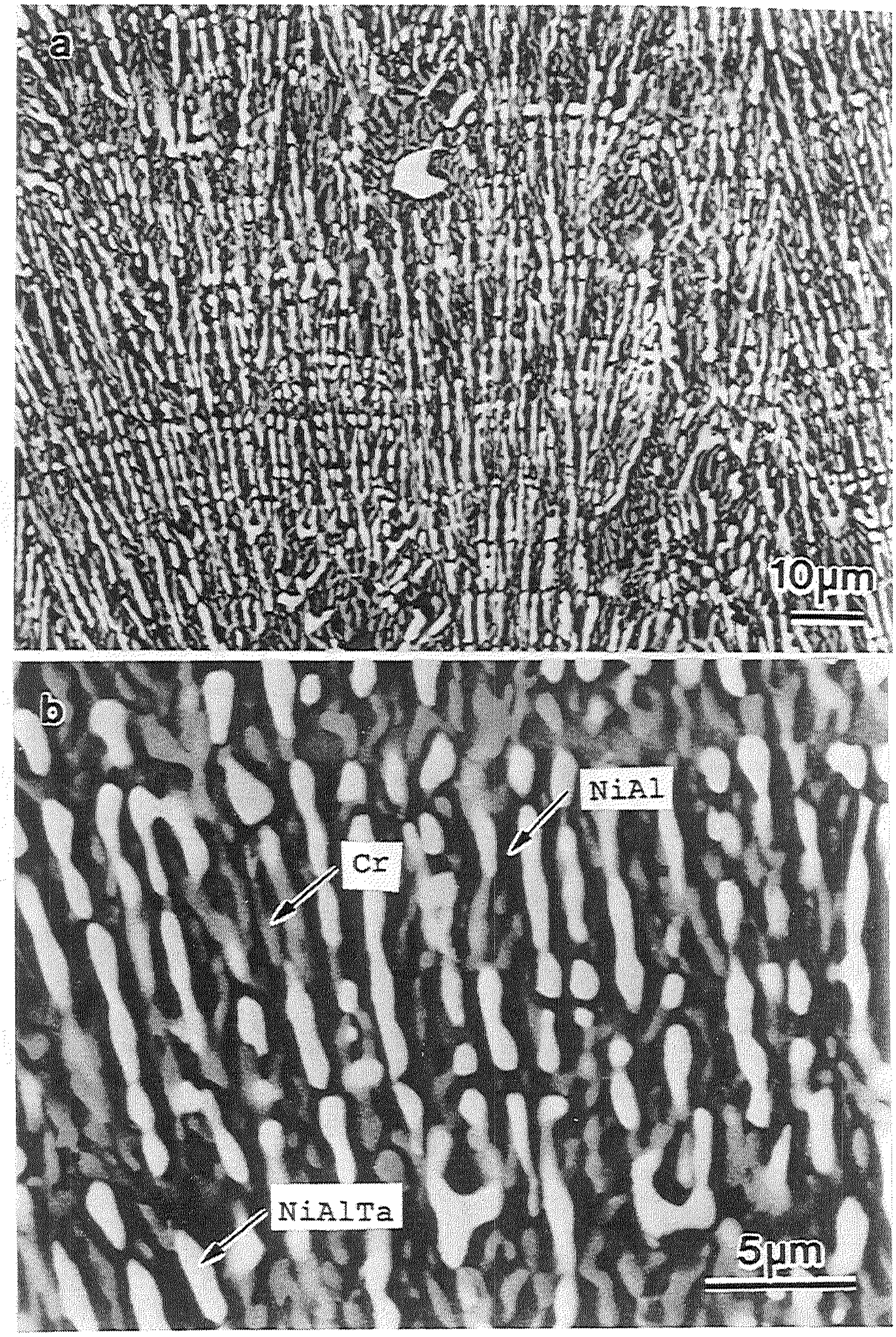

Figure 5.6: Longitudinal SEM photomicrographs of the directionally solidified NiAl-(Cr,Al)NiTa-Cr eutectic.

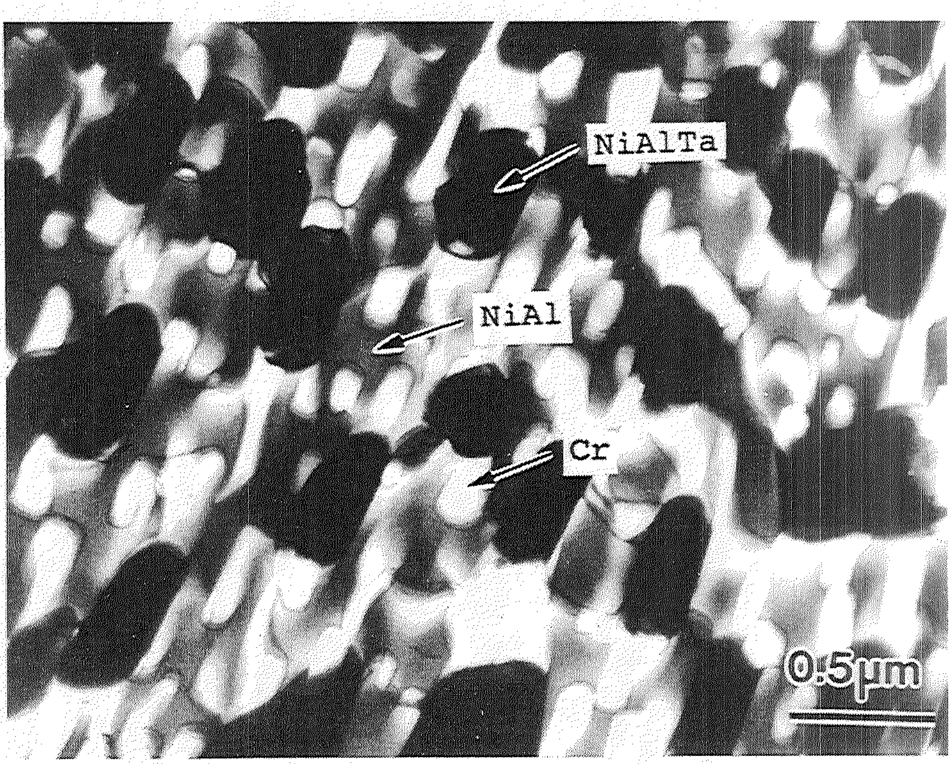

Figure 5.7: TEM photomicrograph of an arc-melted NiAl-(Cr,Al)NiTa-Cr eutectic.

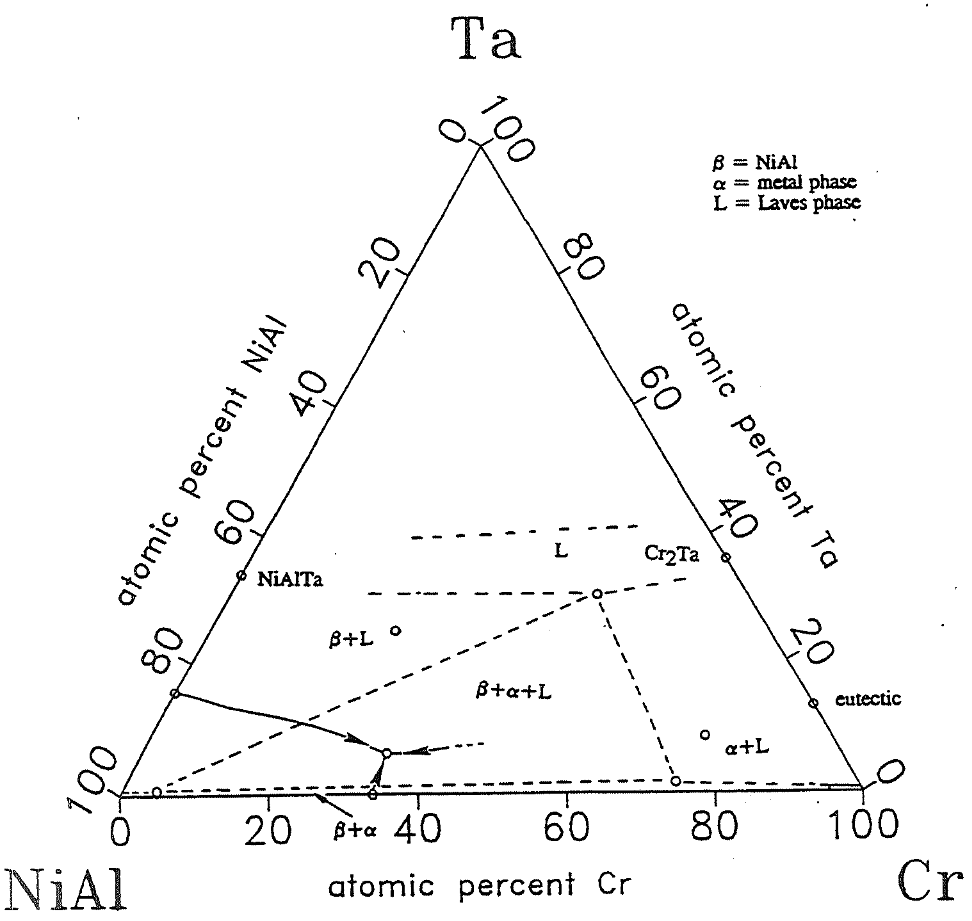

Figure 5.8: Compositions of the eutectic phases at 1673 K and a schematic of the projected liquidus troughs in the NiAl-Cr-Ta system.

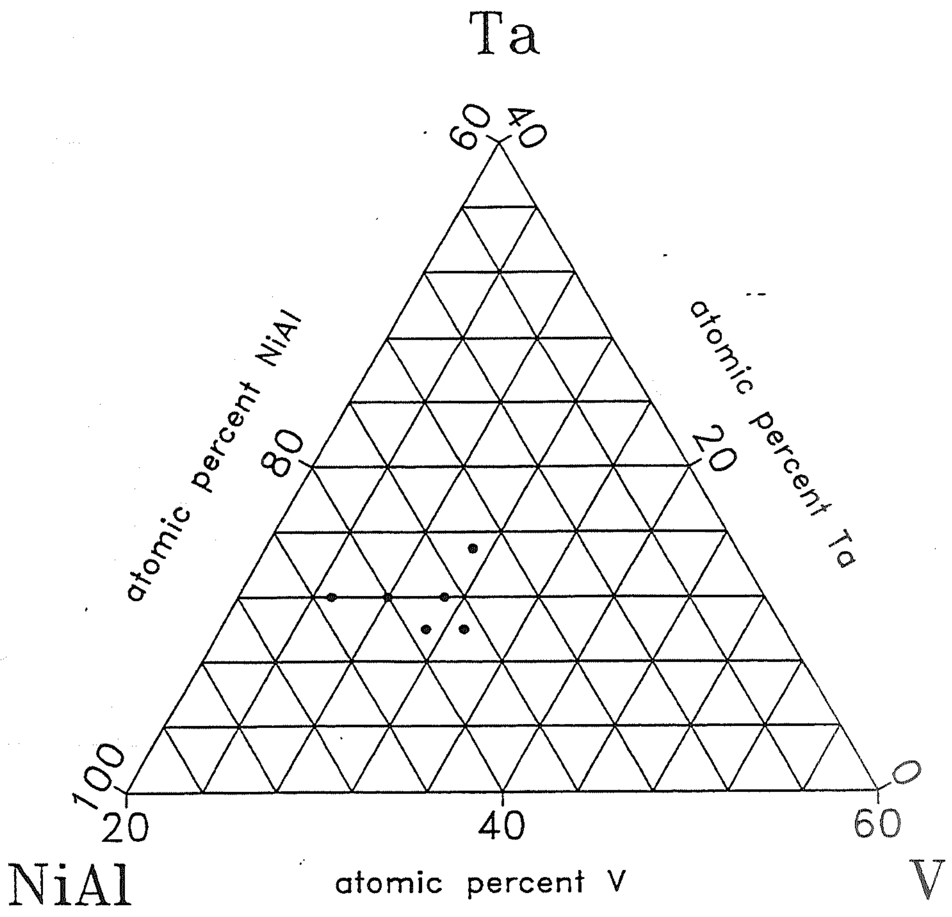

Figure 5.9: Compositions of arc-melted ingots made in the NiAl-V-Ta system.

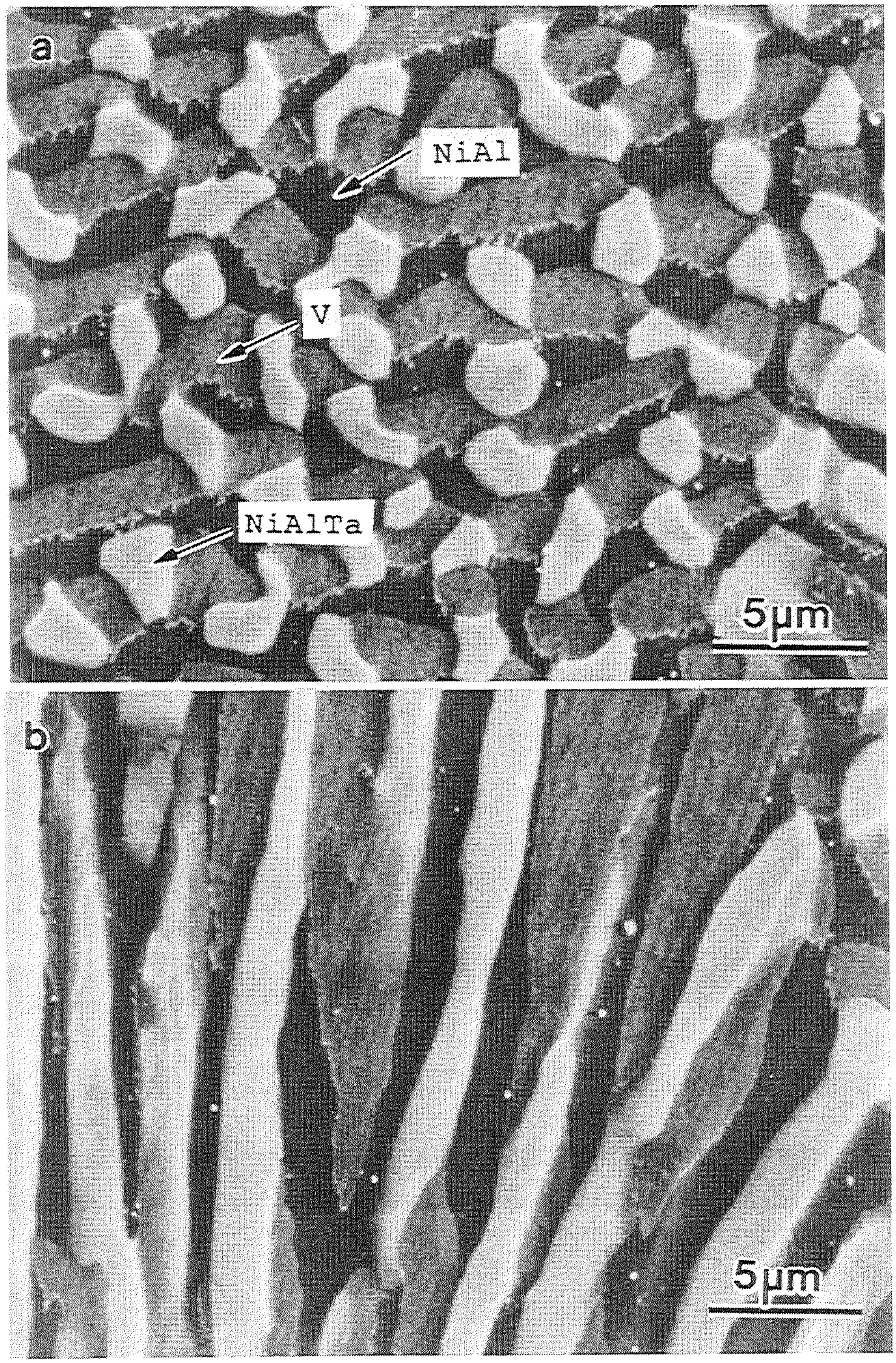

Figure 5.10: Longitudinal SEM photomicrographs of the directionally solidified NiAl-NiAlTa-V eutectic.

microstructures taken from two different sections of the directionally solidified ingot. The change in microstructure between these two sections is due to the poor alignment of the directionally solidified eutectic microstructure.

The phase compositions determined from an arc-melted ingot heat treated at 1533 K for 14.4×10^3 s (4 hours) are shown in Figure 5.11 along with a schematic of the projected liquidus troughs. The relative amounts of each phase as determined by the lever rule calculations and area fractions measurements are in excellent agreement, Table 5.1.

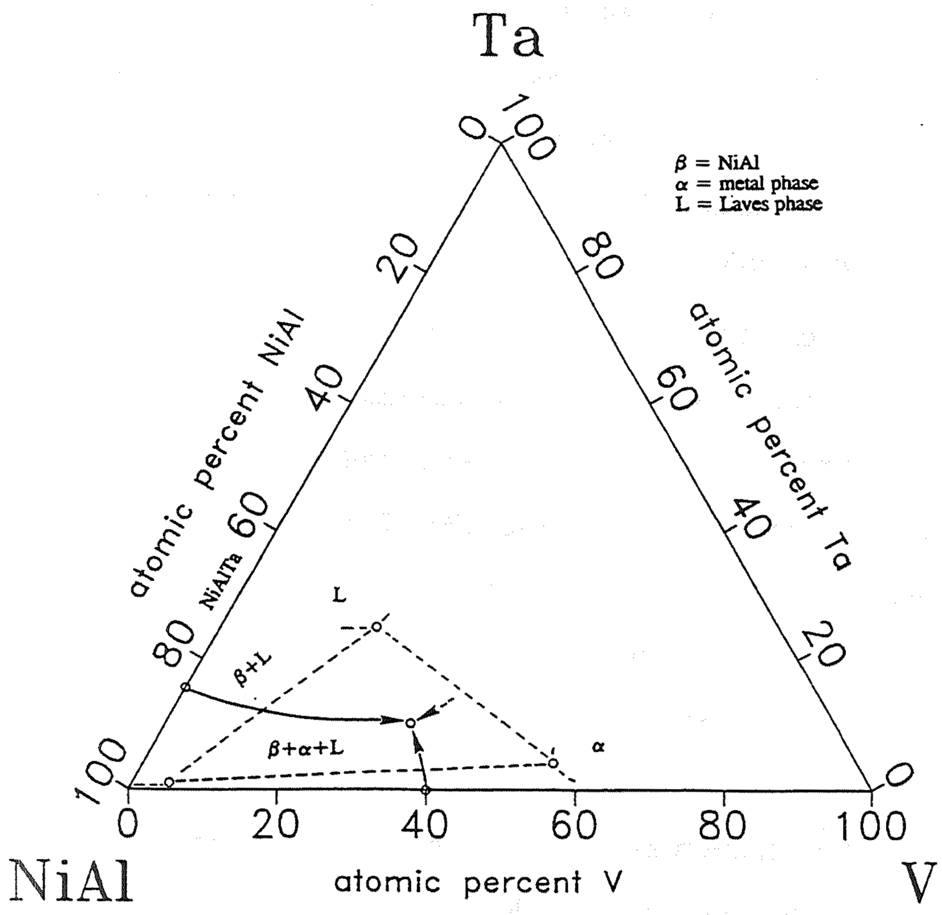

Figure 5.11: Compositions of the eutectic phases at 1533 K and a schematic of the projected liquidus troughs in the NiAl-V-Ta system.

CHAPTER 4

ELEVATED TEMPERATURE STRENGTH

Compressive creep strength of the NiAl-Ta-Mo and the NiAl-Ta-Cr alloys was determined within the temperature range of 1100 to 1400 K. The flow stress and strain rate data for these alloys were fitted to the standard power law equations as previously described in Parts 3 and 4. The creep characteristics for the ternary eutectics are listed in Table 5.2 and the corresponding data over the temperature range of 1100 to 1400 K are plotted in Figures 5.12. and 5.13.

For the NiAl-(Cr,Al)NiTa-Cr eutectic, there may be two creep regimes characterized by similar activation energies but having different stress exponents. A similar result is found for the NiAl-NiAlTa-(Mo,Ta) eutectic where a different equation is needed to describe the 1200 K creep behavior. The lower stress exponent at low deformation rates are likely due to a decrease in the ductile to brittle transition temperature (DBTT) of the ternary eutectic alloys compared to the NiAl-NiAlTa binary system. Sauthoff has shown that DBTT is a function of deformation rates in the NiAl-NiAlTa alloys and decreases with smaller percentages of the Laves phase [6]. The volume fraction of Laves phase in both ternary eutectics is less than that of the NiAl-NiAlTa eutectic, Table 5.1.

In Figure 5.14 and 5.15, the 1300 K compressive strength of both the NiAl-NiAlTa-(Mo,Ta) and the NiAl-(Cr,Al)NiTa-Cr eutectics are compared to single crystal NiAl and the NiAl-NiAlTa eutectic. The 1300 K creep strength of both ternary eutectics are substantially greater than that of binary NiAl but are less than that of the NiAl-NiAlTa eutectic.

Table 5.2: Representative creep behavior of NiAl-(Cr,Al)NiTa-Cr and NiAl-NiAlTa-(Mo,Ta) eutectic alloys.

Alloy	Representative creep behavior
NiAl-(Cr,Al)NiTa-Cr	1100-1300 K
	high stress exponent regime $\dot{\varepsilon} = (9.43\mathrm{x}10^{-13})\sigma^{10.29}\mathrm{exp}(-422.2/RT)$
	low stress exponent regime $\dot{\varepsilon} = (7.84)\sigma^{5.22}\mathrm{exp}(-445.2/RT)$
NiAl-NiAlTa-(Mo,Ta)	
	1200 K $\dot{\varepsilon} = (2.13\mathrm{x}10^{-22})\sigma^{6.18}$
	1300-1400 K $\dot{\varepsilon} = (7.73\mathrm{x}10^{-2})\sigma^{3.6}\mathrm{exp}(-317.9/RT)$

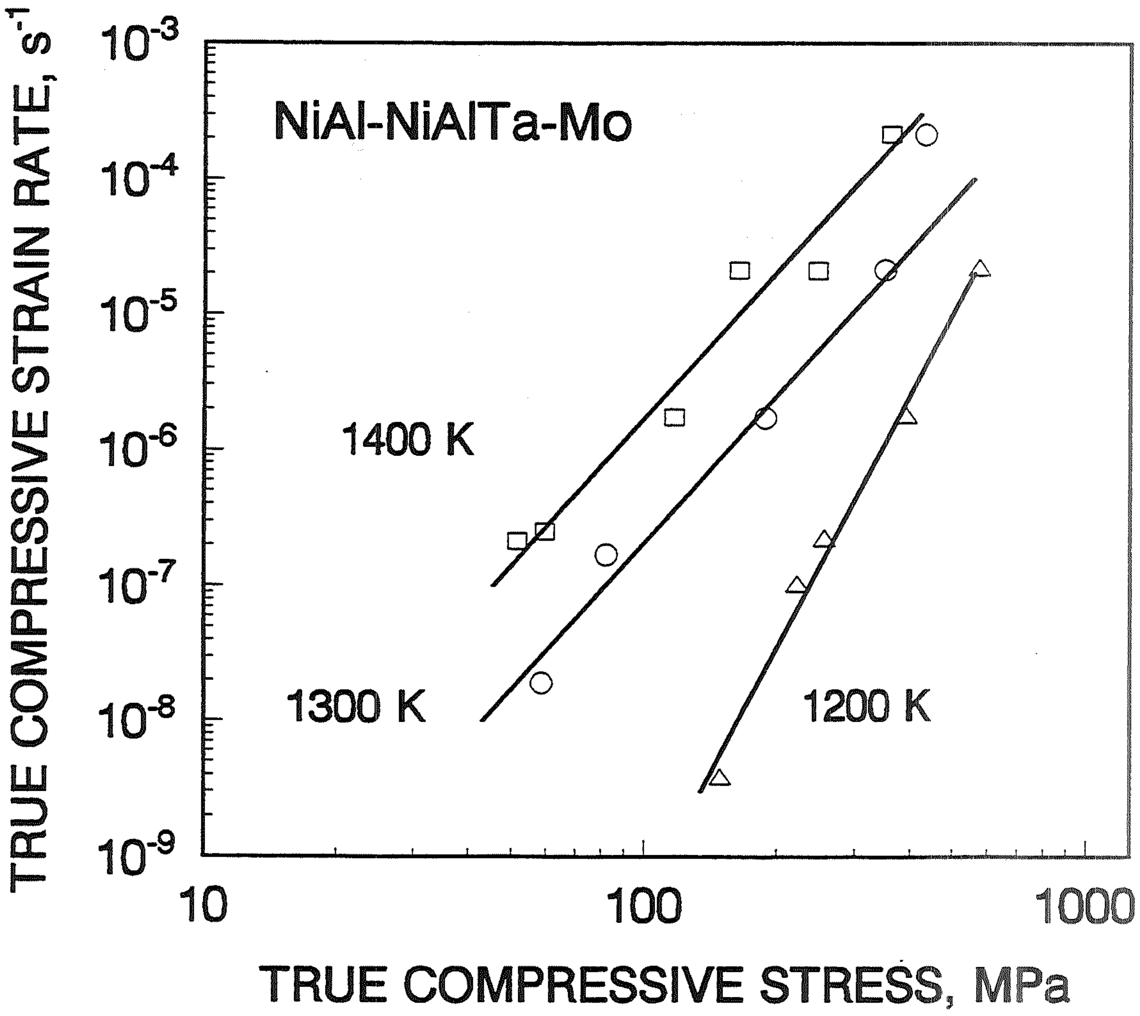

Figure 5.12: Compressive flow stress-strain rate behavior for the NiAl-NiAlTa-(Mo,Ta) eutectic as a function of temperature.

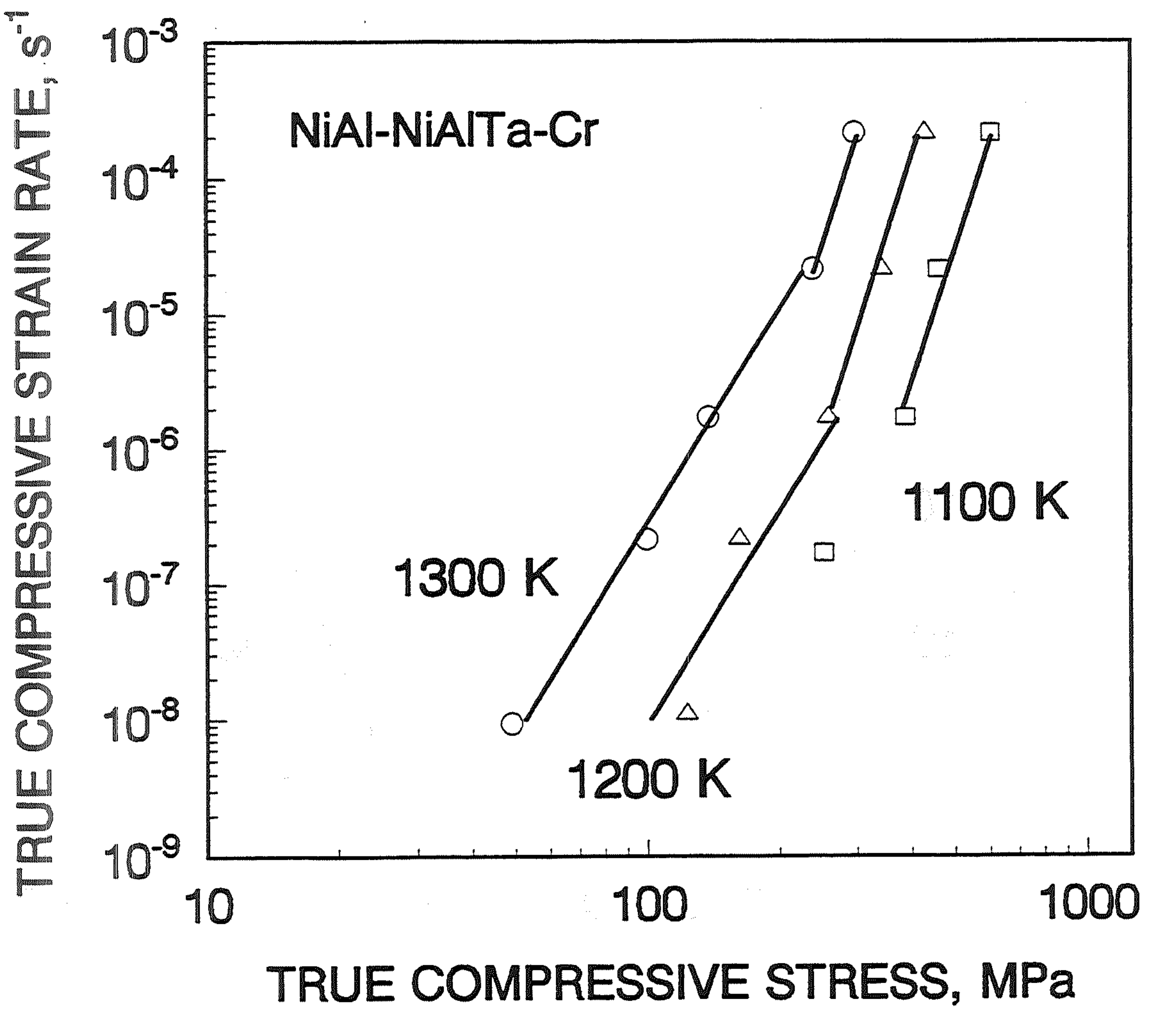

Figure 5.13: Compressive flow stress-strain rate behavior for the NiAl-(Cr,Al)NiTa-Cr eutectic as a function of temperature.

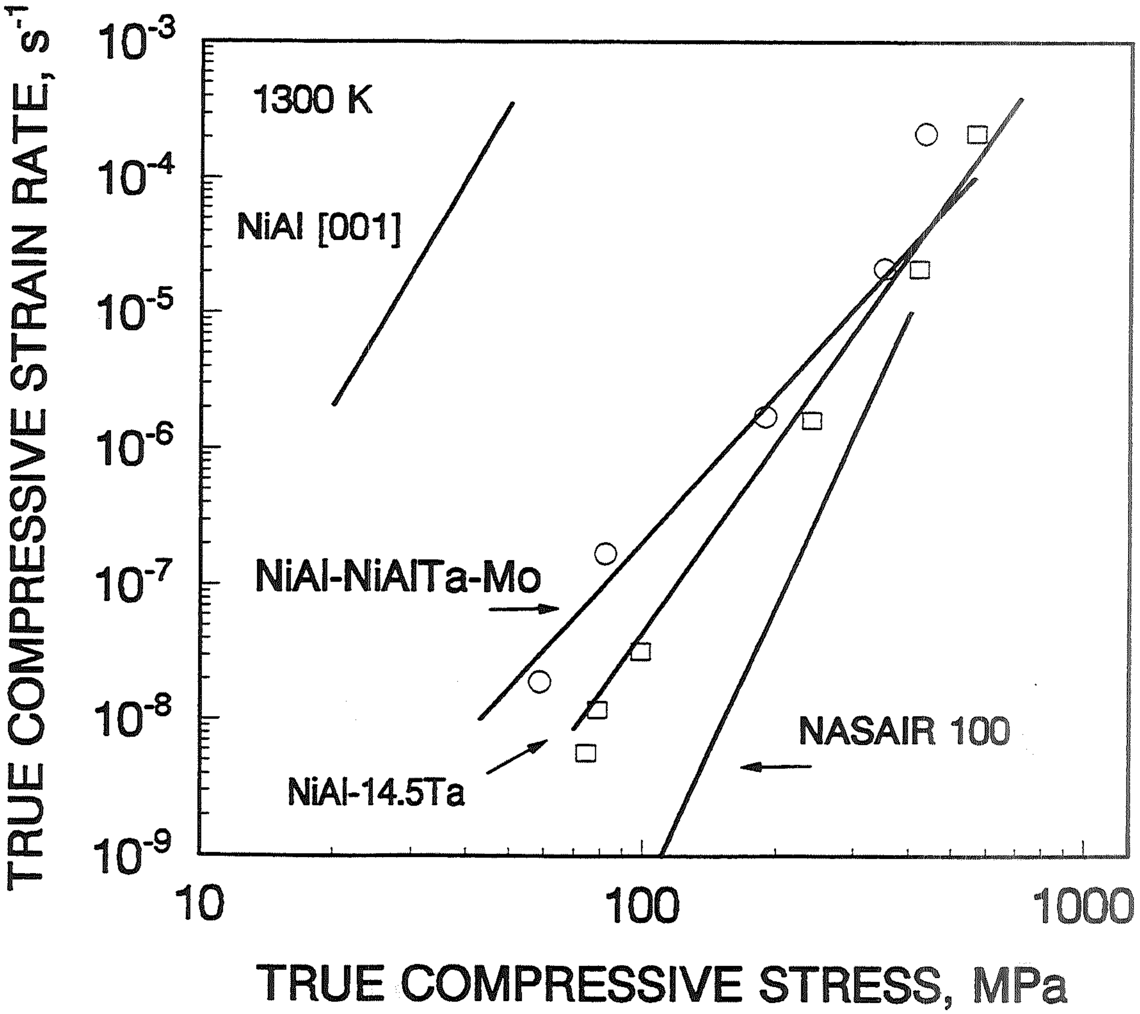

Figure 5.14: 1300 K compressive flow stress-strain rate behavior for the NiAl-NiAlTa-(Mo,Ta) ternary eutectic compared to NiAl and the NiAl-NiAlTa eutectic.

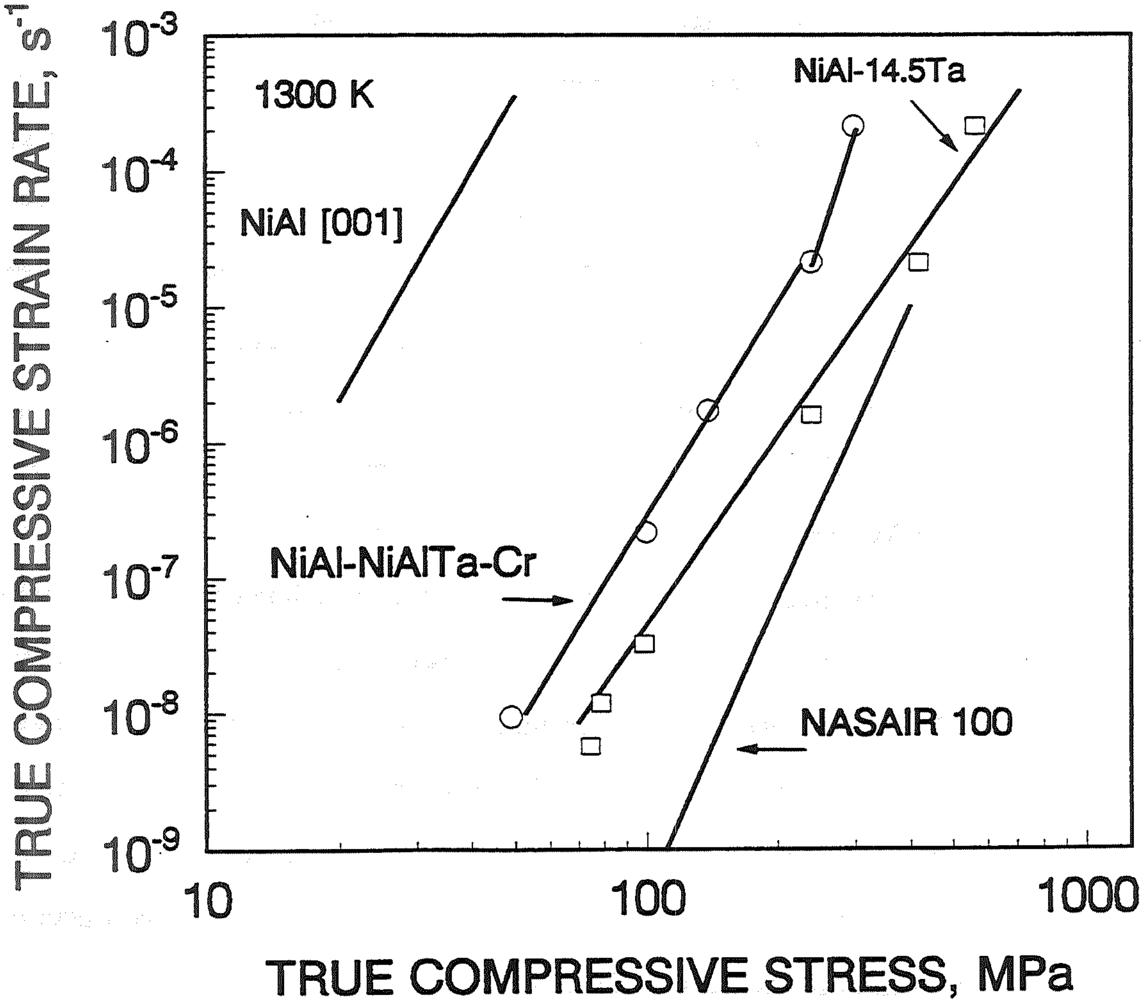

Figure 5.15: 1300 K compressive flow stress-strain rate behavior for the NiAl-(Cr,Al)NiTa-Cr ternary eutectic compared to NiAl and the NiAl-NiAlTa eutectic.

CHAPTER 5

ROOM TEMPERATURE TOUGHNESS

The room temperature fracture toughness values for the NiAl-NiAlTa-refractory metal eutectics are listed in Table 5.3. The fracture toughness of the NiAl-(Cr,Al)NiTa-Cr eutectic (15 MPa√m) lies in between that of the NiAl-NiAlTa eutectic (5 MPa√m) and that of the NiAl-Cr eutectic (20 MPa√m). However the fracture toughness for the NiAl-NiAlTa-(Mo,Ta) and NiAl-NiAlTa-V eutectics were only slightly greater than that of the NiAl-NiAlTa eutectic.

Since the composition of the directionally solidified NiAl-Ta-Mo ingot was off eutectic, a number of heat treatments were performed in an attempt to increase the volume fraction of the metal phase. It was hoped that by heat treating in the three phase region below the ternary eutectic point, a more homogenous distribution of the metal phase might result. However, a coarsening of the metal phase resulted and no significant improvement in the fracture toughness was measured. The fracture surface from the NiAl-Ta-Mo bend sample is shown in 5.16. By comparing secondary and backscattered electron images of the fracture surface, the brittle behavior of this alloy is clearly due to the large volume fraction of the Laves phase. The fracture surface is characterized by cleavage of the Laves phase.

Conversely, the NiAl-Ta-Cr eutectic contains a smaller percentage of the Laves phase and hence has a greater fracture toughness. The fracture surface for this alloy is shown in Figure 5.17. The mode of fracture appears to consist of phase boundary fracture between the NiAl phase and the Laves phase. In addition, cleavage of the NiAl phase is also observed.

Table 5.3: Room temperature fracture toughness of NiAl-NiAlTa-Refractory metal eutectics.

Alloy	Fracture toughness MPa$\sqrt{m}$
NiAl-NiAlTa-(Mo,Ta) as-processed	5.2
(Ni-42Al-12.5Ta-7Mo)	5.2
heat treated 1625 K, 3600 s (1 h)	6.4
	6.8
heat treated 1725 K, 9000 s (2.5 h)	6.7
	9.1
heat treated 1725 K, $14.4x10^3$ s (4 h)	5.7
	5.7
NiAl-(Cr,Al)NiTa-Cr as-processed	15.1
(Ni-30.5Al-6Ta-33Cr)	15.9
	15.2
	13.6
NiAl-NiAlTa-V as-processed	8.2
(Ni-28.5Al-10Ta-33V)	8.7
	8.5
	7.9

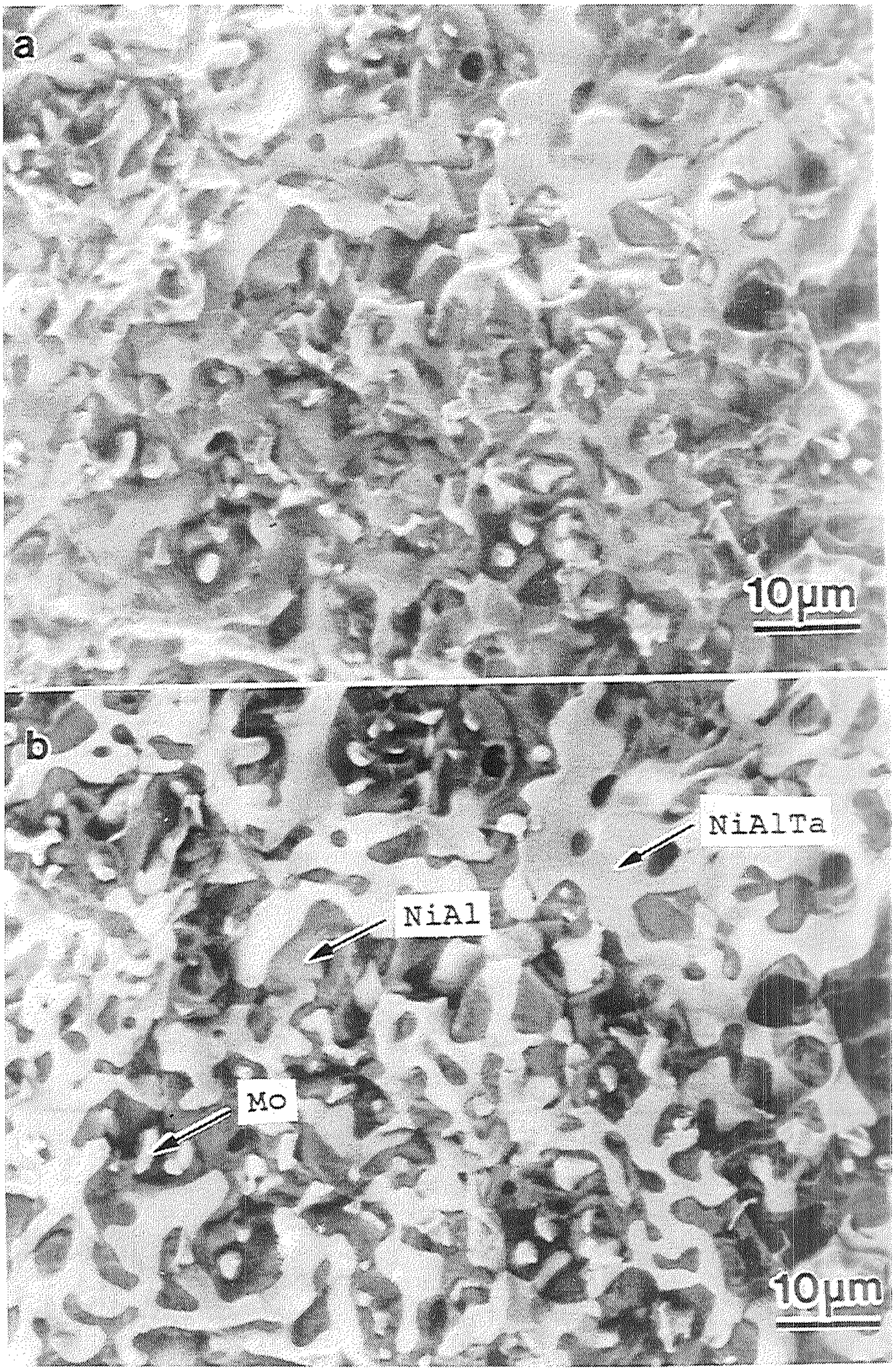

Figure 5.16: SEM photomicrographs of the fracture surface of a broken NiAl-NiAlTa-(Mo,Ta) bend specimen.
(a) secondary electron image.
(b) backscattered electron image.

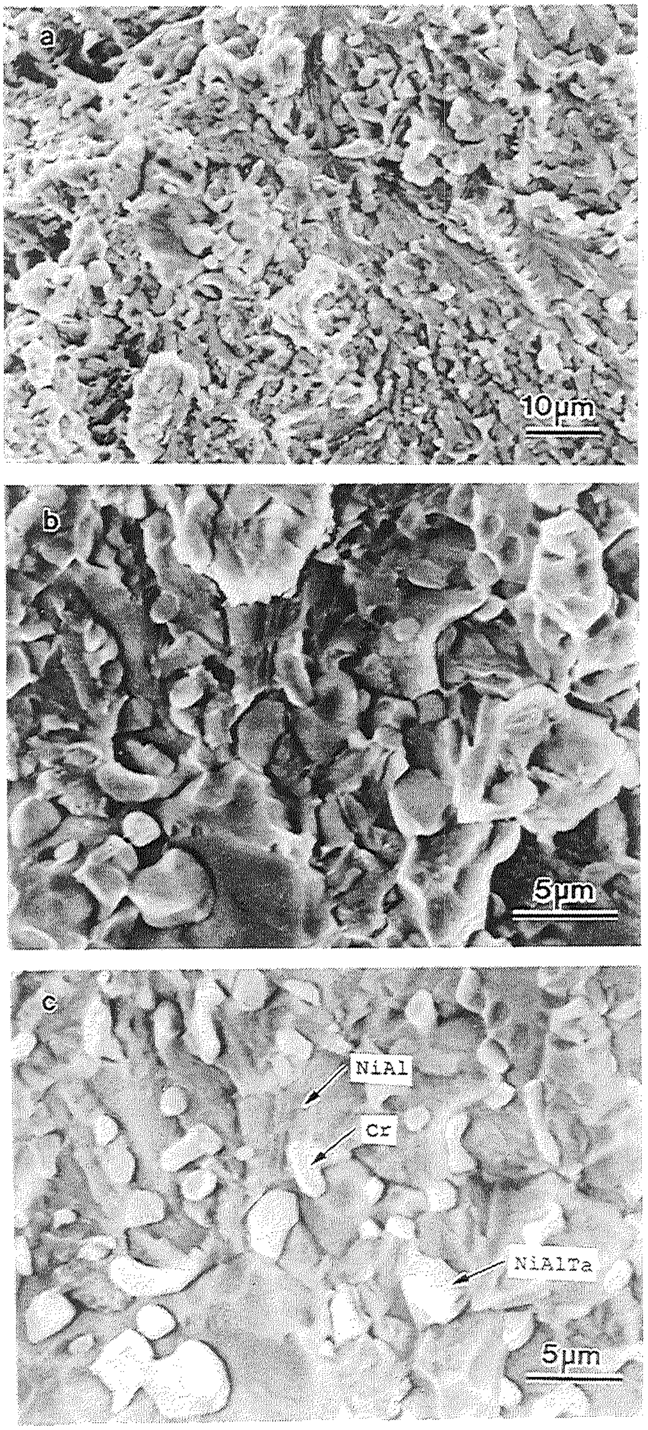

Figure 5.17: SEM photomicrographs of the fracture surface of a broken NiAl-(Cr,Al)NiTa-Cr bend specimen.
(a) and (b) secondary electron image.
(c) backscattered electron image.

Lastly, the fracture surface for the NiAl-NiAlTa-V eutectic is shown in Figure 5.18. The fracture surface for this alloy closely resembles the eutectic microstructure. The toughness of this material was poor. This is attributed to the result that almost no alignment of the phases was produced on directional solidification. The poor alignment is due to the formation of a cellular microstructure upon directional solidification.

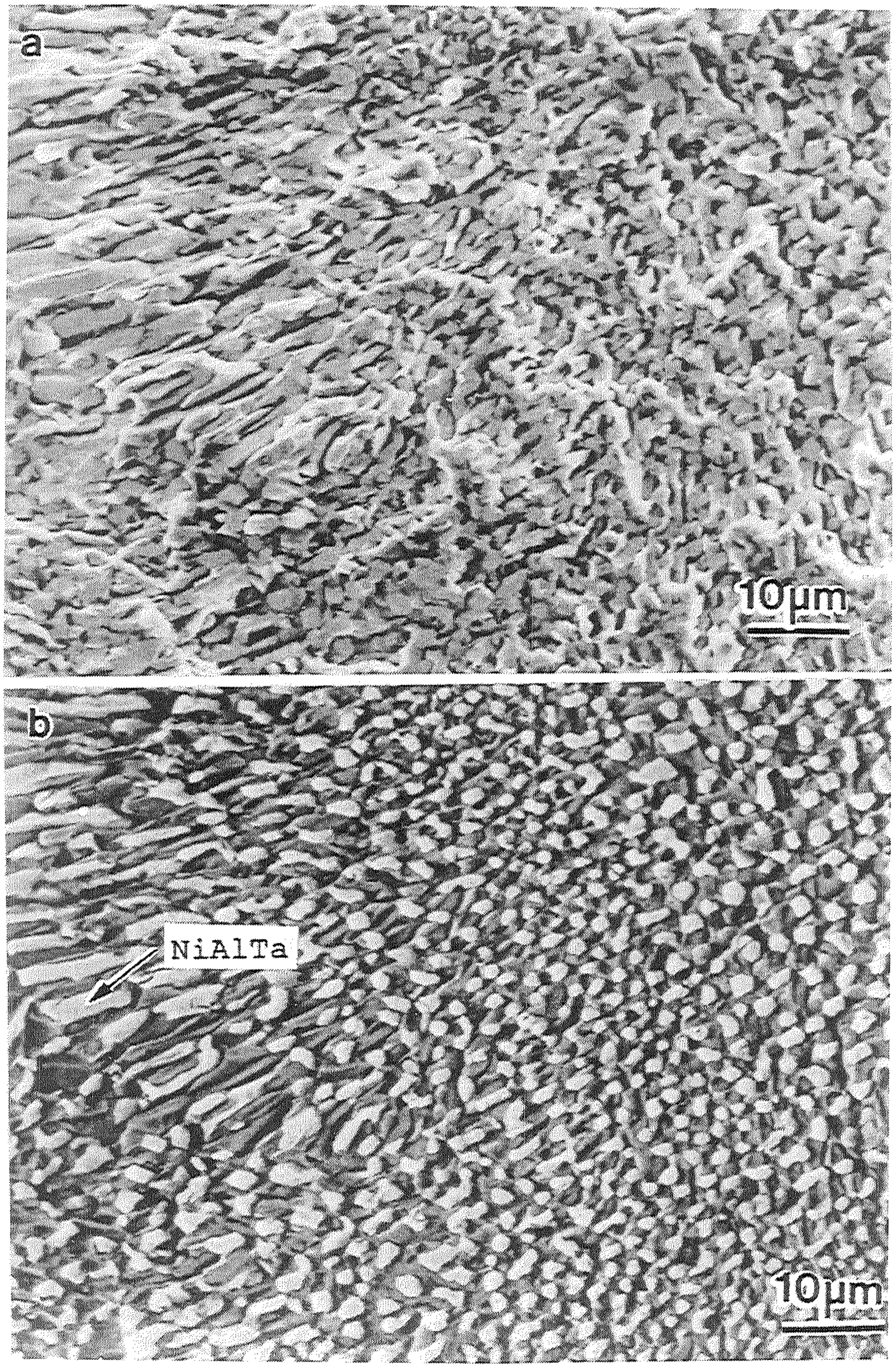

Figure 5.18: SEM photomicrographs of the fracture surface of a broken NiAl-NiAlTa-V bend specimen.
(a) secondary electron image.
(b) backscattered electron image.

CHAPTER 6

DISCUSSION

The ternary eutectic systems were studied to discover if a balance of properties could be achieved by combining the properties of the individual binary eutectics. Of the alloys studied, the ternary eutectic in NiAl-Ta-Cr system came the closest to achieving this goal. The room temperature fracture toughness of this material was greater than that of the NiAl-NiAlTa eutectic by a factor of three. Unfortunately, the creep resistance of this material was no better than that of the NiAl-Cr eutectic.

Since NiAl, NiAlTa, and Cr are all thermodynamically compatible, conventional techniques to produce composite materials formed by joining materials containing the NiAl-NiAlTa and the NiAl-Cr eutectics may be possible. The ternary eutectic represents the lowest melting temperature (1700 K) for alloy compositions within the NiAl, Laves phase, and chromium three phase region shown in Figure 5.8. However, the melting point of the ternary eutectic at 1700 K is not significantly lower than that of the NiAl-Cr binary eutectic (1718 K). From the preliminary mechanical property data, the creep resistance of the ternary eutectic is similar to that of the NiAl-Cr eutectic and the fracture toughness is greater than that of the NiAl-NiAlTa eutectic. Hence, the interface between materials consisting of the separate binary eutectics should be thermodynamically stable and mechanically sound.

REFERENCES

1. R.D. Noebe, R.R. Bowman, and M.V. Nathal, Int. Mat. Rev., 38 (1993), 193-232.
2. Steve Joslin, Ph.D. thesis, University of Tennessee (in progress).
3. M. Durand-Charre, D. David and J. Wang, High Temp. Mat. and Proc, 10 (1991), 1-12.
4. S. Chakravorty and D. R. F. West, Mat. Sci. and Tech., 1 (1985), 978-985.
5. S. Chakravorty and D. R. F. West, Metal Sci., 18 (1984), 207-215.
6. S. Chakravorty, S. Sadiq, and D. R. F. West, J. Mat. Sci., 24 (1989), 577-583.

PART 6: SUMMARY

CHAPTER 1

SUMMARY OF PARTS 2-5

Many ordered intermetallic alloys possess an unique combination of properties making them extremely attractive for high temperature applications. These advantageous properties include: high melting point, high thermal conductivity, low density, excellent oxidation resistance, and low material costs. However, the use of ordered intermetallic alloys for structural applications have been limited due to their brittleness at room temperature. Also, the elevated temperature strength of many intermetallic alloys such as NiAl is poor.

The objective of this research was to improve both the room temperature fracture toughness and elevated strength of NiAl based materials by producing in-situ composites from directional solidification of eutectic alloys. Directional solidification was performed by containerless processing techniques in a levitation zone refiner to minimize alloy contamination. Three classes of NiAl-based in-situ composites were examined. These were the NiAl-Cr eutectic system, the NiAl plus Laves phase eutectics, and ternary eutectic systems containing NiAl, a refractory metal phase, and a Laves phase.

Preliminary mechanical property data for each system is shown in Figure 6.1 [1]. In this figure, the creep resistance at 1300 K and the room temperature fracture toughness of the NiAl-based eutectic alloys are compared to NiAl and a nickel based single crystal superalloy. The NiAl-NiAlTa alloys show the best creep strength. The creep strength of the NiAl-15.5Ta alloy is comparable to that of the superalloy. While the value for NiAl-15.5Ta eutectic alloy is based on a limit number of tests, the result does demonstrate that such strengths are achievable.

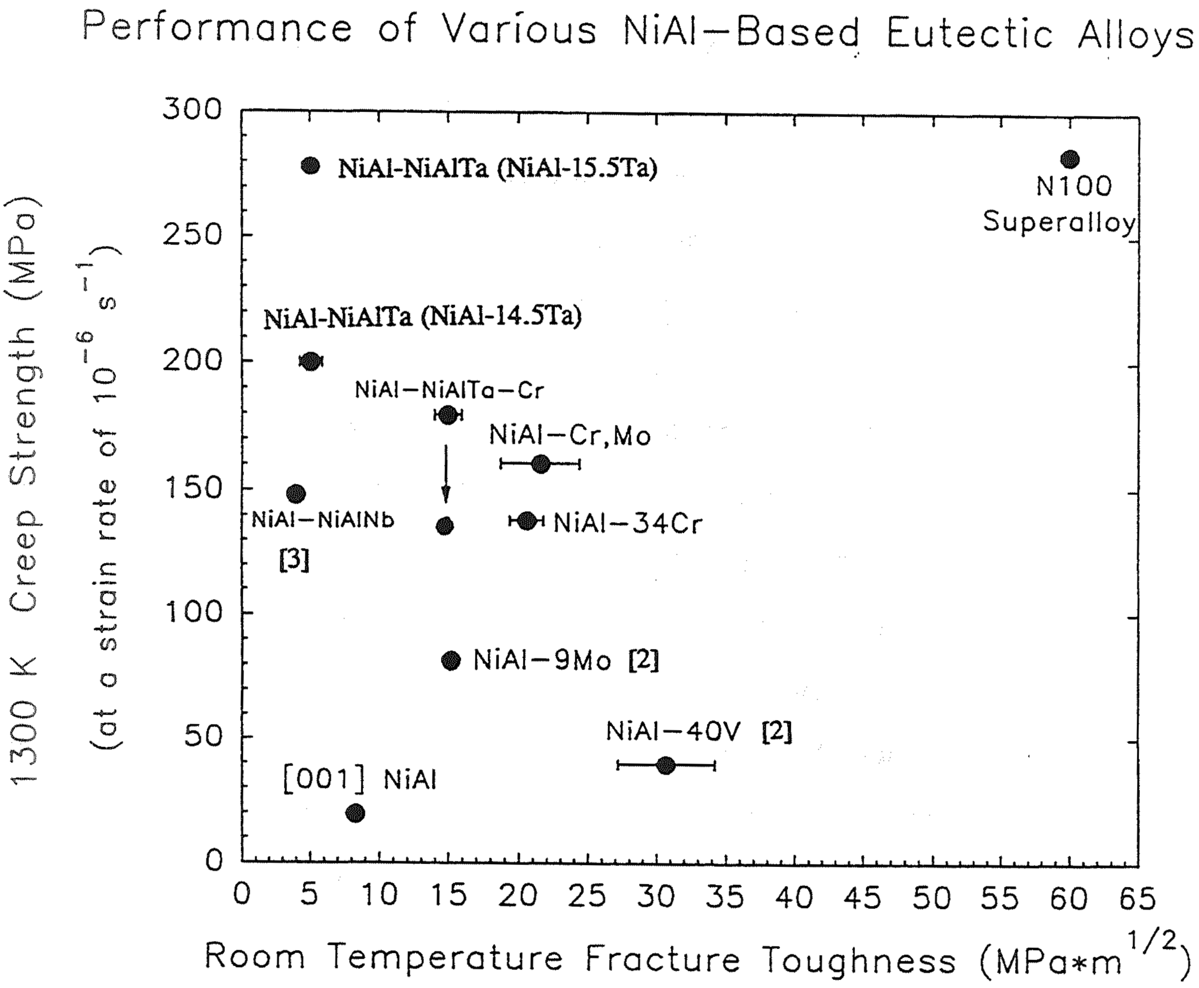

Figure 6.1: Performance of various NiAl-Based eutectic alloys.

The NiAl-(Cr,Mo) eutectic has a reasonable combination of properties when compared to the other NiAl-based eutectics. The NiAl-(Cr,Mo) eutectic has a room temperature fracture toughness of 22 MPa√m and has a much greater creep strength than binary NiAl.

The ternary eutectic systems were studied to discover if a balance of properties could be achieved by combining the properties of the individual binary eutectics. The ternary eutectic in the NiAl-Ta-Cr system came the closest to achieving this goal. The room temperature fracture toughness of this eutectic was intermediate between those of the NiAl-NiAlTa eutectic and the NiAl-Cr eutectic. However, intermediate values for the creep strength of the NiAl-(Cr,Al)NiTa-Cr ternary eutectic were found only at high strain rates ($>10^{-5}$ s^{-1}). At lower strain rates, the creep strength of the ternary eutectic decreased to values near those of the binary NiAl-Cr eutectic.

In conclusion, improvements in both the room temperature fracture toughness and the elevated temperature strength were found for all the eutectics examined when compared to binary NiAl. The NiAl-28Cr-6Mo eutectic was found to have the best combination of properties while the NiAl-15.5Ta eutectic was found to have an excellent high temperature strength. Both these alloys show promise as high temperature structural materials and merit further study.

REFERENCES

1. R.D. Noebe, NASA Lewis Research Center. Figure 6.1 is based on a similar figure compiled by Dr. Noebe that consists of all the material processed at the Univeristy of Tennessee to date (1993).

2. S. M. Joslin, Ph.D. thesis, University of Tennessee (in progress).

3. J.D. Whittenberger, R. Reviere, R.D. Noebe, and B.F. Oliver, Scripta Metall. Mater., 26 (1992), 987-992.

APPENDICES

APPENDIX A: COMPUTER PROGRAMS

```
C
C  ZONE PROCESSOR FOREGROUND PROGRAM
C  RT-11 FORTRAN IV          4/9/1992        DRJ
C
C LINKING PROCEDURE ON RT11 TO PRODUCE FOREGROUND EXECUTABLE
C FROM PROGRAM ZONE.FOR:
C
C     .R LINK
C     * ZONE=ZONE/I/R//
C     * DTLIB
C     * ITELIB
C     * IBVDP
C     * IBUP
C     * //
C     LIBRARY SEARCH? $SHORT
C     LIBRARY SERCH? <return>
C     * ^C ^C
C
C
C LINKING PROCEDURE ON RT11 TO PRODUCE BACKGROUND EXECUTABLE WITH
C OVERLAYS FROM PROGRAMS INGOT.FOR, OTEXT.FOR, OSUB1.FOR AND OSUB2.FOR
C
C     LINK/PROMPT INGOT
C     * OTEXT/O:1
C     * OSUB1/O:1
C     * OSUB2/O:1
C     * //
C
C TO EXECUTE THE PRGORAMS: FRUN ZONE/BUFFER:3000 (then follow prompts)
C
C -- HISTORY --
C
C    4/1/1992  - ADDED MEASUREMET OF SOLID DIAMETER
C    5/10/1992 - OUTPUT ITERFACE POSITION.  ALLOW ANY NUMBER
C                OF AVERAGES OF INTERFACE POSTION.
C    5/11/1992 - PLACE INTERFACE COMPARISON SEARCH ROW
C                INTO THE DAT() MATRIX.
C
C    12/30/1992 - DIRECT OUTPUT TO DELL#2 THROUGH IEEE INTERFACE
C     1/1/1993  - DIRECT OUTPUT TO EITHER DELL#1 OR DELL#2
C
C     1/2/1993  - INCREASE THE SIZE OF DAT() ARRAY TO 7X4
C     1/2/1993  - PUT VARIABLES FOR IEEE INTERFACE IN DAT() ARRAY
C
C     1/9/1993  - ADD COMPLETION ROUTINE TO READ DATA FROM DELL#1
C
C     4/9/1993  - TAKEOUT INTERFACE FINDER FROM RT11 AND CONTROL
C                 INTERFACE FROM DELL#1
C
C     7/14/1993 - CHANGE THE DEFAULT CONDITIONS FOR DELL#1
C                 INTERFACE FINDER
C
C     9/3/1993 -  CORRECT ERROR CHECKING IN THE POWER LOOP
C
C
C PROGRAM DESCRIPTION:
C  Foreground program to setup completion routines and to sample
C  background monitor for user input.  Purpose of the program
C  is to control the diameter, and interface postion for a zone
C  melting procedure.  This is accomplished setting up a power, and
C  stretch/squeeze loop by analizing a digital image of the zone.
C  Programs send and receive data from two IBM pc compatables refered
C  to as DELL#1 and DELL#2.
```

```
C  VARIABLES:
C          DAT()    - matrix holding process and system variables
C          BIAS()   - array which holds the control offsets.
C          FTRANS   - integer array which is received from background
C          FAREA    - work space used to receive background data
C          AREA1    - work space used to call completion routine.
C          IEEE     - byte array containing output data- temperture etc.
C          IOUT     - integer array containing the output data
C
C MATRIX VALUES FOR DAT(I,J):
C  (a) process variables
C       I=1,2,3,4  for diameter, interface postion, rotation, scan.
C       J=1,2,3,4  for gain, time constant, setpoint, last read value
C       note: gain and time constant are not used for rotation and scan.
C             area used for: rot flg., solid dia, search length, width.
C
C  (b) system variables
C       I=5        for system timming values, and printer flag
C       J=1,2,3,4  for completion delay, delay time, comparison row.
C                      and allowable pix change for power loop.
C       I=6        for video graphics setup
C       J=1,2,3,4  for column to start search, row to measure diameter
C                      threshold intensity, empty
C
C  (c) IEEE variables
C       I=7 for ieee bus to DELL computers
C        J=1 flag: communication with Dell#1 ?
C        J=2 flag: comunication with Dell#2 ?
C        J=3 time in ticks to read inteface position from Dell#1
C
C  ROUTINES:  SHED1    - completion routine to control the melt dia.
C             SHED2    - copletion routine to get inteface position
C                        from Dell#1 pc and to control the induced power.
C             LOADF    - completion routine to recieve background values.
C
C  SYSTEM CALLS:
C     IQSET    -  the number of I/O queues reserved.
C     ITIMER   -  calls completion routine after elapsed time interval.
C     IRCVDF   -  receives data and enters a completion subroutine.
C     ISLEEP   -  suspends main program execution for the time period.
C     ISDTTM   -  sets the system date and time.
C     SECNDS   -  returns time in seconds (real)
C
C FROM DTLIB.OBJ:
C     IADC     -  analog to digital conversion  (input to zone melter)
C     IDAC     -  digital to analog conversion  (output to zone melter)
C
C FROM ITELIB.OBJ:  contains all the video graphics library routines.
C
C FROM IBUP.OBJ and IBVDP.OBJ: libraries for the GPIB11 IEEE hardware.
C      IBUP     - send and recieve data via IEEE connection.
C ---------------------------------------------------------------------
C
      PROGRAM ZONE
C
C DECLARE ALL VARIABLES
      EXTERNAL SHED1, SHED2, LOADF
      REAL*4 SECNDS
      BYTE IEEE(20)
      INTEGER*2 IOUT(10),IERR,SIZE, AREA2(4)
      INTEGER*2 FAREA(4),AREA1(4),DAT(7,4),FTRANS(5),ORGIN
      EQUIVALENCE(IOUT,IEEE)
      COMMON /SHD1/  DAT
      COMMON /LDF/ FTRANS
```

```
C
      DATA SIZE/20/           ! length of string data output to DEVICE
      DATA IOUT/10*0/
C
C
C CONVERT 12-BIT NUMBER TO ENGINEERING NUMBER
C     ESS(JJ)    = 7.5*FLOAT(JJ)/2047.          ! st/squeeze (in/min)
C     ETEMP(JJ)  = 1200. + 550.*FLOAT(JJ)/2047. ! temperature (C)
C     EPOWER(JJ) = 100.*FLOAT(JJ)/2047.         ! power (%)
C     ESCAN(JJ)  = 22.8*FLOAT(JJ)/2047.         ! scan velocity (in/hr)
C     EROT(JJ)   = 833.*FLOAT(JJ)/2047.         ! rotational speed (RPM)
C     EPOS(JJ)   = 6.*FLOAT(JJ)/4095.           ! travel pos (-3 to 3in)
C     EDIA(JJ)   = 0.625*FLOAT(JJ)/220.         ! zone diameter (in)
C
C
C INITIALIZE DATA MATRIX
      DATA DAT(1,1)/1420/,DAT(1,2)/1000/,DAT(1,3)/300/, DAT(1,4)/350/
      DATA DAT(2,1)/900/, DAT(2,2)/500/, DAT(2,3)/340/, DAT(2,4)/320/
      DATA DAT(3,1)/8/,   DAT(3,2)/0/,   DAT(3,3)/0/,   DAT(3,4)/0/
      DATA DAT(4,1)/40/,  DAT(4,2)/5/,   DAT(4,3)/0/,   DAT(4,4)/0/
      DATA DAT(5,1)/3/,   DAT(5,2)/10/,  DAT(5,3)/360/, DAT(5,4)/10/
      DATA DAT(6,1)/55/,  DAT(6,2)/320/, DAT(6,3)/70/,  DAT(6,4)/3/
      DATA DAT(7,1)/-1/,  DAT(7,2)/-1/,  DAT(7,3)/45/,  DAT(7,4)/0/
C
C
C CALL STARTUP ROUTINES AND START COMPLETION ROUTINE
      IERR=IQSET(25)                              ! reserve queues
      IERR=IRCVDF(FTRANS,4,FAREA,LOADF)           ! get backgrnd data
      WRITE(5,*) ' TYPE CNTRL-B THEN "RUN INGOT"' ! prompt backgrnd
10    IF (FTRANS(5) .GT. 0) GOTO 12               ! wait on backgrnd
          CALL ISLEEP(0,0,1,0)
          GOTO 10
12      CONTINUE
      DAT(7,4)=FTRANS(5)                      ! DELL#1 or DELL#2
      CALL INITVS                                ! initialize video
      CALL ISDTTM(-1,0,0)                        ! zero clock
      IERR=ITIMER(0,0,0,DAT(5,1),AREA1,1,SHED1)  ! completion routine
      IERR=ITIMER(0,0,DAT(7,3),0,AREA2,2,SHED2)
      ORGIN=IADC(6,0)                            ! initial position
C
C
C MAIN JOB LOOP WHICH EXECUTES EVERY 'DAT(5,2)' SECONDS
100   CALL ISLEEP(0,0,DAT(5,2),0)
         IOUT(1) = INT(SECNDS(0.))          ! time in secs
         IOUT(2) = ORGIN-IADC(6,0)          ! position
         IOUT(3) = IADC(1,0)                ! temperature
         IOUT(4) = DAT(1,4)                 ! liquid zone diameter
         IOUT(5) = IADC(0,0)                ! stretch/squeeze
         IOUT(6) = IADC(3,0)                ! power
         IOUT(7) = DAT(4,4)                 ! scan velocity
         IOUT(8) = DAT(3,4)                 ! rotation
         IOUT(9) = DAT(3,2)                   ! solid diameter
         IOUT(10)= DAT(6,2)+DAT(4,1)-DAT(2,4) ! interface position
         IF (DAT(7,2).GE.0) DAT(7,2) = IBUP(0,2,IOUT,SIZE)
      GOTO 100
C
C
      STOP
      END
C
```

```
C
C Completion routine executes after 'DAT(5,1)' ticks
C     calls the subroutine to control the melt diameter, freezing
C     velocity, and rotational velocity.
C
C
      SUBROUTINE SHED1(ID)
C
      EXTERNAL   SHED1
      INTEGER*2  IERR, AREA1(4)
      INTEGER*2  DAT(7,4)
      COMMON/SHD1/ DAT
C
C
C MAIN JOB LOOP
      CALL CONTRL
C
C
C RECALL THE COMPLETION ROUTINE (RECURSIVE)
      IERR=ITIMER(0,0,0,DAT(5,1),AREA1,1,SHED1)
C
C
      RETURN
      END
C ---------------------------------------------------
C
C Power Control loop completion routine:
C
C     receive the interface position from Dell#1 pc computer and
C     calculate the power output needed to control the zone size.
C
C
C
      SUBROUTINE SHED2(ID)
C
      EXTERNAL   SHED2
      BYTE CDAT(4)
      INTEGER*2  AREA2(4), IALLOW
      INTEGER*2  DAT(7,4), NUMBER
      EQUIVALENCE(NUMBER,CDAT)
      COMMON/SHD1/ DAT
C
C MAIN JOB LOOP
      IALLOW=DAT(5,4)    ! max change in pix position for power change
      IF (DAT(7,1).GT.0) DAT(7,1)=IBUP(1,1,CDAT,4)   ! value from DELL
      IF (DAT(7,1).GT.0.AND.NUMBER.GT.0) DAT(2,4)=NUMBER ! put in matrix
      IF (IABS(NUMBER-DAT(2,3)).GT.IALLOW) GOTO 100 ! allowable change
         CO=GETCO(2)                  ! calculate control output for power
         IF (CO.LT.0) CO=0            ! check limits
         CALL IDAC(0,0,CO)            ! set the power
100   CONTINUE
C
C
C RECALL THE COMPLETION ROUTINE (RECURSIVE)
      IERR=ITIMER(0,0,0,DAT(7,3),AREA2,2,SHED2)
C
C
      RETURN
      END
C
```

```
C
C Completion routine to load background data.
C Action taken by this routine depends on the variable FLAG
C which is loaded from the background.
C
      SUBROUTINE LOADF(ID)
C
      EXTERNAL LOADF
      REAL*4 INTGRL(4)
      INTEGER*2 FAREA(4), FLAG, I, J, VALUE, IERR
      INTEGER*2 DAT(7,4), FTRANS(5), BIAS(4), CHNL(4)
      EQUIVALENCE (FLAG,FTRANS(2))
      EQUIVALENCE (I,FTRANS(3))
      EQUIVALENCE (J,FTRANS(4))
      EQUIVALENCE (VALUE,FTRANS(5))
      COMMON /SHD1/ DAT
      COMMON /CTL/ INTGRL, BIAS
      COMMON /LDF/ FTRANS
      DATA CHNL/0,2,5,4/  ! port for st/sq, power, rot, scan
C
C *** TRANSFER OF CONTROL ***
       IF (FLAG.LT.1) GOTO 10
           DAT(FLAG,3)=DAT(FLAG,4)       ! load setpoint
           INTGRL(FLAG)=0.0              ! clear control equation
           BIAS(FLAG)=IADC(CHNL(FLAG),0) ! needed offset
           BIAS(1)=0                     ! st/sq bias always zero
10    CONTINUE
C
C *** FLAG ACTIONS ***
      IF (FLAG.GE.0) IERR=ISDATW(DAT(I,J),1)   ! send to background
      IF (FLAG.EQ.-1) DAT(I,J)=DAT(I,J)+VALUE ! increment matrix
      IF (FLAG.EQ.-2) BIAS(I)=BIAS(I)+VALUE   ! increment bias array
      IF (FLAG.EQ.-3) DAT(I,J)=VALUE          ! load matrix value
C
C SCAN THE BACKGROUND AGAIN FOR INPUT
      IERR=IRCVDF(FTRANS,4,FAREA,LOADF)
C
      RETURN
      END
C
C -------------------------------------------------------------
C
      SUBROUTINE CONTRL
C
C Set up a power loop, stretch squeeze loop, and ramp to the
C set point values for the rotation and scan velocity.
C The stretch squeeze control is calculated by measuring the diameter
C of the bar with GETLEN.
C NEEDS: libraries DTLIB.OBJ and ITELIB.OBJ
C
      REAL*4 INTGRL(4), RTEMP
      INTEGER*2 GETLEN,GETROW,GETCO,IABS
      INTEGER*2 COUNT,R1,R2,COLUMN,SLEN,XTENS,CO,IFACE
      INTEGER*2 DAT(7,4), BIAS(4), COUNT2, COUNT3
      COMMON /SHD1/ DAT
      COMMON /CTL/ INTGRL, BIAS
      COMMON /GTLN/ COLUMN,SLEN,XTENS
      DATA COUNT/0/, COUNT2/0/, COUNT3/0/, RTEMP/0.0/
C
      COLUMN=DAT(6,1)       ! horizontal position of interface search
      XTENS=DAT(6,3)        ! threshold pixel intensity
      R1=DAT(6,2)           ! vertical position at start of search
      R2=DAT(6,2)+DAT(4,1) ! vertical position at end of search
      SLEN=DAT(4,2)         ! length of search.
```

```
C
C GRAB A SCREEN TO PROCESS
      CALL GETSCR(R1,R2,DAT(1,4),DAT(2,4),DAT(1,3),DAT(2,3),DAT(5,3))
C
C MEASURE THE DIAMETER
      DAT(1,4)=GETLEN(R1,25,485,XTENS)
      CO=GETCO(1)
      CALL IDAC(1,0,CO)
C
C
      COUNT2=COUNT2+1                          ! do rotation and scan
      IF (COUNT2.LT.DAT(3,1)) GOTO 20          ! only after a certain
      COUNT2=0                                 ! number of passes.
C
C RAMP TO THE ROTATION SETPOINT
      DAT(3,4)=IADC(5,0)
      IF (DAT(3,3).LT.BIAS(3)) BIAS(3)=BIAS(3)-1  ! closed loop
      IF (DAT(3,3).GT.BIAS(3)) BIAS(3)=BIAS(3)+1
      CALL IDAC(3,0,BIAS(3))
C
C
C RAMP TO THE TRANSLATION SETPOINT
      DAT(4,4)=IADC(4,0)
      IF (DAT(4,3).LT.BIAS(4)) BIAS(4)=BIAS(4)-1  ! closed loop
      IF (DAT(4,3).GT.BIAS(4)) BIAS(4)=BIAS(4)+1
      CALL IDAC(2,0,BIAS(4))
C
20    CONTINUE
C
C
C MEASURE SOLID DIAMETER AT END OF INTERFACE SEARCH AREA
      COUNT3=COUNT3+1
      IF (COUNT3.LT.(2*DAT(5,2))) GOTO 30
        COUNT3=0
        DAT(3,2)=GETLEN(R2,25,485,XTENS)
30    CONTINUE
C
      RETURN
      END
C ----------------------------------------------------------
C
      SUBROUTINE INITVS
C
C INITIALIZE THE VIDEO SYSTEM
C    The following subprograms are contained in the library
C    "ITELIB.OBJ" and access the analog processor and
C    the frame buffer hardware.
C
      CALL SELGRP(1)          ! select video group
      CALL SELTAP(0)          ! select type of analog processor
      CALL INITFB(0)          ! initialize frame buffer
      CALL INITAP             ! initialize analog processor
      CALL SELLT(0,0)         ! select lookup table
      CALL DOLNLT(0)          ! linearize lookup table
      CALL SELLT(2,0)         ! select lookup table
      CALL DOLNLT(0)          ! linearize lookup table
      CALL SELPLL(0)          ! select sync source
      CALL SELGFB(0)          ! select graphics frame buffer
      CALL GRAB(0,1,0)        ! acquire an image & store in memory
      CALL SELGPI(175)        ! select graphics pen intensity
C
      RETURN
      END
C
```

```
C
      SUBROUTINE GETSCR(R1,R2,DIA,ROW,DSET,RSET,SRCH)
C
C  GET A SCREEN FOR PROCESSING
C    Use calls from ITELIB to store image in memory.  The needed
C    operator information is placed on the image.  The info must be
C    kept away from areas which will be processed.
C
C
      INTEGER*2 R1,R2,DIA,ROW,I,COLUMN,SLEN,XTENS,DSET,RSET,SRCH
      COMMON/GTLN/ COLUMN, SLEN, XTENS
C
      CALL GRAB(0,1,0)                              ! get image
      CALL GRLINE(5,ROW,20,ROW)                     ! interface position
      CALL GRLINE(16,RSET,23,RSET)                  ! interface setpoint
      CALL GRLINE(COLUMN,R1-2,COLUMN+SLEN,R1-2)     ! top search line
      CALL GRLINE(COLUMN,R2+3,COLUMN+SLEN,R2+3)     ! bottom search line
      CALL GRRECT(150,R1-100,350,R1-85)             ! draw rectangle
      CALL GRLINE(DIA-30,R1-100,DIA-30,R1-85)       ! show diameter change
      CALL GRLINE(DSET-30,R1-92,DSET-30,R1-81)      ! diameter setpoint
C
      RETURN
      END
C
C
      INTEGER FUNCTION GETLEN(ROW,COLUMN,SLEN,XTENS)
C
C  GET THE LENGTH OF THE LINE SEQMENT AT ROW
C     The line segment has a maximum length of SLEN and starts
C     at COLUMN.  The length is found by counting the number
C     of pixels with a intensity greater than XTENS.  Uses ITELIB.
C
C
      BYTE IN(512)
      INTEGER*2 ROW, LENGTH, COLUMN, SLEN, XTENS, I
C
      LENGTH=0
      CALL READHL(0,COLUMN,ROW,SLEN,IN)
      DO 10 I=1,SLEN
          IF ((IN(I).LT.0).OR.(IN(I).GE.XTENS)) LENGTH=LENGTH+1
10    CONTINUE
      GETLEN=LENGTH
C
      RETURN
      END
C
C -----------------------------------------------------------
C
C Function to calculate the control output and
C to send this to the zone melter.
C I - the control variable: dia, interface, rot., scan
C
      INTEGER FUNCTION GETCO(I)
C
      INTEGER*2 DAT(7,4)
      INTEGER*2 BIAS(4), I
      REAL*4 INTGRL(4), ERROR, GAIN, CONST, STIME, CO
      COMMON/SHD1/ DAT
      COMMON/CTL/ INTGRL, BIAS
C
```

```
      STIME=FLOAT(DAT(5,1)+12)
      GAIN=FLOAT(DAT(I,1))/100.              ! scale gain
      CONST=GAIN/(FLOAT(DAT(I,2))*10.0)      ! gain/(time const)
      ERROR=DAT(I,3)-DAT(I,4)                ! error=setpt-measured
      INTGRL(I)=INTGRL(I)+CONST*ERROR*STIME  ! kII(error)dt
      CO=GAIN*ERROR+INTGRL(I)+FLOAT(BIAS(I)) ! the control output
      IF (CO .GT.  2047.0) CO= 2047.0
      IF (CO .LT. -2048.0) CO=-2048.0
      GETCO=IFIX(CO)
C
      RETURN
      END


C *** program INGOT.FOR ***
C BACKGROUND PROGRAM FOR ZONE.REL
C RT-11 FORTRAN IV        1/5/1992              DRJ
C
C   5/10/1992 - TAKE OUT SEARCH AREA CHANGE.
C               ALLOW CHANGE OF NUMBER OF INTERFACE AVERAGES.
C   5/11/1992 - ADD KEYBOARD ROUTINE FOR CHANGING THE COMPARISON
C               SEARCH ROW.
C   1/1/1993 -  TELL FOREGROUND TO SEND OUTPUT TO DELL#1 OR DELL#2
C   1/2/1993 -  SPLIT PROGRAM INTO MODULES FOR THE OVERLAY LINKER
C   7/14/1993 - ADD PARALLEL PROCESSING TEXT
C
      PROGRAM INGOT
C
      INTEGER*2  CHOICE,SPCBAR,FLAG,II,JJ,IVAL,SETPTS(6),FVAL(2)
      INTEGER*2  DELL1, DELL2
      REAL*4  CONV(4), SVAL
      COMMON SETPTS, CONV, FVAL
      DATA SETPTS/6*0/
      DATA CONV/2.84091E-3, 1.0, 0.406937, 0.0111383/
C
      CALL IQSET(10)
      WRITE(5,*) ' PRESS <SPACEBAR> TO BEGIN.'
      IVAL=SPCBAR()
      CALL SETPAR(-99,4,4,IVAL)         ! activate the foreground.
C
C KEYBOARD MENU
10    WRITE(5,11)
11    FORMAT('1 '/'1 ')
C
      WRITE(5,*) 'OUTPUT: TIME  TRAVEL  TEMP  ZONE-DIA  ST/SQ  POWER',
     *  '  SCAN  ROT  BAR-DIA  INTFC'
      WRITE(5,*) '       sec    in      C       in     in/min   %  ',
     *  '  in/hr  rpm    in     pixel'
      WRITE(5,*)  ' '
      WRITE(5,*)  ' '
      WRITE(5,*)  ' THE SET POINT VALUES ARE:'
      WRITE(5,12) ' DIAMETER  =',FLOAT(SETPTS(1)*CONV(1))
      WRITE(5,12) ' INTERFACE =',FLOAT(SETPTS(2)*CONV(2))
      WRITE(5,12) ' ROTATION  =',FLOAT(SETPTS(3)*CONV(3))
      WRITE(5,12) ' SCAN VEL. =',FLOAT(SETPTS(4)*CONV(4))
12    FORMAT(4X,A12,F9.3)
      CALL SETPAR(0,7,1,IVAL)
      DELL1=FVAL(2)
      CALL SETPAR(0,7,2,IVAL)
      DELL2=FVAL(2)
      WRITE(5,*) '  '
      IF (DELL1.GT.0) WRITE(5,*) ' RECIEVING DATA FROM DELL#1'
```

```
      IF (DELL1.LE.0) WRITE(5,*) ' *NOT* RECIEVING DATA FROM DELL#1'
      IF (DELL2.GT.0) WRITE(5,*) ' SENDING DATA TO DELL#2'
      IF (DELL2.LE.0) WRITE(5,*) ' *NOT* SENDING DATA TO DELL#2'
C
      CALL ITEXT(1,II,JJ)
      IVAL=SPCBAR()
      IF (IVAL.NE.32) GOTO 10
C
C PARAMETER MENU
      CALL ITEXT(2,II,JJ)
      II=CHOICE(1,8)                   ! pick what row in matrix.
      IF (II.EQ.8) GOTO 10
C
C       graphics tuning menu
      IF (II.NE.5) GOTO 30
         CALL ITEXT(3,II,JJ)
         CALL QUERY(4,1)    ! change dist between liq and solid dia meas.
         GOTO 10
30    CONTINUE
C
C       cool down routine
      IF (II.NE.6) GOTO 45
          CALL ITEXT(4,II,JJ)
          IVAL=CHOICE(1,2)
          IF (IVAL.EQ.2) GOTO 10
          WRITE(5,*) ' cooling rate (53kW)/(N hr) N=[1-20]?'
          IVAL=CHOICE(1,20)
          CALL SETPAR(-3,7,1,-1)      ! don't load data from DELL#1
          CALL SETPAR(2,2,3,JJ)     ! do transfer of control
          WRITE(5,48)                 ! prompt user
          JJ=SPCBAR()                 ! pause till spcbar hit
          WRITE(5,*) ' ***WORKING***'
43        CALL ISLEEP(0,0,IVAL,0)     ! do cooldown
               CALL SETPAR(-2,2,2,-1)
               GOTO 43
45    CONTINUE
C
C     setup parallel processing (activate dells)
      IF (II.NE.7) GOTO 46
          CALL ITEXT(6,II,JJ)
          IVAL=CHOICE(1,3)
          IF (IVAL.EQ.3) GOTO 10
          IF (IVAL.EQ.1) CALL SETPAR(-3,7,1,1)
          IF (IVAL.EQ.2) CALL SETPAR(-3,7,2,1)
          GOTO 10
46    CONTINUE
C
C CONTROL OPTIONS MENU   ( II is between 1 and 4. )
      CALL ITEXT(5,II,JJ)
      JJ=CHOICE(1,5)                          ! Get row of matrix.
      IF (JJ.EQ.5) GOTO 10
      IF ((II.EQ.3).AND.(JJ.LT.3)) GOTO 10    ! Can't change gain or
      IF ((II.EQ.4).AND.(JJ.LT.3)) GOTO 10    ! const for rot, scan.
      IF (JJ.LT.4) CALL QUERY(II,JJ)          ! Change parameter value
      IF (JJ.NE.4) GOTO 50                    ! or do a control transfer.
          CALL SETPAR(II,II,3,IVAL)
          SETPTS(II)=FVAL(2)
          WRITE(5,47) CONV(II)*FLOAT(SETPTS(II))
47        FORMAT(1X,/'  SETPOINT=',F9.3)
            WRITE(5,48)
48        FORMAT(1X,/'  switch to REMOTE then/or hit the SPACEBAR'/)
          IVAL=SPCBAR()
50    CONTINUE
      GOTO 10
```

```
C
C
      STOP
      END
C
C
C rountine to send data to foreground
C
      SUBROUTINE SETPAR(FLAG,I,J,VAL)
C
      INTEGER*2 DAT(4), FVAL(2), SETPTS(6), FLAG, I, J, VAL, IERR
      REAL*4 CONV(4)
      COMMON SETPTS, CONV, FVAL
C
      DAT(1)=FLAG
      DAT(2)=I
      DAT(3)=J
      DAT(4)=VAL
      IERR=ISDATW(DAT,4)
      IF (FLAG.GE.0) IERR=IRCVDW(FVAL,1)
      IF ((FLAG.EQ.-1).AND.(J.EQ.3)) SETPTS(I)=SETPTS(I)+VAL
C
      RETURN
      END
C


C *** program ITEXT.FOR  (for overlay with INGOT.FOR) ***
C
      SUBROUTINE ITEXT(MENU,II,JJ)
C
      INTEGER*2 MENU,II,JJ
C
      IF (MENU.NE.1) GOTO 20
      WRITE(5,14)
14    FORMAT(1X///)
      WRITE(5,*) '                 *** Key Board Control ***'
      WRITE(5,*) '            dia. interface  rot. scan  hor.   vert.'
      WRITE(5,*) ' increase    W       R        Y    I     >      P'
      WRITE(5,*) ' decrease    A       D        G    J     <      L'
      WRITE(5,*) ' '
      WRITE(5,*) ' CTRL-P/L moves search comparison length UP or DOWN.'
        WRITE(5,*) ' CTRL-R/D increase/decrease the power without',
     *                 'changing the tuning.'
      WRITE(5,*) ' Note: 0.1 kW equals about 7 keystrokes.'
      WRITE(5,*) ' '
        WRITE(5,*) ' Z=print time.          SPACEBAR=menu.'
      WRITE(5,*) ' '
C
C PARAMETER MENU
20    IF (MENU.NE.2) GOTO 30
      WRITE(5,25)
25    FORMAT('1 '/'1 ')
      WRITE(5,*) ' *** SELECTION MENU ***'
      WRITE(5,*) ' '
      WRITE(5,*) ' choose by number.'
      WRITE(5,*) ' (1) DIAMETER'
      WRITE(5,*) ' (2) INTERFACE'
      WRITE(5,*) ' (3) ROTATION'
      WRITE(5,*) ' (4) SCAN VEL.'
      WRITE(5,*) ' (5) SOLID DIAMETER'
      WRITE(5,*) ' (6) COOL-DOWN'
      WRITE(5,*) ' (7) ACTIVATE DELL COMPUTERS'
      WRITE(5,*) ' (8) EXIT'
```

```
C
C        graphics tuning menu
30     IF (MENU.NE.3) GOTO 40
          WRITE(5,25)
          WRITE(5,*) '    *** SOLID DIAMETER MEASURMENT ***'
          WRITE(5,*) ' '
          WRITE(5,*) ' the solid diameter is measured at the'
          WRITE(5,*) ' lower horizonatal line.  You can change'
          WRITE(5,*) ' the distance between the liquid diameter'
          WRITE(5,*) ' line (upper) and the solid diameter line.'
          WRITE(5,*) ' Changing this value will not effect the'
          WRITE(5,*) ' the liquid diameter control.'
C
C        cool down routine
40     IF (MENU.NE.4) GOTO 50
           WRITE(5,*) ' '
           WRITE(5,*) '   *** COOL-DOWN ROUTINE ***'
           WRITE(5,*) ' '
           WRITE(5,*) ' The cool down program allows the power'
           WRITE(5,*) ' to be ramped down evenly to advoid'
           WRITE(5,*) ' thermally shocking the ingot.'
           WRITE(5,*) ' '
           WRITE(5,*) ' Do cool-down? (1=yes,2=no)'
C
C CONTROL OPTIONS MENU    ( II is between 1 and 4. )
50     IF (MENU.NE.5) GOTO 60
       WRITE(5,*) ' '
       WRITE(5,*) ' '
       IF (II.EQ.1) WRITE(5,*) ' *** DIAMETER CONTROL ***'
       IF (II.EQ.2) WRITE(5,*) ' *** INTERFACE POSITON CONTROL ***'
       IF (II.EQ.3) WRITE(5,*) ' *** ROTATION RAMP ***'
       IF (II.EQ.4) WRITE(5,*) ' *** SCAN VELOCITY RAMP ***'
       WRITE(5,*) ' '
       WRITE(5,*) ' do or change the following:'
       WRITE(5,*) ' (1) GAIN'
       WRITE(5,*) ' (2) TIME CONSTANT'
       WRITE(5,*) ' (3) SETPOINT'
       WRITE(5,*) ' (4) TRANSFER CONTROL'
       WRITE(5,*) ' (5) EXIT'
C
C
60     IF (MENU.NE.6) GOTO 70
       WRITE(5,*) ' '
       WRITE(5,*) '(1) ACTIVATE DELL#1 FOR INTERFACE CONTROL'
       WRITE(5,*) '(2) ACTIVATE DELL#2 FOR DATA DOWNLOAD'
       WRITE(5,*) '(3) EXIT'
C
70     RETURN
       END


C *** program OSUB1.FOR (for overlay with INGOT.FOR) ***
C
C routine to wait until the space bar is hit or perform
C a function directly from the keyboard.
C
       INTEGER FUNCTION SPCBAR()
C
       INTEGER*2 KEY, I, J, SETPTS(6), FVAL(2), VAL
       REAL*4 CONV(4)
       COMMON SETPTS, CONV, FVAL
C
```

```
C GET A KEY
10        CALL IPOKE("44,IPEEK("44).OR."10000)
          KEY=ITTINR()
          CALL IPOKE("44,IPEEK("44).AND..NOT."10000)
          CALL RCTRLO
C
C KEYBOARD CONTROL
          IF (KEY.EQ.32) GOTO 200
          IF (KEY.EQ.87) CALL SETPAR(-1,1,3,1)   ! W
          IF (KEY.EQ.65) CALL SETPAR(-1,1,3,-1)  ! A
          IF (KEY.EQ.82) CALL SETPAR(-1,2,3,1)   ! R
          IF (KEY.EQ.68) CALL SETPAR(-1,2,3,-1)  ! D
          IF (KEY.EQ.89) CALL SETPAR(-1,3,3,1)   ! Y
          IF (KEY.EQ.71) CALL SETPAR(-1,3,3,-1)  ! G
          IF (KEY.EQ.73) CALL SETPAR(-1,4,3,1)   ! I
          IF (KEY.EQ.74) CALL SETPAR(-1,4,3,-1)  ! J
          IF (KEY.EQ.46) CALL SETPAR(-1,6,1,1)   ! .
          IF (KEY.EQ.44) CALL SETPAR(-1,6,1,-1)  ! ,
          IF (KEY.EQ.62) CALL SETPAR(-1,6,1,5)   ! >
          IF (KEY.EQ.60) CALL SETPAR(-1,6,1,-5)  ! <
          IF (KEY.EQ.80) CALL SETPAR(-1,6,2,-1)  ! P
          IF (KEY.EQ.76) CALL SETPAR(-1,6,2,1)   ! L
          IF (KEY.EQ.18) CALL SETPAR(-2,2,2,1)   ! CTL R
          IF (KEY.EQ.4)  CALL SETPAR(-2,2,2,-1)  ! CTL D
          IF (KEY.EQ.16) CALL SETPAR(-1,5,3,-1)  ! CTL P
          IF (KEY.EQ.12) CALL SETPAR(-1,5,3,1)   ! CTL L
          IF (KEY.EQ.13) GOTO 200                ! <RET>
          IF (KEY.NE.90) GOTO 190                ! CTL Z
              WRITE(5,187)
187           FORMAT(1X,//'  print time? [1-300]',$)
            READ(5,*) I
              IF (I.GT.0) CALL SETPAR(-3,5,2,I)
              GOTO 200
190       CONTINUE
          IF (KEY.NE.27) GOTO 195                ! Esc
              WRITE(5,193)
193         FORMAT(1X,//' enter MATRIX elements I, J:  '$)
              READ(5,*) I,J
              CALL SETPAR(0,I,J,VAL)
              WRITE(5,*) 'OLD VALUE=',FVAL(2),' ENTER NEW VALUE'
            READ(5,*) VAL
              CALL SETPAR(-3,I,J,VAL)
              GOTO 200
195       CONTINUE
      GOTO 10
200   CONTINUE
C
C
      SPCBAR=KEY
      RETURN
      END
```

```
C *** program OSUB2.FOR (for overlay with INOGT.FOR) ***
C
C rountine to get an integer number from the
C user within the range of M1 to M2.
C
      INTEGER FUNCTION CHOICE(M1,M2)
C
      INTEGER*2 M1, M2, CH
5     WRITE(5,10)
10    FORMAT(1X,' choice: '$)
      READ(5,20) CH
20    FORMAT (I4)
      IF ((CH.LT.M1).OR.(CH.GT.M2)) GOTO 5
      CHOICE=CH
      RETURN
      END
C ---------------------------------------------
C routine to see if user wishes to change the setpoint
C value or the control parameters.
C
      SUBROUTINE QUERY(II,JJ)
C
      INTEGER*2 FLAG,II,JJ,IVAL,ANS,CHOICE
      INTEGER*2 SCAN, ROT, DIA, FVAL(2), SETPTS(6)
      REAL*4 CONV(4), VALUE
      COMMON SETPTS, CONV, FVAL
C
      FLAG=0                              ! flag to show value
      CALL SETPAR(FLAG,II,JJ,IVAL)
      VALUE=FLOAT(FVAL(2))
C
      IF ((JJ.EQ.3).AND.(II.LT.5)) VALUE=CONV(II)*VALUE
      WRITE(5,12) VALUE
12    FORMAT(1X,/1X,' VALUE=',F9.3/)
      WRITE(5,*) ' change value? (1=YES, 2=NO)'
      ANS=CHOICE(1,2)
      FLAG=-99
C
      IF (ANS.NE.1) GOTO 100
50       WRITE(5,55)
55       FORMAT('  Enter new value: '$)
         READ (5,*) VALUE
         IF (VALUE.LT.-32768.) GOTO 50
         IF (VALUE.GT. 32767.) GOTO 50
         WRITE(5,57) VALUE
57       FORMAT (1X,' Input value=',F9.3)
         WRITE(5,*) ' correct? (1=YES, 2=NO)'
         ANS=CHOICE(1,2)
         IF (ANS.EQ.2) GOTO 50
         FLAG=-3                         ! flag for substitution
         IVAL=IFIX(VALUE)
         IF (JJ.NE.3) GOTO 90
            IF (II.LT.5) IVAL=IFIX(VALUE/CONV(II)+0.5)
            SETPTS(II)=IVAL
90       CONTINUE
100   CONTINUE
      CALL SETPAR(FLAG,II,JJ,IVAL)
C
C
      RETURN
      END
```

```
C 3/23/1993   ver 1.7    DRJ
C SOLID-LIQUID INTERFACE FINDER
C
C HARDWARE REQUIRED:  DT-IRIS VIDEO BOARD
C                     NATIONAL INSTRUMENTS IEEE BOARD
C
C SUBROUTINE CALLED:  IVIDEO - SET UP CAMERA AND VIDEO SYSTEM
C                     SEARCH - ROUTINE TO FIND S/L INTERFACE
C                     INKEY  - KEY BOARD SCAN FROM FORUTIL LIBRARY
C                     GETDIA - FIND THE ZONE LENGTH AT A GIVEN PIXEL ROW
C
C COMPLLE AND LINK PROCEDURE:
C  fl ZONE.FOR MFIBL.OBJ IVIDEO ISFORLIB.LIB FORUTIL.LIB
C
C      where   MFIBL.OBJ = GPIB IEEE LIBRARY
C              ISFORLIB.LIB = DATA TRANSLATION VIDEO BOARD LIBRARY
C              FORUTIL.LIB = UTILITY LIBRARY -- KEYBOARD ROUTINES ETC.
C              IVIDEO.OBJ = INITIALIZE VIDEO BOARD SUBROUTINE
C
$INCLUDE:'ISDEFS.FOR'   ! VIDEO DEFINITIONS (comes with video hardware)
$INCLUDE:'ISERRS.FOR'   ! VIDEO ERRORS DEFINITIONS
C
C  VARIABLES:  TOP    - TOP ROW OF SEARCH AREA
C              WIDTH  - WIDTH OF SEARCH AREA
C              DSET   - DIAMETER LENGTH USED TO DEFINE THE INTERFACE
C ------------------------------------------------------------
C
      INTEGER*2 STATUS,DSET/30/,KEY,INKEY,GETDIA,SEARCH
      INTEGER*2 OFFSET/20/, TOP/310/, WIDTH/35/, COL/50/
      INTEGER*2 IFACE, SLEN/40/, SCOL/1/, ITMP,I,IAVG/6/
      REAL  XFACE
      EXTERNAL INKEY
C
      write(*,*) ' '
      WRITE(*,*) ' INTERFACE FINDER-2'
      WRITE(*,*) ' '
      WRITE(*,*) ' This program locates the interface by sweeping'
      WRITE(*,*) ' out an area near the interface.  Horizontal lines'
      WRITE(*,*) ' are scanned across this area.  The interface is'
      WRITE(*,*) ' located when the bright length of the scan line'
      WRITE(*,*) ' matches the length of a line scanned in the solid.'
      WRITE(*,*) ' '
      WRITE(*,*) ' use arrow keys to place the 2 dots that'
      WRITE(*,*) ' mark the left edge of the scan area *IN FRONT*'
      WRITE(*,*) ' of the interface.'
      write(*,*) ' '
      write(*,*) ' small increments: arrow keys '
      write(*,*) ' large increments: control left and right arrows'
      write(*,*) '                   page-up and page-down keys'
      write(*,*) ' '
      CALL IVIDEO                                 ! initialize video
      PAUSE 'HIT RETURN TO BEGIN'
      write (*,*) ' ----ok-----'
C
      DO WHILE(.TRUE.)
         XFACE = 0.0
         DO I=1,IAVG
           CALL USER(DSET,TOP,WIDTH,COL,SLEN,SCOL)     ! user input
           STATUS = ISACQ(0,1)                         ! aquire image
           STATUS = ISDISP(1)                          ! display image
           ITMP=SEARCH(TOP,WIDTH,COL,DSET,SLEN,SCOL)  ! find interface
           XFACE = XFACE + ITMP
         ENDDO
```

```
            XFACE=XFACE/IAVG + 0.5
            IFACE=XFACE
            CALL SEND(IFACE)                           ! send info to DEC
         ENDDO
C
         STATUS = ISEND()    ! close out video routines
C
         STOP
         END
C
         INTEGER*2 FUNCTION SEARCH(TOP,WIDTH,COL,DSET,SLEN,SCOL)
C
C
$INCLUDE:'ISDEFS.FOR'
$INCLUDE:'ISERRS.FOR'
C
         INTEGER*2 TOP,WIDTH,COL,STATUS,BOTTOM,SLEN,SCOL
         INTEGER*2 DIA, DSET, GETDIA, ROW2, I, ISET, ITFC
         LOGICAL FLAG
C
C *** DRAW SEARCH ARE ON VIDEO SCREEN ***
         BOTTOM=TOP+WIDTH
         STATUS = ISPUTP(0,TOP,COL,1,255)
         STATUS = ISPUTP(0,BOTTOM,COL,1,255)
C
C *** SEARCH FOR THE INTERFACE ***
         DSET=GETDIA(BOTTOM,SCOL,SLEN)-2
         FLAG=.TRUE.
         ITFC= -1
         DO I=TOP+1, TOP+WIDTH-1           ! want this loop to execute
            DIA=GETDIA(I,SCOL,SLEN)        ! for the same amout of time
            IF (DIA.GE.DSET.AND.FLAG) THEN  ! each time to prevent timing
               ITFC=I                      ! erorrs on DEC RT-11.
               FLAG=.FALSE.
            ENDIF
         ENDDO
C
C *** MARK THE INTERFACE ON THE VIDEO
         STATUS = ISPUTP(0,ITFC,COL,1,255)
C
         SEARCH=ITFC
         RETURN
         END
C
C -------------------------------------------------------
C
         INTEGER*2 FUNCTION GETDIA(ROW2,SCOL,SLEN)
C
$INCLUDE:'ISDEFS.FOR'
$INCLUDE:'ISERRS.FOR'
C
         INTEGER*2 I, STATUS, LEN,  PIXELS(512), ROW2, ITENS/60/
         INTEGER*2 SCOL,SLEN
         LEN = 0
         STATUS = ISGETP(0,ROW2,SCOL,SLEN,PIXELS)
         DO I=1,SLEN
            IF (PIXELS(I).GT.ITENS) LEN=LEN+1
         ENDDO
         GETDIA=LEN
         RETURN
         END
C
```

```
C
      SUBROUTINE USER(DSET,TOP,WIDTH,COL,SLEN,SCOL)
      INTEGER*2 DSET,TOP,WIDTH,KEY,COL,SLEN,SCOL
C
      KEY=INKEY()                          ! ---user input---
      IF (KEY.EQ.18432) TOP=TOP-1          !  up arrow
      IF (KEY.EQ.20480) TOP=TOP+1          !  down arrow
      IF (KEY.EQ.19200) COL=COL-1          !  left arrow
      IF (KEY.EQ.19712) COL=COL+1          !  right arrow
      IF (KEY.EQ.29696) COL=COL+10         !  ctrl arrow
      IF (KEY.EQ.29440) COL=COL-10         !  ctrl arrow
      IF (KEY.EQ.18688) TOP=TOP-10         !  page up
      IF (KEY.EQ.20736) TOP=TOP+10         !  page down
      SCOL=COL
C
      RETURN
      END
C
C -----------------------------------------------------
C  Send the interface position to the DEC RT-11
C
       SUBROUTINE SEND(INUMBER)
C
       INTEGER*2 IBSTA,IBERR,IBCNT,INUMBER
       INTEGER*2 BOARD,NUMBER,COUNT/4/
       CHARACTER*4 DATA
       EQUIVALENCE (NUMBER,DATA)
       EXTERNAL IBSTA,IBERR,IBCNT
C
       NUMBER=INUMBER
       BOARD=IBFIND("GPIB0 ")
       CALL IBWRT(BOARD,DATA,COUNT)
C
       RETURN
       END


C----------------------------------------------


C ** from file VIDEO.FOR ***

       SUBROUTINE IVIDEO
C
$INCLUDE:'ISDEFS.FOR'
$INCLUDE:'ISERRS.FOR'
C
       INTEGER*2 STATUS
C
       STATUS = ISINIT()    !  open chaannel to device driver
       STATUS = ISINTS(0)   ! select input look-up table 0
       STATUS = ISOUTS(0)   ! select output look-up table 0
       STATUS = ISSYNC(1)   ! select sync source 1=external sync
       STATUS = ISDISP(1)   ! enable display circuitry (on)
       STATUS = ISINFR(0)   ! select frame buffer 0 for input
       STATUS = ISOTFR(0)   ! seclect frame buffer 0 for output
       STATUS = ISPASS()    ! real-time acquisition and display
C
       RETURN
       END
```

```
REM $INCLUDE: 'qbdecl4.bas'
 '
 ' QUICK BASIC PROGRAM: (example program) to download data on DELL#2
 '     from RT-11 computer during directional solidification.
 '
 ' HARDWARE REQUIRED: NATIONAL INSTRUMENTS IEEE BOARD
 '
 ' OTHER FILES NEEDED (included with hardware)
 '     qbdecl4.bas - delcarations for IEEE routines
 '     qbib4.qlb   - quikbasic subroutines
 '
 ' IEEE ROUTINES CALLED: ibfind - setup hardware
 '                       ibtmo  - set timeout
 '
 ' IEEE VARIABLES USED:  iberr% - error code, 13=none
 '                       ibcnt% - number of bytes read
 '------------------------------------------------------
 '
 DIM N(10):                    ' the data array
 N$ = "GPIBO":                 ' the ieee board
 CALL IBFIND(N$, BOARD%):      ' locate and setup the ieee board
 TIMEOUT% = 15:                ' timeout of 100 seconds  (15)
 CALL IBTMO(BOARD%, TIMEOUT%): ' set the timeout
 '
 '  *** read ten integers values from RT-11 ***
 CLS : PRINT " waiting ..."
 WHILE (IBERR% = 13)
    IBERR% = -99: IBCNT% = 0
    RD$ = SPACE$(50):                ' the data buffer
    CALL IBRD(BOARD%, RD$):          ' ieee read fucntion
    FOR Z = 0 TO 18 STEP 2
       H1 = ASC(MID$(RD$, 2 + Z, 1)):       ' low byte of I*2 integer
       H2 = ASC(MID$(RD$, 1 + Z, 1)):       ' high byte of I*2 integer
       NN = 256 * H1 + H2:                  ' calculate the I*2 integer
       IF NN > 32767 THEN NN = NN - 65536!: ' range from -32768, +32767
       N(Z / 2 + 1) = NN                    ' place data in array
    NEXT Z
 '
 '  convert 12-bit number to engineering number
 '  N(1)                          : ' time in seconds
    N(2) = 6 * N(2) / 4095:          ' position
    N(3) = 1200 + 550 * N(3) / 2047: ' temerature
    N(4) = .625 * N(4) / 220:        ' liquid diameter
    N(5) = 7.5 * N(5) / 2047:        ' st/squeeze
    N(6) = 100 * N(6) / 2047:        ' power
    N(7) = 22.8 * N(7) / 2047:       ' scan
    N(8) = 833 * N(8) / 2047:        ' rotation
    N(9) = .625 * N(9) / 220:        ' solid diameter
 '  N(10)                         : ' interface position
 '
 '  *** WRITE DATA TO SCREEN ***
 '
    U$ = "###.###": UU$ = "####.##"
    PRINT USING "######"; N(1);
    PRINT USING U$; N(2);
    PRINT USING "######.# "; N(3);
    PRINT USING U$; N(4) * SF; N(5);
    PRINT USING UU$; N(6); N(7); : PRINT USING "  " + UU$; N(8);
    PRINT USING " " + U$; N(9) * SF;
    PRINT USING "  #####"; N(10)
 WEND
 PRINT "ERROR CODE="; IBERR%
 END
```

APPENDIX B: DIFFERENTIAL THERMAL ANALYSIS RESULTS

OPERATOR: A.PALCZER	NETZSCH STA 429/409	ATM. HELIUM	
DATE: 5/24/93	REFERENCE : CRUCIBLE	FLOW = 60 cc/min	
RUN No. NOEBE	CRUCIBLE : AL203	HEAT RATE = 10 C/min	
TG Setting : 0mg	FILE NAME : NIALTA	SAMPLE WT. = 1531.5 mg	
DTA Setting : .1mV	MATERIAL: NIAL/NIALTA	REF WEIGHT = 0 mg	

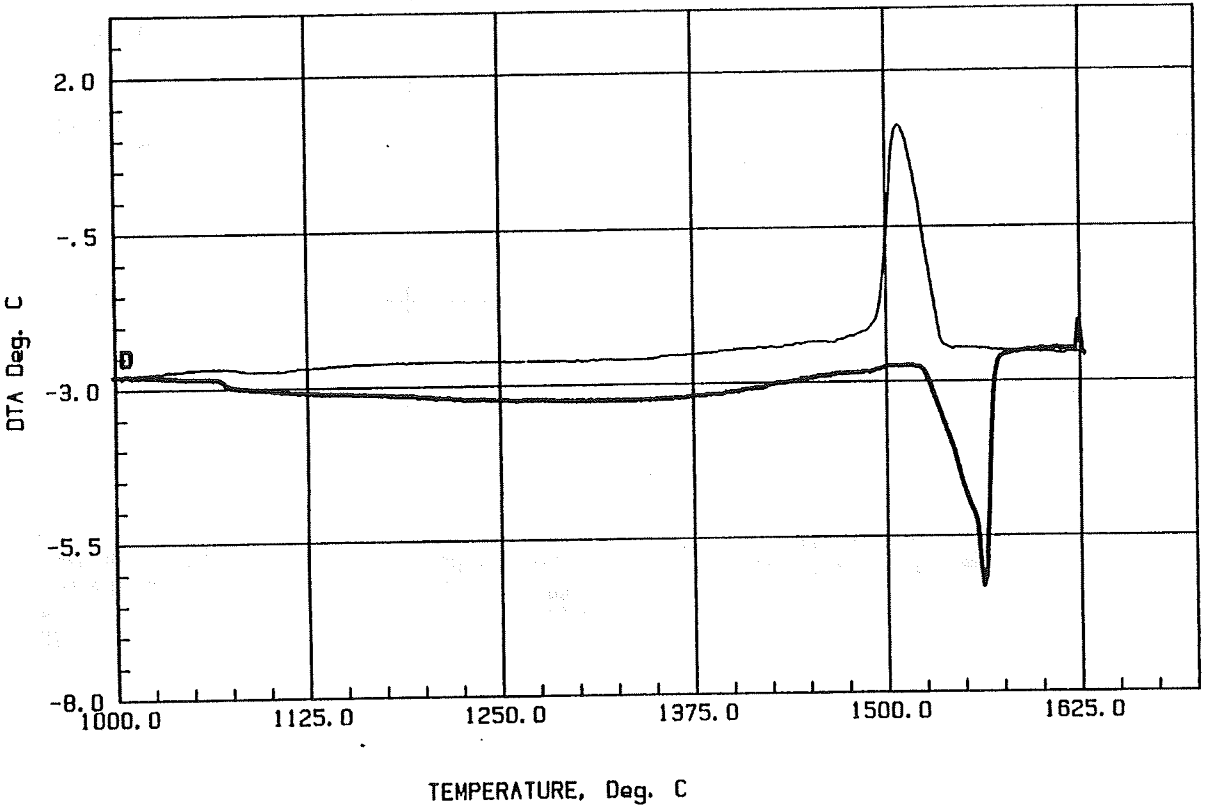

Figure B.1: DTA scan for material taken from a directionally solidified NiAl-14.5Ta ingot

OPERATOR: A.PALCZER DATE: 11/2/93 RUN No.R.NOEBE TG Setting : 0mg DTA Setting : .05mV	NETZSCH STA 429/409 REFERENCE : CRUCIBLE CRUCIBLE : AL203 FILE NAME : TaMo MATERIAL:NiAlTaMo	ATM. HELIUM FLOW = 60 cc/min HEAT RATE = 10 C/min SAMPLE WT.= 1568.6 mg REF WEIGHT = 0 mg

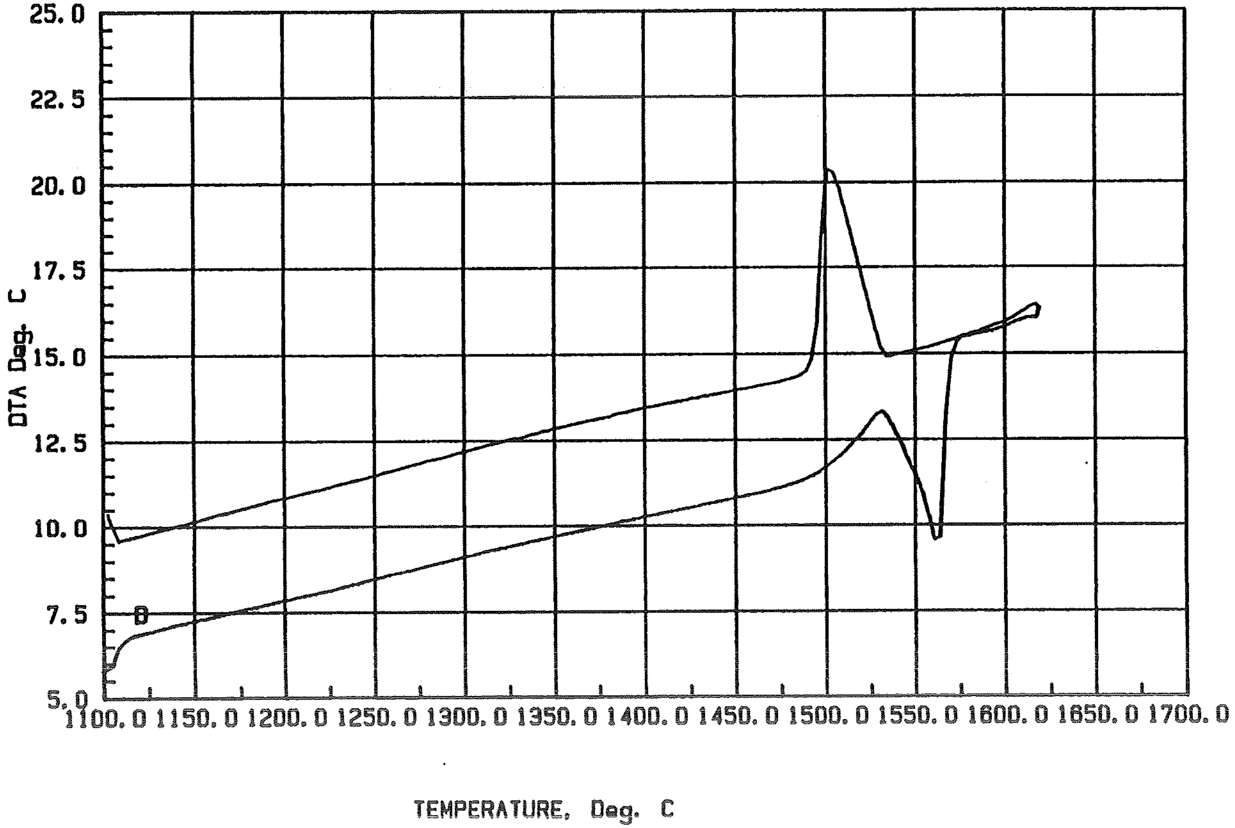

Figure B.2: DTA scan for material taken from a directionally solidified Ni-42-12.5Ta-7Mo ingot.

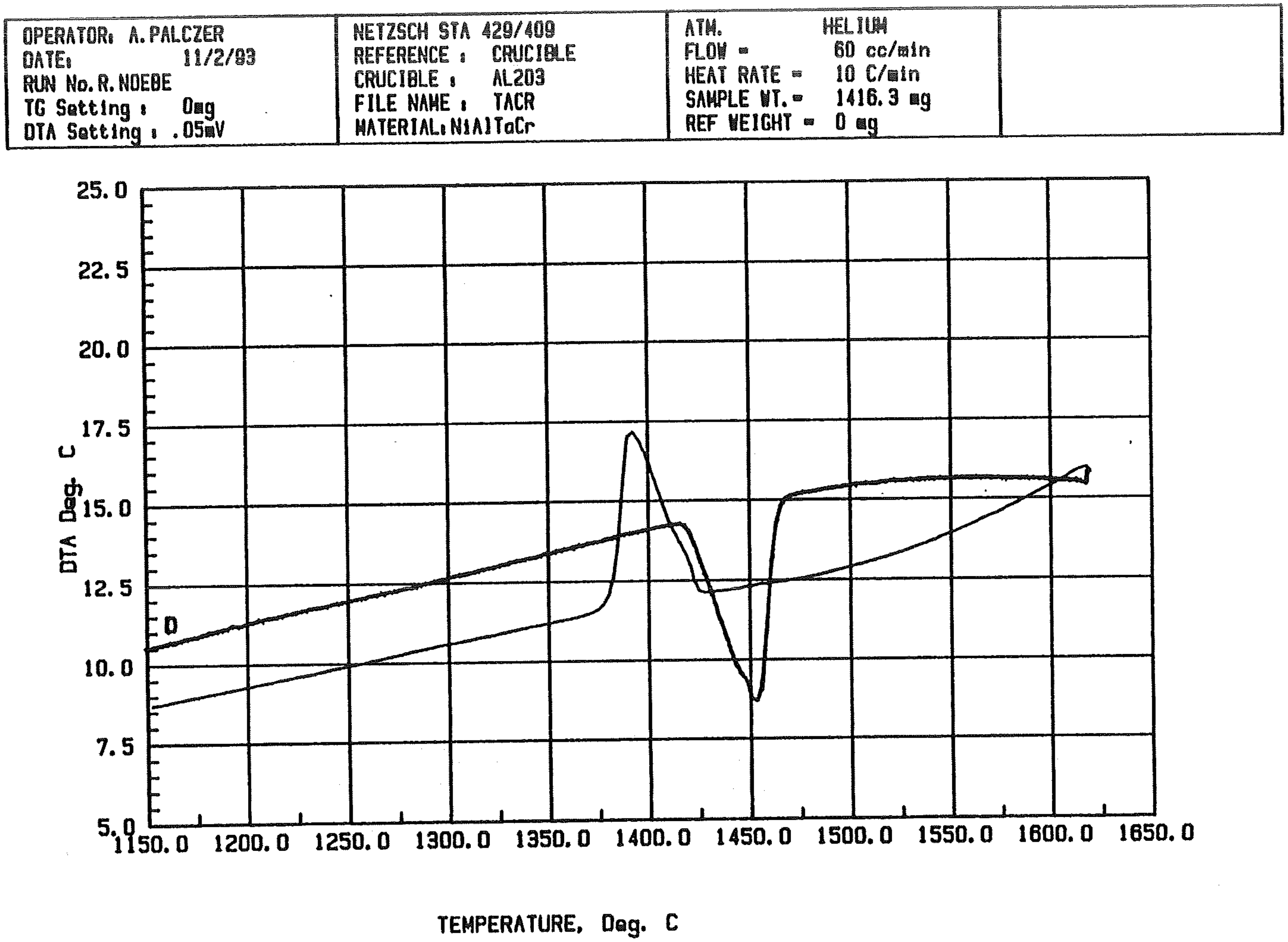

OPERATOR: A.PALCZER
DATE: 11/2/93
RUN No. R.NOEBE
TG Setting : 0mg
DTA Setting : .05mV

NETZSCH STA 429/409
REFERENCE : CRUCIBLE
CRUCIBLE : AL203
FILE NAME : TACR
MATERIAL: NiAlTaCr

ATM. HELIUM
FLOW = 60 cc/min
HEAT RATE = 10 C/min
SAMPLE WT. = 1416.3 mg
REF WEIGHT = 0 mg

Figure B.3: DTA scan for material taken from a directionally solidified Ni-30.5Al-6Ta-33Cr ingot.

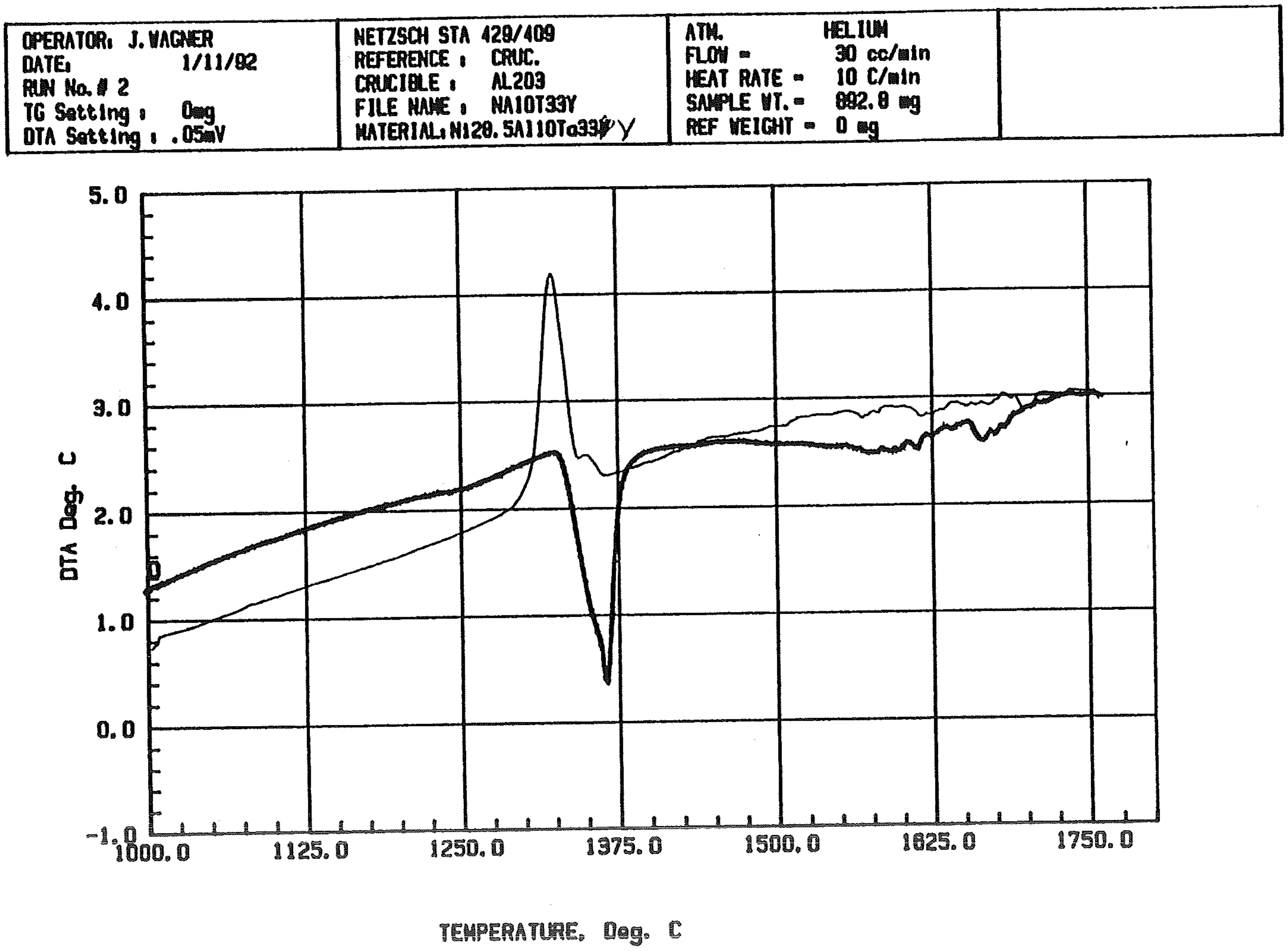

OPERATOR: J.WAGNER
DATE: 1/11/92
RUN No.# 2
TG Setting : 0mg
DTA Setting : .05mV

NETZSCH STA 429/409
REFERENCE : CRUC.
CRUCIBLE : AL203
FILE NAME : NA10T33Y
MATERIAL: Ni28.5Al10Ta33 Y

ATM. HELIUM
FLOW = 30 cc/min
HEAT RATE = 10 C/min
SAMPLE WT. = 892.8 mg
REF WEIGHT = 0 mg

Figure B.4: DTA scan for material taken from an arc-melted Ni-28.5Al-10Ta-33V ingot.

VITA

David Ray Johnson was born in [redacted] on [redacted] He received a Bachelor of Science degree in Engineering Science and Mechanics from the University of Tennessee, Knoxville in June 1987. The following fall he enrolled in the graduate program in Metallurgical Engineering under the supervision of Dr. W.T. Becker. A Master's degree was awarded in May 1990. The thesis was entitled "Toughness of Tempered Bainitic Microstructures in a 4150 Steel." A Doctor of Philosophy in Metallurgical Engineering was awarded in May 1994. After graduation, he received a post-doctoral fellowship to study at Kyoto University, Japan.

REPORT DOCUMENTATION PAGE

Form Approved
OMB No. 0704-0188

1. AGENCY USE ONLY *(Leave blank)*	**2. REPORT DATE** May 1994	**3. REPORT TYPE AND DATES COVERED** Final Contractor Report

4. TITLE AND SUBTITLE

Processing and Mechanical Properties of NiAl-Based In-Situ Composites

5. FUNDING NUMBERS

WU–505–6352
G–NAG3–876

6. AUTHOR(S)

David R. Johnson

7. PERFORMING ORGANIZATION NAME(S) AND ADDRESS(ES)

The University of Tennessee at Knoxville
Knoxville, Tennessee

8. PERFORMING ORGANIZATION REPORT NUMBER

E–8864

9. SPONSORING/MONITORING AGENCY NAME(S) AND ADDRESS(ES)

National Aeronautics and Space Administration
Lewis Research Center
Cleveland, Ohio 44135–3191

10. SPONSORING/MONITORING AGENCY REPORT NUMBER

NASA CR–195333

11. SUPPLEMENTARY NOTES

This report was submitted as a dissertation in partial fulfillment of the requirements for the degree Doctor of Philosophy to The University of Tennessee at Knoxville, Knoxville, Tennessee. Project Manager, Ronald D. Noebe, Materials Division, organization code, 5180, NASA Lewis Research Center, (216) 433–2093.

12a. DISTRIBUTION/AVAILABILITY STATEMENT

Unclassified - Unlimited
Subject Category 26

12b. DISTRIBUTION CODE

13. ABSTRACT ***(Maximum 200 words)***

In-situ composites based on the NiAl-Cr eutectic system were successfully produced by containerless processing and evaluated. The NiAl-Cr alloys had a fibrous microstructure while the NiAl-(Cr,Mo) alloys containing 1 at.% or more molybdenum exhibited a lamellar structure. The NiAl-28Cr-6Mo eutectic displays promising high temperature strength while still maintaining a reasonable room temperature fracture toughness when compared to other NiAl-based materials. The Laves phase NiAlTa was used to strengthen NiAl and very promising creep strengths were found for the directionally solidified NiAl-NiAlTa eutectic. The eutectic composition was found to be near NiAl-15.5Ta (at.%) and well aligned microstructures were produced at this composition. An off-eutectic composition of NiAl-14.5Ta was also processed, consisting of NiAl dendrites surrounded by aligned eutectic regions. The room temperature toughness of these two phase alloys was similar to that of polycrystalline NiAl even with the presence of the brittle Laves phase NiAlTa. Polyphase in-situ composites were generated by directional solidification of ternary eutectics. The systems investigated were the Ni-Al-Ta-X(X=Cr, Mo, or V) alloys. Ternary eutectics were found in each of these systems and both the eutectic composition and temperature were determined. Of these ternary eutectics, the one in the NiAl-Ta-Cr system was found to be the most promising. The fracture toughness of the NiAl-(Cr,Al)NiTa-Cr eutectic was intermediate between those of the NiAl-NiAlTa eutectic and the NiAl-Cr eutectic. The creep strength of this ternary eutectic was similar to or greater than that of the NiAl-Cr eutectic.

14. SUBJECT TERMS

NiAl Composite; Eutectic; NiAl-Cr; NiAl-NiAlTa; Laves

15. NUMBER OF PAGES

205

16. PRICE CODE

A10

17. SECURITY CLASSIFICATION OF REPORT Unclassified	**18. SECURITY CLASSIFICATION OF THIS PAGE** Unclassified	**19. SECURITY CLASSIFICATION OF ABSTRACT** Unclassified	**20. LIMITATION OF ABSTRACT**